Characterisation of Anatomical and Functional Deficits in a Mouse Model of Rett Syndrome

Shih-Ming Weng
MD, MSc

Submitted in fulfilment of the requirements for the degree of PhD
School of Life Sciences
College of Medical, Veterinary and Life Science
University of Glasgow
Glasgow, G12 8QQ

September 2011

Abstract

Rett syndrome (RTT), a disorder caused almost exclusively by mutations in the X-linked gene, *MECP2*, has a clinical phenotype thought to be primarily of neurological origin. Disruption of *Mecp2* in mice results in a prominent RTT-like phenotype and *Mecp2* knock-out animal models provide an excellent platform for investigating the role of MeCP2 in the brain development. In this thesis, I used the *Mecp2-stop* mouse model to address the effects of MeCP2 deficiency in the central nervous system. First, I assessed the genotype-phenotype relationship at the level of the whole organism by detailed temporal mapping of the RTT-like neurological signs. I also addressed the genotype-phenotype relationship at the level of neuronal networks by assessing alterations in neuronal (cortical) density including potential alterations across morphologically discrete cell subtypes. Finally, I also investigated the genotype-phenotype relationship at the level of the synapse by assessing RTT-related changed in synaptic plasticity.

Whole organism phenotyping using observational scoring revealed the male hemizygous *Mecp2*-mutant mice (*Mecp2*$^{stop/y}$) to show an early (from ~5 weeks) and aggressive onset of signs including locomotor and other general features. Correlated studies at the level of the synapse revealed the severity of gross organismal pathology to mirror a progressive decline in both short- and long-term forms of synaptic plasticity as measured in the CA1 region of the hippocampus. Specifically, extracellular field recordings in acute hippocampal slices from strongly symptomatic *Mecp2-stop* mice showed long-term plasticity (LTP) at the Schaffer-collateral-to-CA1 pyramidal synapse to be 40.2 ± 1.6 % of age-matched wild-type littermate controls. In addition, putative presynaptic short-term forms of plasticity (post-tetanic potentiation (PTP) and paired-pulse facilitation (PPF)) were also decreased in the *Mecp2-stop* hippocampus (45 ± 18.8 % and 78 ± 0.1 % of wild type for PTP and PPF respectively; all $p<0.05$). Moreover, the impairment in LTP was associated with symptom severity score whereby mice with a more 'severe' symptom score showed a more profound deficit in LTP.

Refined axon stimulation protocols revealed evidence of pronounced LTP saturation in symptomatic *Mecp2*$^{stop/y}$ mice, suggesting an LTP 'ceiling' effect. I

therefore assessed the action of the weak NMDA receptor blocker memantine, shown previously to reverse LTP saturation-related LTP deficits, in the hippocampus of control and *Mecp2-stop* mice. Application of memantine (1μM), resulted in substantial reversal of short-term plasticity deficits in the *Mecp2-stop* samples, without affecting plasticity in wild-type mice. However, systemic administration of memantine (30mg/Kg) in vivo did not have any observable effect on RTT-like phenotype at the organismal level including symptom onset, progression and survival.

Utilising immunohistochemistry (NeuN) and histological staining (DAPI) to quantify cell density in layer five of the somatosensory cortex, I demonstrated that the symptomatic *Mecp2-stop* mouse had a higher cortical cell density compared to wild-type controls (1.28 times of whole cortical cell density and 1.41 times of neuronal cell density). Detailed analyses of distinct neuronal subpopulations (parvalbumin-, somatostatin-, calretinin- and calbindin-immunopositive cells) showed that calretinin (CR)- and somatostatin (SOM)-immunopositive cells had a lower cell density in *Mecp2-stop* mouse somatosensory cortex. However, the distribution patterns of different neuronal subtypes (using the same markers) in *Mecp2-stop* hippocampus were preserved and were grossly similar to those of WT brains.

In summary, in this thesis, I demonstrated that the cell densities of CR- and SOM- positive neurons were altered in the somatosensory cortex in symptomatic *Mecp2-stop* mice. At the synaptic functional level, I showed both short-term and long-term plasticity deficits in the hippocampus of *Mecp2-stop* brains. Memantine, a clinically widely-used Alzheimer drug, partially restored the synaptic plasticity deficits *in vitro*. These data together supported that deficits in specific neuronal populations and progressive functional synaptic impairment may be key features in the RTT brain and also demonstrated the potential for the pharmacological restoration of synaptic plasticity function.

Table of Contents

List of Tables

List of Figures

Acknowledgements

When I was a secondary school student, I read an essay paragraph of a famous Chinese scientist and writer, Chih-Fan Chen（陳之藩）:

“因為需要感謝的人太多了，就感謝天罷。”

(We appreciate all the contributions and support from many. If we simplify it into just one sentence, which is “All thanks be to God.”

Now, I truly realise what he was trying to convey, after several decades. As it comes to the end of my time in Glasgow and completion of this thesis, I would like to express my highest gratitude to my supervisors Dr Mark Bailey and Dr Stuart Cobb for their support and guidance from the initial to the final level in my course of study. I truthfully appreciate the opportunity to participate in this interesting and challenging project. I still remember in February 2007, the first time I visited University of Glasgow, at that time I actually couldn’t expect what is waiting for me for the next four years. As a paediatric neurologist, I am confident to make clinical decisions day by day; however, without Mark and Stuart, I have no idea how I can reach this final stage of my PhD. Sincerely from the bottom of my heart, thanks very much.

When I first started my PhD project in 2007, there is only one PhD student in Dr Cobb’s. Fortunately, Dr Jian Gan is from China, and we can communicate directly in mother tongue. Particularly, Jian is the electrophysiology expert and I relied on his guidance and support for the initial two years of my PhD, not only in the lab but also outside campus. I really appreciate to have such a good friend in my life.

I would like to thank both Dr Rosie Spike and Faye McLeod, who have greatly contributed to my thesis. This work would not be attainable without the anatomical studies and western blot experiments they carried out.

To Paul Turko, Dr Kamal Gadalla and Joe Wu, thank you not only for sharing scientific knowledge and discussing projects with me, and also for accompanying me to pass the darkest period of my PhD life.

As an assessor of my PhD, Prof Imre Vida always inspires me with creative suggestions. Without the support of his lab and Dr Sam Booker, I couldn’t complete the immunohistochemistry part of my project.

I would also like to thank many people who work in the West Medical and Davidson building with me: Graham for the immediate help on the day of thesis

submission and the Congo stories, Louise for chatting and staying in the vegetarian team with me in many occasions and everyone else mentioned previously, it is indeed my pleasure to work with all of you.
My gratitude also extends to Dr David Hughes for the technical support in operating confocal microscope at the Spinal Cord Group and smart suggestions for my thesis, also Dr Andrew Irving for the valuable advice in my viva.
I also thank many Taiwanese students in Glasgow and Tao relatives in London and Telford for turning my PhD life more colourful and enjoyable.
I am also grateful to Prof Tzu-Bi Shih, Prof Huei-Fang Shang, the Rett Syndrome Association Scotland and the Ministry of Education Taiwan for providing the opportunity, funds and support for this study.
Last but not least, I owe my deepest gratitude to my parents, my dear wife, my brother and friends. Thank you for your unconditional love and tolerate my bad temper all the time!

Dedication

To my most loving parents, my beloved wife and my brother

給我摯愛的父母，太太與我弟弟

Author's Declaration

I declare that the work presented in this thesis is entirely my own with all exceptions being clearly indicated or/and properly cited in the context, and all citations have been provided in the reference list.

Signature: Shih-Ming Weng

The work has not been presented in part or alone for any other degree programme. Some of the work contained here has been published in part: a list follows.

Weng SM, McLeod F, Bailey ME & Cobb SR (2011) Synaptic plasticity deficits in an experimental model of rett syndrome: long-term potentiation saturation and its pharmacological reversal. ***Neuroscience***, 180, 314-321.

Weng SM, Bailey ME & Cobb SR (2011) Rett Syndrome: From Bed to Bench. ***Pediatrics and Neonatology***, 52(6), 309-16.

Abbreviations

Ab	antibody
ACSF	artificial cerebrospinal fluid
AMPA	α-amino-3-hydroxy-5-methyl-4-isoxazolepropionic acid
ANOVA	analysis of variance
BDNF	Brain-derived neurotrophic factor
bp	base pair
CA (1,2,3)	cornus ammonis (1,2,3)
Ca^{2+}	Calcium
CB	Calbindin
CNS	Central nervous system
CpG	Cytosine-guanine dinucleotide
CR	Calretinin
DG	dentate gyrus
DNA	Deoxyribonucleic acid
EC	entorhinal cortex
EDTA	ethylenediaminetetraacetic acid
EPSP	excitatory postsynaptic potential
fEPSP	field excitatory postsynaptic potential
GABA	γ-aminobutyric acid
GFP	green fluorescent protein
HFS	high frequency stimulation
Hz	hertz
I/O	input/output
IgG	immunoglobulin G
LTD	long term depression
LTP	long term potentiation
mA	milliampere
MBD	Methyl-CpG binding domain
MECP2	Methyl-CpG binding protein 2
MF	mossy fibre
nM	nanomolar
NEO	Neomycin
NMDA	N-methyl-D-aspartic acid
PB	phosphate buffer
PBS	phosphate-buffered saline
PCR	polymerase chain reaction
PP	perforant path
PPF	paired-pulse facilitation
PTP	post-tetanus potentiation
PV	parvalbumin
RNA	Ribonucleic acid
RTT	Rett syndrome
SEM	standard error of mean
SOM	somatostatin
STP	short term plasticity
WT	wild type
μA	microampere
μg	microgram
μm	micrometre
μM	micromolar

1 Introduction

1.1 General introduction

Rett syndrome is a postnatal progressive neurological disorder that alters normal brain development during early childhood. Brain development is a complicated but highly organised process. It includes the processes that generate, shape, and reshape the nervous system, from the earliest stages of embryogenesis to the final years of life. At the embryonic stage, the brain emerges as the neural tube. The anterior part of the neural tube is the telencephalon, which later expands rapidly and eventually gives rise to the brain. Newly-generated neurons migrate to different parts of the developing brain and are organised into different brain structures. After neurons immigrate to their designated regions, they project axons and dendrites and connect with each other via synapses to form networks. The synaptic connection between neurons is the foundation of functional neural circuits that mediate sensory and motor processing and underlie behaviour. Most essential neurodevelopment occurs in the first five to ten years of human life. Therefore, it is not surprising that most prevalent neurodevelopmental disorders have early onsets, and symptoms can involve motor, sensory, autonomic or higher cognitive dysfunctions. Rett syndrome is a neurodevelopmental disorder and represents a significant cause of mental retardation in girls. Genetic studies have revealed that Rett syndrome is due to the mutation of *MECP2* (Amir *et al.*, 1999), and knock-out animal models provide an excellent platform for investigating the role of *MECP2* in brain development. In this thesis, I used the *Mecp2-stop* mouse model to assess the genotype-phenotype relationship and the progress patterns of symptoms. At the cellular level, I quantified alterations in neuronal subtype densities and their distributions in the brain, and finally evaluated synaptic functions in the RTT brain to further realise the pathologic mechanism which underlies Rett syndrome.

1.2 Rett syndrome

Rett syndrome (RTT; MIM 312750) was first identified by Dr Andreas Rett in 1966, after he observed twenty-two patients with similar unique symptoms (Rett, 1966). The constellation of features that represent RTT became more widely recognized as a specific neurodevelopmental disorder after subsequent larger studies by Dr Bengt Hagberg (Hagberg *et al.*, 1983). In 1999, Amir *et al.* discovered the genetic basis of RTT (>95% of cases of classical RTT) to be mutations in the gene *MECP2* (Amir *et al.*, 1999). A few years earlier, Dr Adrian Bird and his colleagues identified MeCP2 (methyl-CpG binding protein 2) as a novel protein that binds to methylated CpG dinucleotides within the mammalian genome (Lewis *et al.*, 1992). Methylation of CpGs is associated with gene silencing and alterations in chromatin structure. Whilst the exact function of MeCP2 is still not known, it is an abundant nuclear protein and is considered likely to regulate gene expression, whether through the silencing or activation of specific genes or through more global regulation of transcriptional processes (Klose & Bird, 2006; Chahrour *et al.*, 2008; Skene *et al.*, 2010).

An important feature in the aetiology of RTT is the fact that *MECP2* is located on the X chromosome, Xq28 (Quaderi *et al.*, 1994). Most mutations are sporadic and rarely inherited. Moreover, mutations in males typically result in severe infantile encephalopathy due to complete absence of functional MeCP2. In contrast, females are heterozygous for the mutation with, due to X chromosome inactivation, approximately half of the cells expressing the mutant *MECP2* allele but with the other half expressing a functional allele. Thus, RTT is a disease that is almost exclusively seen in females.

1.2.1 Clinical Features of RTT

Rett syndrome is a predominantly neurological disorder and a primary cause of severe mental retardation in girls with an incidence of approximately 1 in 10,000 female births (Neul *et al.*, 2010). Patients with RTT appear to develop normally up to 6–18 months of age. They typically achieve normal neurodevelopmental milestones, from gross and fine motor functions to social communication skills. The head circumference of Rett girls is normal at birth; however, it begins to decelerate in its growth at 2 to 3 months of age (Schultz *et*

al., 1993). Distinctive aspects contributing to the diagnosis include developmental regression, with accompanying loss of hand skills, mobility skills and speech, and stereotypical hand movements. As the syndrome progresses, social withdrawal and loss of language become apparent with features reminiscent of autism (Nomura, 2005). The onset of mental deterioration is accompanied by loss of motor coordination and the development of ataxia and gait apraxia. Associated features, such as microcephaly, respiratory/autonomic abnormalities (Julu *et al.*, 2001), seizures, scoliosis, growth deficits and early hypotonia, are very prevalent.

Among these symptoms, the most significant is seizure disorder, which ranges from simple convulsion to intractable epilepsy (Jian *et al.*, 2006). Neurophysiological evaluations show cortical hyperexcitability on the electroencephalogram (EEG), which represents a loss of expected developmental features and the occurrence of rhythmic slow activity, primarily in the frontal-central regions. However, most events presumed to be seizures are without EEG correlation during video-EEG recording (Percy, 2008). Other associated abnormalities during the post-regression phase include teeth grinding, night laughing or crying, screaming fits, low mood, and anxiety episodes elicited by distressful external events (Mount *et al.*, 2001). Most girls with RTT lose mobility, and are often wheelchair-bound during their teenage years. Impairment of the autonomic nervous system in Rett syndrome is suggested by an increased incidence of long Q–T intervals during electrocardiographic recordings, and this can contribute to the higher incidence rate of sudden unexpected death in RTT patients. Other autonomic abnormalities include hypotrophy, cold blue feet, severe constipation, oropharyngeal dysfunction, and cardiac abnormalities, including tachycardia and sinus bradycardia. Even with high risk of sudden death due to respiratory and cardiac dysfunctions, several patients survive till the sixth or seventh decade of life with limited mobility (Hagberg, 2005).

1.2.2 Genetic Basis of RTT

RTT cases are usually the result of dominantly-acting sporadic mutations in the X-linked gene *MECP2*, which encodes methyl-CpG-binding protein 2 (MeCP2) (Amir *et al.*, 1999). MeCP2 is expressed quite widely throughout the body, with notably high expression in postnatal neurons (LaSalle *et al.*, 2001; Shahbazian *et*

al., 2002; Zhou *et al.*, 2006). However, the question remains as to why disruption of a ubiquitously expressed protein results in a predominantly neurological phenotype (Zhou *et al.*, 2006). Most pathogenic mutations in *MECP2* cause RTT in heterozygous females, while mutations leading to other phenotypic outcomes are also known (Moretti & Zoghbi, 2006). Since most RTT cases are sporadic, it was difficult to map the disease locus by traditional linkage analysis. Instead, using information from families under the rare circumstances in which the mutant *MECP2* is inherited, the Xq28 region was identified, and subsequent screening of candidate genes in RTT patients revealed mutations in *MECP2* (Amir *et al.*, 1999). Boys inheriting a mutant *MECP2* allele are much more severely affected, presenting with infantile encephalopathy and usually not surviving infancy. Since most *MECP2* mutations leading to RTT involve loss of function of the mutant allele, RTT can be modelled using gene knockout mice that recapitulate many of the key clinical signs that characterize RTT in humans (Chen *et al.*, 2001; Guy *et al.*, 2007).

MECP2 is located on the X chromosome and is subject to X chromosome inactivation (XCI), such that in each cell in a heterozygous female RTT patient expresses only the normal or the mutant *MECP2* allele. The XCI process is random and results in an approximately 50:50 phenotypic mixture of cells. Previous studies of the distribution pattern of brain cells expressing normal and mutant *MECP2* alleles have revealed that MeCP2-negative cells tend not to be clustered and are well-mixed with MeCP2-positive cells in a mosaic pattern (Guy *et al.*, 2007). However, a number of studies have reported that the skewing of XCI ratio is away from 50:50 in RTT patients (Knudsen *et al.*, 2006; Schanen *et al.*, 1997). It is well-known that several rare familial cases of RTT are attributed to that mothers of these patients carry the causative mutation, but are highly skewed towards expression of the normal allele (Villard *et al.*, 2001). A study investigating the skewing phenomenon of XCI in sporadic RTT cases (Archer *et al.*, 2007) revealed that most RTT patients had degrees of skewing towards expression of the normal allele and this phenomenon could partially explain the phenotypic variability of RTT. The tendency that MeCP2-positive cells are generated more or survive longer still needs to be verified since most skewing studies were conducted in peripheral tissues with a higher cell turnover rate rather than in brain regions.

MeCP2 is a member of a family of proteins that bind regions of DNA enriched with methylated CpG regions (MBD family) (Hendrich & Bird, 1998). MeCP2 was initially identified in rat cells based on its ability to bind methylated DNA and was found to bind a single symmetrically methylated CpG independent of sequence context (Meehan *et al.*, 1989; Lewis *et al.*, 1992). MeCP2 RNA is ubiquitously transcribed in the whole body; however, protein expression shows tissue specificity. In the adult mouse, MeCP2 is highly abundant in the brain, lung and spleen, less abundant in the kidney and heart, and almost negligible in the liver, stomach and small intestine (Shahbazian *et al.*, 2002). The quantification of MeCP2 in adult mouse brain has shown nearly 16 million molecules of MeCP2 per nucleus in neurons, with almost an order of magnitude less in glial cells and 30- fold less in liver cells (Skene *et al.*, 2010). In mice, the neuronal MeCP2 level is low at birth and elevates significantly during the first 3 weeks of life (Kishi & Macklis, 2004; Skene *et al.*, 2010).

MeCP2 contains six functional domains encoded by exon 3 and 4, including a methyl-CpG binding domain (MBD), two high mobility group protein-like domains (HMGD), a transcriptional repression domain (TRD) (Nan *et al.*, 1993; Nan *et al.*, 1997), and two C-terminal domains (CTD) (see structure of MeCP2 and common mutation sites in RTT in figure 1.1). The MBD domain is necessary and sufficient to bind a single symmetrically methylated CpG in the major groove of DNA, covering a region of 12bp surrounding the methyl-CpG site (Nan *et al.*, 1993). MeCP2 binds methylated DNA *in vitro* and *in vivo*, and is capable of binding to DNA in a nucleosomal context without targeted disruption of the nucleosome (Nan *et al.*, 1997; Kudo, 1998). The domain responsible for conferring gene silencing was mapped to the middle of the protein and defined as the transcriptional repression domain (TRD). The TRD overlaps with a nuclear localisation signal and is capable of repressing transcription *in vitro* and *in vivo* (Nan *et al.*, 1997). The C-terminal domain (CTD) could be divided into CTDα and CTDβ. The CTDβ contains the WW binding domain, which is involved in splicing factor interactions. MeCP2 was classically considered to be a methylation-dependent transcriptional repressor (Nan *et al.*, 1998). However, other studies suggest additional or alternative roles, including an enhancer of transcription (Chahrour *et al.*, 2008), a global regulator of chromatin structure (Horike *et al.*, 2005) or a global dampener of transcriptional noise (Skene *et al.*, 2010).

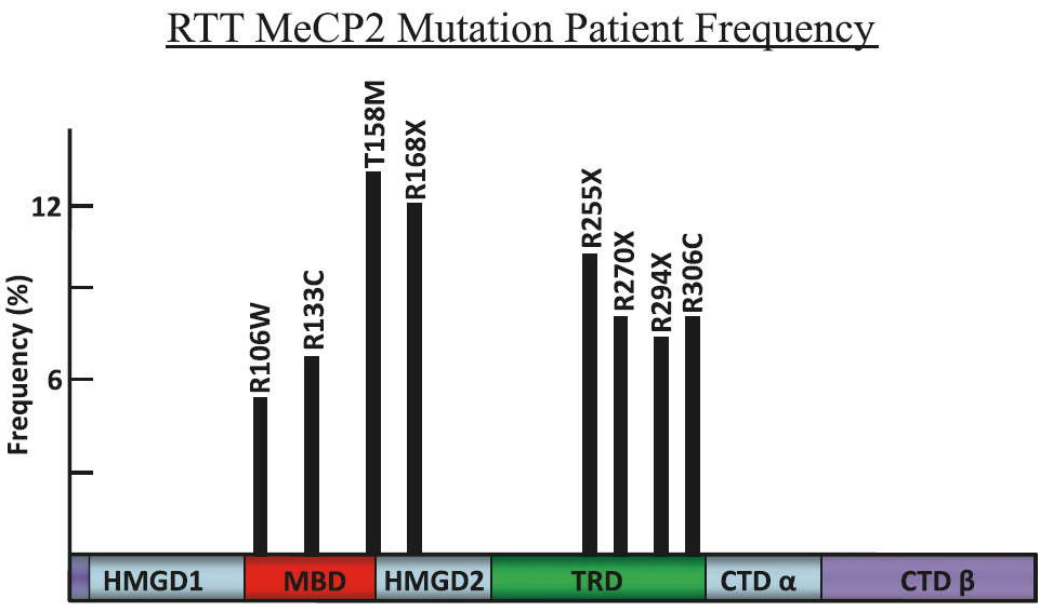

Figure 1.1 Illustrated structure of MeCP2 and the location and frequency of common MeCP2 mutations in RTT patients.

R106W, arginine to tryptophan point mutation at residue 106; R133C, arginine to cysteine point mutation at residue 133; T158M, threonine to methionine point mutation at residue 158; R168X, arginine to stop codon at residue 168; R255X, arginine to stop codon at residue 255; R294X, arginine to stop codon at residue 294; R306C, arginine to cysteine point mutation at residue 306. Adopted and modified from Zlatanova *et al.,* 2005 (Zlatanova *et al.,* 2005).

MeCP2 is expressed in a range of tissues but is especially abundant in post-mitotic neurons. Mice lacking MeCP2 in neurons show overt RTT-like symptoms, whereas mice in which the expression of MeCP2 is driven in neurons alone are reported to show a normal phenotype (Luikenhuis *et al.*, 2004). While MeCP2 is present at low levels in astrocytes, and MeCP2 deficiency in these cells may confer subtle non-cell autonomous actions on neuronal phenotype (Ballas *et al.*, 2009; Maezawa *et al.*, 2009), a body of evidence points to the overt RTT-like symptoms being due mainly to MeCP2 deficiency in the nervous system and neurons in particular.

1.2.3 Neuropathology in RTT patients

The average one-year-old infant brain weight in RTT patients is 900 g. The weight of the Rett syndrome brain is significantly less than that of the brain of age-matched controls in autopsy studies (Armstrong, 2005). Observation of MeCP2 expression has shown that it is primarily distributed in post-mitotic neurons (Shahbazian *et al.*, 2005). The weight of the Rett brain does not decrease significantly with age, so atrophy does not account for the small cell

size (Armstrong, 2005). Instead, RTT is characterised by lack of brain growth which is not generalised, since some structures such as the cerebral hemispheres are affected more than other structures such as the cerebellum (Armstrong, 2005). Alterations in volume mainly occur in prefrontal, posterior frontal, and anterior temporal regions, with preservation in the posterior temporal and posterior occipital regions (Reiss *et al.*, 1993; Subramaniam *et al.*, 1997).

Neurochemical studies based on RTT patient data are relatively limited. Nevertheless, cerebrospinal fluid and brain tissues have been analysed with respect to levels of various transmitters, receptors, and additional trophic factors. Abnormalities have been reported in most systems, including in acetylcholine (Wenk & Mobley, 1996; Wenk, 1997; Wenk & Hauss-Wegrzyniak, 1999), dopamine (Zoghbi *et al.*, 1985; Brucke *et al.*, 1987; Zoghbi *et al.*, 1989; Lekman *et al.*, 1990; Percy, 1992), serotonin (Segawa & Nomura, 1990; Segawa & Nomura, 1992), glutamate (Hamberger *et al.*, 1992; Lappalainen & Riikonen, 1996), substance P (Matsuishi *et al.*, 1997; Deguchi *et al.*, 2000), and nerve growth factor (Lappalainen *et al.*, 1996; Riikonen & Vanhala, 1999). The age of the patient with Rett syndrome (Lekman *et al.*, 1990) and the severity of the symptoms (Percy, 1992) influence measurements. The reduced levels of acetylcholine and cholinergic markers (Armstrong, 2005) are one of the most consistent findings (Wenk, 1997).

1.2.4 Animal models of RTT

Several mouse genetic models of RTT have been developed through interruption of murine *Mecp2*, and these models accurately recapitulate the cardinal signs that characterise RTT in humans (Chen *et al.*, 2001; Guy *et al.*, 2001; Shahbazian *et al.*, 2002; Luikenhuis *et al.*, 2004; Guy *et al.*, 2007). RTT models are proving invaluable in helping understand the underlying pathology and neuronal dysfunction in RTT, as well as providing insights into the pathophysiology of neurodevelopmental disorders more generally. *Mecp2*-null male mice develop motor impairment, tremor, breathing abnormalities and limb stereotypies (Chen *et al.*, 2001; Guy *et al.*, 2001; Guy *et al.*, 2007). In most of the models, the null males demonstrate apparently normal early development before the onset of overt signs at about 6 weeks of age, and progression is usually fairly aggressive, with death at about 16–20 weeks. Females

heterozygous for *Mecp2* show a more delayed onset of symptoms. The symptom severity increases over a period of weeks to months, as in human females; these then stabilise and the mice show an apparently normal lifespan.

Three RTT models have been widely used. The first of these is the Jaenisch model (Chen *et al.*, 2001), which utilised the *cre-lox* recombination system to delete *Mecp2* exon 3 in this model. Normal development is observed in null model for the first five weeks, following which mice develop nervousness, body trembling, piloerection and occasional breathing abnormalities. Mice typically experience weight loss at 8 weeks and most die by 10 weeks. Reduced brain weight and neuronal size in hippocampus, cerebral cortex, and cerebellum have been reported. The second model is the Bird model (Guy *et al.*, 2001), which was generated by targeted deletion of exons 3 and 4 of *Mecp2* in embryonic stem cells to produce a complete null in terms of the production of MeCP2 protein. Hemizygous males are normal till 3 to 8 weeks, but later develop stiff uncoordinated gait, hindlimb clasping, irregular breathing and uneven teeth wear. Symptoms progress rapidly after 10 weeks, with weight loss and death at around 12-16 weeks. In contrast, the heterozygous females develop inertia and hindlimb clasping at around 3 months, and breathing abnormalities (irregular breathing patterns) and decreased mobility after 6 months. They survive longer than males and are fertile. The *Mecp2*$^{308/y}$ model (Shahbazian *et al.*, 2002) is a milder model and was generated by insertion of a truncating *Mecp2* mutation. A stop codon (after amino acid 308) produces a protein that is truncated yet retains the MBD, TRD domains and nuclear localisation signal motif. Males appear normal till 6 weeks and later develop tremors, motor impairment, hypoactivity, anxiety behaviour, seizures, kyphosis, and stereotypic forelimb motions. Survival is much longer than MeCP2 null models, with males living to 10 months and being fertile. Females also survive and have milder symptoms than seen in the null (complete absence of protein) models.

Most RTT model studies have focused on global deletion or truncation of *Mecp2* (Chen *et al.*, 2001; Guy *et al.*, 2001; Shahbazian *et al.*, 2002; Pelka *et al.*, 2006; Stearns *et al.*, 2007). Behavioural studies in these mice have revealed altered gait and motor defects including hypoactivity, paw stereotypies and balance and swimming impairments. Such mice also display an anxiety phenotype including reduced exploration, increased thigmotaxis (movement toward or away from

mechanical stimulus) and altered plus and zero maze behaviour. Motor dysfunction limits the application of certain cognitive tests, but impairments in fear conditioning and novel object recognition have been reported (Pelka *et al.*, 2006; Stearns *et al.*, 2007). In the *Mecp2*$^{308/y}$ model, which generates truncated MeCP2 and displays significantly milder symptoms, mice show impairments in hippocampal-dependent spatial memory as well as social memory (Moretti *et al.*, 2006).

Like in RTT patients, *Mecp2*-mutant mice have smaller cortical neurons packed at a higher density than their wild-type littermates (Chen *et al.*, 2001; Kishi & Macklis, 2004; Stearns *et al.*, 2007). Moreover, pyramidal neurons in the cortex (Kishi & Macklis, 2004) as well as in hippocampal CA3 region, and granule cells of the dentate gyrus show reduced dendritic complexity (Ballas *et al.*, 2009). Furthermore, Jaenisch *Mecp2*-mutant mice show a disorganised olfactory neuroepithelium indicative of delayed terminal differentiation (Matarazzo *et al.*, 2004). However, dendritic branching in layer III and V pyramidal neurons of the frontal cortex of male *Mecp2*$^{308/y}$ mice was comparable to that in controls (Moretti *et al.*, 2006). In the Bird model, pyramidal neurons from the somatosensory cortex of six-week-old mice show lower spine densities compared with wild-type controls (Fukuda *et al.*, 2005). Newly generated granule cells in the dentate gyrus of eight-week-old Jaenisch model mutant mice also show impaired dendritic spine density and distribution (Smrt *et al.*, 2007). In female heterozygous mice, the onset of this dendritic spine phenotype is delayed and more severe in *Mecp2*-lacking neurons than in *Mecp2*-expressing neurons, suggesting both cell autonomous and non-cell autonomous effects (Belichenko *et al.*, 2009). The intensity of PSD-95 (an abundant postsynaptic protein) is also lower in layer V pyramidal neurons of the motor cortex of MeCP2-null mice (Tropea *et al.*, 2009). As far as pre-synaptic terminals are concerned, the motor cortex of Bird model mice shows defects in axonal fasciculation (Belichenko *et al.*, 2009). Moreover, the intensity of VGLUT1 (a pre-synaptic protein) is lower in the dendritic region of the hippocampal CA1 region from MeCP2-null mice; however, the post-synaptic dendritic marker MAP-2 was not different. The authors interpreted this as showing that *Mecp2* deletion caused a reduction in the number of mature synapses in area CA1, consistent with their results from dissociated neuronal cultures (Chao *et al.*, 2007).

1.2.5 Synaptic Function Studies in RTT models

Anatomical studies have shown changes in neuronal structure and synaptic connectivity (Armstrong *et al.*, 1995; Belichenko *et al.*, 1997; Armstrong *et al.*, 1998; Chao *et al.*, 2007). For instance, the neuronal soma is smaller in the absence of MeCP2 (15-25% smaller in hippocampal CA2 region), and cells are more densely packed (Kaufmann & Moser, 2000; Chen *et al.*, 2001; Armstrong, 2005; Taneja *et al.*, 2009). Mutation of MeCP2 is also associated with an abnormal number of axons (~33% increased in *Mecp2*-mutant mice) (Belichenko *et al.*, 2009) and a defect in axonal targeting (Matarazzo *et al.*, 2004; Palmer *et al.*, 2008; Belichenko *et al.*, 2009). These results indicate a decrease in the number of synapses in RTT brains, which has been confirmed for glutamatergic synapses in primary neuronal cultures (Chao *et al.*, 2007).

Electrophysiological studies in mice show subtle changes in neuronal electrical properties within cortical areas (Dani *et al.*, 2005; Kline *et al.*, 2010) and more pronounced changes in other regions such as the brain stem and locus ceruleus (Medrihan *et al.*, 2008; Taneja *et al.*, 2009). Overt changes in synaptic function include reduced synaptic plasticity (Asaka *et al.*, 2006; Moretti *et al.*, 2006; Guy *et al.*, 2007; Nelson *et al.*, 2008) and changes in basal inhibitory and excitatory synaptic transmission (Dani *et al.*, 2005; Medrihan *et al.*, 2008; Nelson *et al.*, 2008; D'Cruz *et al.*, 2010; Kline *et al.*, 2010; Maliszewska-Cyna *et al.*, 2010). At the network level there is a shift in the balance of excitatory/inhibitory (E/I) currents, with increased excitatory and decreased inhibitory neurotransmission in the hippocampus and cortex (Dani *et al.*, 2005; Nelson *et al.*, 2006; Chao *et al.*, 2007; Zhang *et al.*, 2008; Wood & Shepherd, 2010). This is supported by data showing defects of GABAergic neurotransmission in the brainstem (Medrihan *et al.*, 2008). Recently, the mouse model with MeCP2 deficiency solely in GABAergic neurons has recapitulated most of the phenotypic features displayed by *Mecp2*-null mice, including synaptic dysfunctions (Chao *et al.*, 2010). Although GABAergic interneurons constitute only around 10% of the total neuronal population, GABA is the major inhibitory neurotransmitter in the brain and the GABAergic interneuron serves as the coordinator of the neuronal networks (Watanabe *et al.*, 2002). As a result, defects in the inhibitory neurons are likely to affect most neuronal networks and mimic the phenotypes in the *Mecp2*-null mouse. This conclusion is in line with previous reports stating that

the E/I balance is shifted, showing higher excitatory and lower inhibitory neurotransmission. Since GABAergic interneurons are a constellation of diverse neuron groups varying according to their firing signatures, biochemical markers, morphologies, innervating patterns, and distributions (Ascoli *et al.*, 2008; Klausberger & Somogyi, 2008), it is essential to assess the effect of MeCP2 deficiency not only in total GABAergic interneurons but also in distinct subtypes.

The synaptic dysfunction also has been shown by assessing the levels of neurotransmitters, and was in line with the RTT brain autopsy studies (see section 1.2.3). In mice, reduced levels of serotonin (5- hydroxytryptamine), adrenaline, and dopamine have been found in the *Mecp2*-null brain(Ide *et al.*, 2005; Samaco *et al.*, 2009; Isoda *et al.*, 2010; Santos *et al.*, 2010). These are associated with regional defects in the expression of key rate-limiting enzymes tyrosine hydroxylase and tryptophan hydroxylase 2 in the brainstem, the substantia nigra, and the raphe nuclei (Viemari *et al.*, 2005; Samaco *et al.*, 2009; Taneja *et al.*, 2009), and this conclusion suggests that restoration of the monoamine system may be one of the options for rescuing RTT phenotypes (see section 1.5.6).

According to the studies of *Mecp2*-mutant mouse models, synaptic plasticity (long-term potentiation, LTP) appears to be normal in young *Mecp2*-mutant mice (Asaka *et al.*, 2006; Guy *et al.*, 2007; Dani & Nelson, 2009), but shows impairment when tested in older mice upon onset of overt RTT-like signs (Asaka *et al.*, 2006; Guy *et al.*, 2007). In addition, the degree of LTP impairment appears to correlate with the severity of the RTT-like neurological phenotype (Gadalla *et al.*, 2011). Regarding the long-term depression (LTD), another form of NMDA-receptor-dependent long-lasting synaptic plasticity, it is considered to be essential during early development and has also been investigated in different *Mecp2*-mutant mouse models. In the Bird *Mecp2* knockout model, low-frequency afferent stimulation (LFS, 15 min at 1 Hz) induced a smaller or absent LTD in hippocampal CA1 region of symptomatic mutant mice (Asaka *et al.*, 2006). Similarly, LTD induced in area CA1 by paired-pulse low-frequency stimulation of its afferent fibers was impaired in hippocampal slices from symptomatic *Mecp2*$^{308/Y}$ mice (Moretti *et al.*, 2006). In the same *Mecp2*$^{308/Y}$ model, they also investigated LTD by exposing slices to the group I mGluR agonist DHPG (50μm) for 10 min. DHPG-induced LTD was similar in WT and *Mecp2*$^{308/Y}$ mice, indicating

that mutation of *Mecp2* does not alter group I mGluR-induced signalling (Moretti *et al.*, 2006). Moreover, in the symptomatic *Mecp2-stop* female (Guy *et al.*, 2007), the authors also attempted to assess LFS-induced LTD. However, since LTD is difficult to experimentally induce *in vitro* from tissue derived from older animals (*Mecp2-stop* females became symptomatic usually after 3 months old), the LTD data was absent and incomparable in both WT and symptomatic groups (Dr Jian Gan, personal communication). The precise mechanisms underlying the involvement of MeCP2 in regulating morphological and functional aspects of synaptic signalling are yet to be identified. However, synaptic plasticity deficits are one of the most consistent findings and may provide important insights into RTT-like pathogenesis as well as serve as a target system for therapeutic interventions.

1.2.6 Therapeutic Approaches toward RTT

It appears that lack of functional MeCP2 results in a nervous system primed to malfunction at a critical point during postnatal brain development. However, function can be restored (including normal plasticity) to a large degree by the reintroduction of MeCP2 (Guy *et al.*, 2007). In the study by Guy and colleagues (Guy *et al.*, 2007), endogenous *Mecp2* was silenced by insertion of *lox-stop* cassette allowing the mice to develop symptoms (and plasticity deficits) before reintroducing MeCP2 into the brain by pharmacological reactivation of the gene. This reactivation resulted in a pronounced improvement in neurological signs and reduced mortality in the mice. Similar strategies to reintroduce or rebalance MeCP2 levels have been adopted by other groups using different genetic approaches, and these studies have demonstrated improvements in motor function and a reversal of brain weight and neuronal morphology deficits (Luikenhuis *et al.*, 2004; Giacometti *et al.*, 2007; Jugloff *et al.*, 2008). Another genetic strategy has been to overexpress Bdnf, a potent modulator of synaptic plasticity/function that is dysregulated in MeCP2 mutant mice, which again reverses signs such as locomotor deficits (Martinowich *et al.*, 2003). Whilst none of these studies represent a therapeutic strategy that can be applied to human patients, they nevertheless demonstrate the concept of phenotypic reversibility in mouse models of RTT and suggest that the *Mecp2*-mutant mice represent a viable platform for testing future pharmacological and genetic strategies that can be translated for clinical use.

The most obvious strategy in RTT is one of gene therapy. This approach has been successful in disorders such as thalassemia (Perumbeti & Malik, 2010), sickle cell disease (Olowoyeye & Okwundu, 2010), cystic fibrosis (Davies & Alton, 2010), and some cancers (Voutsinas & Stravopodis, 2009; Al-Humadi *et al.*, 2010; Sangro & Prieto, 2010; Vachani *et al.*, 2010), but the application of gene therapy to CNS disorders is a particular challenge. Whilst conceptually straightforward, RTT being a monogenic disorder, the application of gene therapy in RTT is likely to be problematic on numerous counts. For instance, it is likely to be necessary to express MeCP2 in the correct cell types and at the correct levels since overexpression of MeCP2 is also known to be detrimental (Collins *et al.*, 2004). A related complication is that females with RTT have a mosaic expression of MeCP2, with cells expressing the mutant allele and other cells expressing the normal allele and producing functional protein (Hoffbuhr *et al.*, 2002). It is possible that a targeted strategy would be required, whereby the transgene is activated only in the 'mutant' cells and overexpression avoided in the cells with the 'healthy' allele, which are presumably functioning normally. This is an active current area of research but there is relatively little published literature as yet. Using lentiviral delivery of *Mecp2* driven by the endogenous *Mecp2* promoter, Rastegar and colleagues achieved natural expression patterns of MeCP2 and concomitant reversal of dendritic maturation phenotypes *in vitro*, but this approach has not yet been tested *in vivo* (Rastegar *et al.*, 2009).

In contrast to the limited gene therapy literature, a significant number of studies have investigated pharmacological interventions in models of RTT. Several modulators of synaptic function / plasticity have been tested, including the AMPA receptor modulator CX546, the IGF-1 tripeptide, the monoamine reuptake inhibitor desipramine and the Alzheimer drug memantine. In addition to the pharmacological strategies targeting neuronal mechanisms downstream of the MeCP2 deficiency, another approach is to target the MeCP2 mutation itself. This may be applied to specific but common mutations in MeCP2 leading to premature stop codons. Gentamycin, a widely used antibiotic agent, has this capacity and can provide modest (10–22%) read-through of common nonsense mutations in *Mecp2*-mutant transfected HeLa cells (Brendel *et al.*, 2009). Whether this approach can be successfully applied *in vivo* or indeed in the clinic remains to be established.

The studies focusing on AMPA receptor modulators (the ampakine CX546) are based on the fact that levels of BDNF are considered to be regulated by MeCP2 binding (Chen *et al.*, 2003) and that aberrant levels of BDNF have concomitant effects on neurite outgrowth and synaptic maturation and maintenance. Mice treated with daily dosing of CX546 showed enhanced levels of BDNF and an improvement in the breathing phenotype (irregular breathing patterns) that is a prominent feature of RTT patients and seen in *Mecp2*-mutant mice (Nag *et al.*, 2009).

In addition to BDNF (via ampakines), another growth factor that has received attention is IGF-1 (Insulin-like growth factor 1) which is a well-known regulator of synaptic maturation and plasticity. The activity of IGF-1 is regulated by a range of IGF binding proteins. One of these, IGFBP3, has a binding site for the MeCP2 (Chang *et al.*, 2004) and MeCP2-null mice and RTT patients express aberrantly high levels of this protein which would be expected in turn to inhibit IGF-1 signalling (Itoh *et al.*, 2007). An active tripeptide fragment of IGF-1 has been shown to enhance lifespan, improve locomotor function and breathing pattern and heart rate abnormalities in MeCP2-null mice (Tropea *et al.*, 2009). At the cellular level, reversed structural and cortical plasticity deficits were also observed following IGF-1 tripeptide treatment (Tropea *et al.*, 2009), and clinical trials using recombinant IGF-1 are now underway.

For some time there has been an interest in monoamine systems with respect to RTT. There are consistent reports that levels of monoamine markers are reduced in the RTT brain and in MeCP2-null mice (Zoghbi *et al.*, 1985; Zoghbi *et al.*, 1989; Percy, 1992; Viemari *et al.*, 2005). To counter these deficits, drugs such as desipramine (an inhibitor of monoamine uptake) have been tested in MeCP2-null mice (Roux *et al.*, 2007; Zanella *et al.*, 2008). Repeated administration of desipramine improves breathing and prolongs lifespan in RTT mice and at a cellular level, reverses the depletion in brain stem tyrosine hydroxylase (Roux *et al.*, 2007).

1.2.7 Limitations of RTT research

For the past decade, RTT research shifted from the clinical observations to the molecular and cellular neuroscience levels. However, there are still questions that need to be addressed.

Firstly, the symptom progress pattern is not compatible between human and mouse models. For the RTT patients, generally the symptom onset is 12 to 18 months, and most symptoms occur in the early toddler stage (Chahrour & Zoghbi, 2007). In contrast, the heterozygous females of *Mecp2*-null models normally develop symptoms only once they have reached the adult stage. Several previous reports offered species differences or effects of X chromosome inactivation ratio as explanations, but the exact link between mutant MeCP2 and phenotype development is not yet confirmed. This is worthy of further investigation since decoding of the genotype-phenotype relationship is essential for the understanding of the pathologic mechanism that underlies RTT.

Seizures are one of the most prevalent symptoms of RTT (Chahrour & Zoghbi, 2007). In RTT patients, seizures vary from the focal convulsion to intractable epilepsy (Jian *et al.*, 2006). This observation is in line with a recent study demonstrating that deletion of MeCP2 exclusively in GABAergic inhibitory neurons recapitulated most RTT-like symptoms, particularly seizure disorder and hyperexcitable neuronal networks (Chao *et al.*, 2010). In the brain, neurons are classified into two main groups. One is the excitatory neuron (glutamergic neuron), and the other is the inhibitory neuron (GABAergic neuron). Two hypotheses can fit the phenomenon observed in the RTT mouse model. The first of these is an imbalance between the excitatory and the inhibitory populations. The population imbalance could originate from imbalanced neurogenesis processes deriving embryonic neurodevelopment, or from the fact that inhibitory neurons are more vulnerable than excitatory neurons directly or indirectly influenced by the mutant MeCP2 protein. It is worth comparing the neuronal population change in distinct cell types to further determine whether MeCP2 is essential to the development or integrity of specific neuronal subtypes.

The second hypothesis is that the electric property changes are associated with synaptic deficits in the *Mecp2*-null models. Synaptic dysfunctions have been

reported in various anatomical and electrophysiological studies in RTT animal models (Asaka *et al.*, 2006; Moretti *et al.*, 2006; Guy *et al.*, 2007; Nelson *et al.*, 2008). There are still several debates on the link between synaptic plasticity deficits and general phenotype development in RTT animals (Dani & Nelson, 2009). To dissect the synaptic abnormalities in the RTT brain, it is necessary to adopt more accurate experimental schemes for synaptic functional assessment; this will be beneficial for further understanding of the synaptopathy in RTT and for future clinical treatment.

In this thesis, my main focus is on the influence of MeCP2 dysfunction in the brain, especially in the cerebral cortex and the hippocampus. Therefore, in the following sections, general descriptions of the cerebral cortex and the hippocampus are included, followed by the introduction of the synapse, its structures and functions in the brain.

1.3 Cerebral cortex

The cerebral cortex is the neural tissue that lies as an outermost layer, 2 to 4 mm thick, of the cerebrum in mammalian brains (Bentivoglio *et al.*, 2003). It plays a key role in higher-level psycho-physical functions, such as memory, attention, perceptual awareness, thought, language, and consciousness. The phylogenetically more ancient part of the cerebral cortex, the hippocampus, has at most three cellular layers, and is divided into subfields (see section 1.3.5). The most phylogenetically recent part of the cerebral cortex is the neocortex, which is differentiated into six horizontal layers, each of which has a different composition of neurons and connectivity.

1.3.1 Layer structures in the neocortex

Different cortical layers each contain characteristic distributions of neuronal cell types and connections with other cortical regions. Staining cross-sections of the cortex has revealed the position of neuronal cell bodies and the intracortical axon tracts, which have allowed neuroanatomists to produce a detailed

description of the laminar structure of the mammalian brain. After the work of Korbinian Brodmann, the neurons of the cerebral neocortex are grouped into six main layers (Bentivoglio *et al.*, 2003), from the pial surface to the white matter (see figure 1.1).

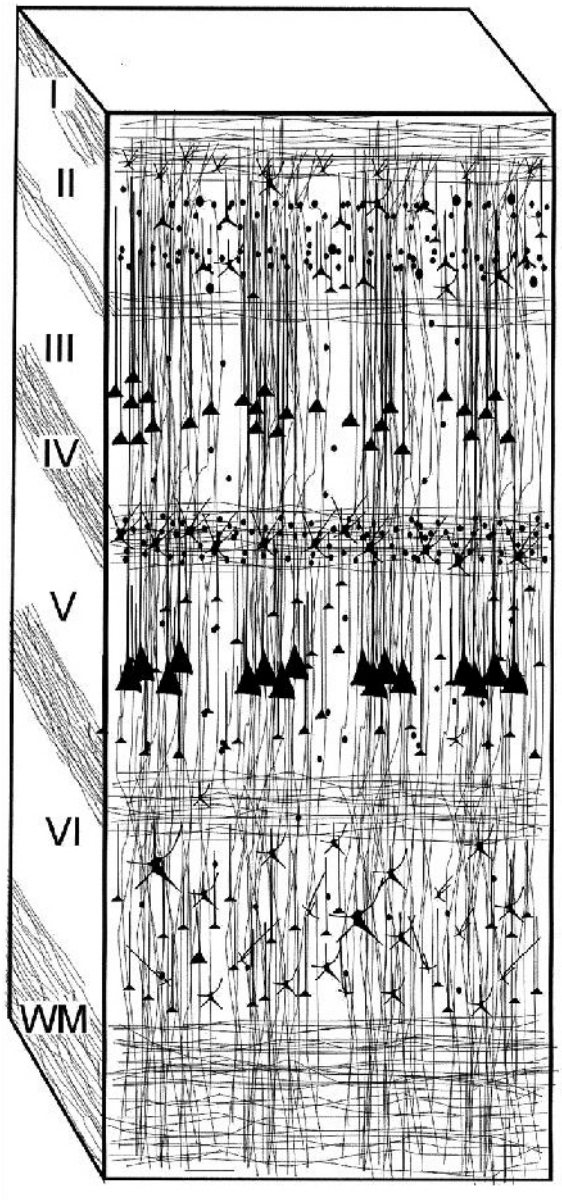

Figure 1.2 Illustration of layer structures in the neocortex.

The diagram of cortical layers I to VI, and WM represents the white matter layer. Adopted and modified from Bentivoglio *et al.,* 2003 (Bentivoglio *et al.*, 2003).

Layer I, the molecular layer, contains only a few scattered neurons and these are all inhibitory neurons. It also consists of extensions of apical dendritic tufts of pyramidal neurons located at layers II and III. Inputs to the apical tufts are thought to be essential for learning and attention functions.

Layer II, the external granular layer, contains mainly small pyramidal neurons and inhibitory neurons, principally bipolar cells and double bouquet cells. It also contains apical dendrites from pyramidal cells whose cell bodies are found in layers V and VI.

Layer III, the external pyramidal layer, contains mainly small and medium-size pyramidal neurons, and few non-pyramidal neurons with vertically-oriented intracortical axons. Layers I to III are the main targets of interhemispheric corticocortical afferents, and layer III is the principal source of corticocortical efferents.

Layer IV, the internal granular layer, is the exclusive location of a class of small excitatory cells called spiny stellate cells. It also contains a variety of inhibitory cells, and is the main target of thalamocortical afferents from thalamus neurons.

Layer V, the internal pyramidal layer, contains large pyramidal neurons. It is the principal source of subcortical efferents. Large pyramidal cells which send axons leaving the cortex and targeting the basal ganglia, the brain stem and the spinal cord can be observed in layer V. Chandelier cells, which are inhibitory cells that make synaptic connections only to the axons protruding from other neurons, are often found in layer V.

Layer VI, the polymorphic layer, contains few large pyramidal neurons and many small spindle-like pyramidal and multiform neurons. Layer VI sends efferent fibres back to the thalamus, establishing the precise reciprocal interconnection between the cortex and the thalamus. Layer VI also contains a class of inhibitory neurons called Martinotti cells, whose axonal outputs make long projections across all layers of the neocortex.

1.3.2 Cell types in the neocortex

Neurons in the neocortex can be categorised as below (Connors & Gutnick, 1990),

1. Pyramidal cells. Pyramidal cells consist of about 60-70% of all neurons in the neocortex. They are the only neurons that send signals out of their local areas to other regions of the brain. Most pyramidal cells belong to the regular spiking neuron group. The signalling-type classification was defined by experimental observations of the neuronal response when a pyramidal cell is injected with a constant excitatory current.

2. Spiny Stellate Cells (SSCs). SSCs make up the other type of excitatory neurons in neocortex. They are found only in layer IV and fromabout 10% of the total population of neurons. SSCs are locally projecting interneurons only. SSCs belong to the regular spiking group as far as their signalling behaviour is concerned.

3. Inhibitory interneurons. The remaining 20-30% of cortical neurons are inhibitory interneurons and can be further classified by electric properties (Connors & Gutnick, 1990). 50% of these neurons are classified as Class-I GABAergic cells. They are found in all cortical layers and belong to the fast-spiking group. About 15% of inhibitory interneurons in the neocortex are Class-II GABAergic cells. These neurons exhibit a low spiking threshold and are known as low threshold spiking cells. Class-II cells are observed in layers II-VI of the neocortex. Class-III inhibitory interneurons make up another 15% of all inhibitory interneurons in the neocortex. They express VIP (vasoactive intestinal peptide) and display an irregular spiking pattern. There are also other inhibitory interneurons that cannot be classified; these account for 20% of all inhibitory interneurons in the neocortex.

1.3.3 Classification of cortical inhibitory interneurons by expression of calcium-binding proteins

Cortical inhibitory interneurons can be also classified into distinct classes on the basis of calcium-binding protein (CBP) expression. Parvalbumin (PV), calbindin (CB) and calretinin (CR) belong to the large family of CBPs, which are characterised by the presence of a variable number of helix-loop-helix motives binding calcium ions. The major function of these three CBPs is buffering of intracellular calcium. CB and CR are bound to cellular structures, while PV is freely mobile in axons, neuronal soma and nuclei. Data from different brain regions suggest that these proteins are involved in regulating calcium pools for synaptic plasticity functions (Schwaller *et al.*, 2002; Schmidt *et al.*, 2007; Mojumder *et al.*, 2008).

Previous analyses have demonstrated that neurochemical markers such as CBPs represent relevant tools to define the chemo-architecture of the neocortex and that they are observed in distinct neuronal subpopulations. Inhibitory neurons that express CBPs PV, CB and CR form three largely non-overlapping

subpopulations. In the rat neocortex layer V, it has been demonstrated that 50% of all inhibitory cells express PV, 15% express CR and 30% express CB (Wonders & Anderson, 2006). The density of CB+ and CR+ neurons is greater in layers II–III, while PV+ interneurons were most often found in the middle cortical layers (Zaitsev *et al.*, 2005). CB and CR expressing interneurons share many morphological similarities and are mainly bipolar, bi-tufted and double bouquet neurons. PV+ neurons are common in layers II–V and classified as basket cells and chandelier cells (DeFelipe, 1997; DeFelipe, 1999). In the majority of mammalian representatives, balanced representation of the three CBPs was demonstrated (Hof & Sherwood, 2005).

1.3.4 Hippocampus

The hippocampus is part of the limbic system in mammalian brains and is essential for memory formation as well as spatial navigation functions (Bliss & Collingridge, 1993; Wilson & McNaughton, 1993; Malenka & Bear, 2004; McNaughton *et al.*, 2006). The clear laminated structures and highly organised excitatory and inhibitory input-output networks have made the hippocampus one of the most widely investigated regions in the brain. Therefore, the hippocampus is an excellent platform for experimental projects ranging from synaptic physiology, neural plasticity, spatial learning and memory to clinical conditions such as epilepsy, schizophrenia, Alzheimer's disease, and autism (Bliss & Lomo, 1973; Best & White, 1999; Burke & Barnes, 2006; Boyer *et al.*, 2007).

1.3.4.1 Structures of the hippocampus

The hippocampus is shaped a sea-horse seated in the medial temporal lobe of the mammal's brain, and consists of three main subdivisions: CA1, CA3 (CA: cornus ammonis) and the dentate gyrus (DG) (figure 1.2). In addition to these subdivisions, the hippocampus has three distinct cell layers. A single layer of pyramidal cells, the stratum pyramidale, has afferent fibres running transversely above (stratum oriens) and below (stratum radiatum and stratum lacunosum-moleculare) them. The dentate gyrus also consists of three layers; a polymorphic layer (the hilus), a granular layer (stratum granulosum) and a molecular layer (stratum moleculare).

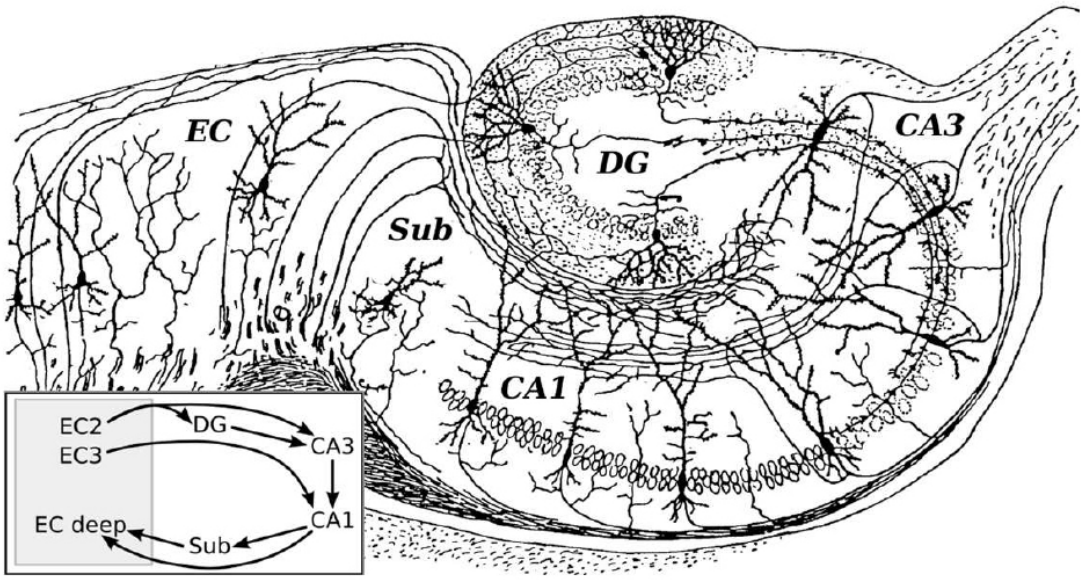

Figure 1.3 Illustration of the hippocampus showing the excitatory trisynaptic pathway. Adapted and modified from classical illustration of hippocampal formation showing the excitatory trisynaptic pathway as drawn by Santiago Ramon y Cajal (Ramón y Cajal, 1952, 1955). Insert shows the schematic representation of main excitatory pathways and the direction of information flow. Source: http://en.wikipedia.org/wiki/Hippocampus

1.3.4.2 Cell types in the hippocampus

The main neurons in the CA3 and CA1 regions of hippocampus are pyramidal neurons. There are approximately 210000 pyramidal cells in the rat hippocampal CA3 region, while in the CA1 nearly 320000 are observed (Boss *et al.*, 1987). Pyramidal cells are mainly seated in the stratum pyramidale, sending out apical dendrites through the stratum radiatum to the stratum lacunosum-moleculare and basal dendrites through the stratum oriens. As for the dentate gyrus, the principal cells are granule cells, and there are an estimated 700000 of these in rat hippocampi (Boss *et al.*, 1985; Boss *et al.*, 1987). Interneurons, however, are inhibitory neurons that appear widely distributed throughout the hippocampus and can be found in the stratum oriens, pyramidale and radiatum. Several subtypes of these neurons exist in the hippocampus, including basket cells, axo-axonic cells, bistratified cells, etc. All the inhibitory interneurons comprise around 10% of the total neuronal population, and are responsible for general inhibition and modulation of network activities (Freund & Buzsaki, 1996; Jonas *et al.*, 2004; Ascoli *et al.*, 2008; Klausberger & Somogyi, 2008).

1.3.4.3 Neuronal circuits in the hippocampus

The excitatory circuits in the hippocampus are characterised as conveying unidirectional flow of information through a well-characterised “trisynaptic” pathway (Bliss & Gardner-Medwin, 1973; Malenka & Nicoll, 1999) (see figure 1.2). Pyramidal cells in the entorihnal cortex (EC) layer II send axon projections into the DG (the perforant pathway). The perforant path serves as the major input of the hippocampus. Subsequently, the mossy fibre (MF) delivers information flows from the DG granule cells into the CA3 area of the hippocampus. The pyramidal cells in the CA3 then innervate the CA1 area of the hippocampus through long axon projections called Schaffer collaterals (SC) to allow signals to be transmitted from the CA3 into the CA1. Finally, the CA1 pyramidal cells project axons into subiculum, which directs projections back to the EC. As a relay, the information flows start from the superficial layers and finish in the deep layers of the entorhinal cortex (EC), and this is simply presented as the EC-DG-CA3-CA1-EC pathway.

1.4 Synapse

In previous section 1.3.5.3, the excitatory circuits in the hippocampus are well-illustrated. The neuronal circuits, at the cellular level, consist of connections between neurons. Neurons make contact with each other, and play essential roles in coordinating neural activities within neuronal circuits. A contact between neurons is termed as a ‘synapse’, which originates from ‘synaptein’, combining the Greek "syn-" ("together") and "haptein" ("to clasp"); this term was first applied by British neurophysiologist Charles Sherrington. The interactions among neurons at the synapse are conducted by transmitting electrical signals from one neuron to the other. Two main forms of synaptic transmission, electrical and chemical, are responsible for the connection within the synapse.

1.4.1 Chemical synaptic transmission

Chemical synaptic transmission is known as the classical synaptic transmission. It has four phases:

1) The action potential initiated from the presynaptic neuron activates voltage-dependent calcium channels located at the presynaptic terminal to allow the calcium influx.

2) The elevation of calcium concentration triggers neurotransmitters to be released from the pre-synaptic terminal.

3) Neurotransmitters cross the synaptic cleft, and then bind to neurotransmitter receptors on the postsynaptic neuron.

4) After the neurotransmitters have acted on neurotransmitter receptors on the postsynaptic neuron, the neurotransmitter receptors generate a change of local resting membrane potential.

It is also termed an electrical-chemical-electrical transmission, since the action potential is transferred into the "chemical" form when delivering from the presynaptic to the postsynaptic neuron, and is transferred back again to the "electrical" form at the postsynaptic terminal to be sent through the postsynaptic neuron.

The critical phase of chemical synaptic transmission is the release of neurotransmitters. The release of neurotransmitters is characterised by a mechanism involving the exocytosis and the recycling of synaptic vesicles and can be divided into four steps as below,

1) Docking. Vesicles containing neurotransmitters are tethered to the active zone of the pre-synaptic terminal.

2) Priming. In this step, all the protein and lipid modification and rearrangement in the active zone has been done to make synaptic vesicles "readily releasable" and competent to fusion (Lloyd & Bellen, 2001).

3) Fusion. The activation of calcium channel is triggered by the calcium influx, and then synaptic vesicles fuse with the pre-synaptic membrane, leading to the release of neurotransmitters into synaptic cleft. These three steps combine to from the process of "exocytosis".

4) Recycling. Vesicles have been are recycled back to the pre-synaptic terminal, reloaded with neurotransmitters, and transported to the releasable pool.

1.4.2 Electrical synaptic transmission

Unlike the electrical-chemical-electrical transduction in classical chemical synapses, the information flow between neurons can be passed through direct electrical coupling established by the electrical synapses in the brain (Eccles, 1982; Jessell & Kandel, 1993). Electrical synapse, which is known as the gap junction, allows charged ions and transmitters to flow through the gap-junction channel connexons between adjacent neurons (Bennett, 1997; Bennett & Zukin, 2004). Compared to the chemical synapse, most transmissions at electrical synapses are bidirectional. Electrical synapse and chemical synapse can coexist at one single synaptic formation (Shapovalov, 1980). Functionally, electrical synapses are particularly essential in local inhibitory circuits consisting of GABA-releasing interneurons to generate gamma oscillation (Galarreta & Hestrin, 2001).

1.4.3 Postsynaptic potential

The neurotransmitter is released from the presynaptic terminal, diffused through the synaptic cleft, and bound with specific receptors on the postsynaptic membrane. The binding of the neurotransmitter to specific receptors induces conformation change of the receptor proteins, and subsequently leads the opening of ion channels to alter the permeability of certain ions.

The permeability alteration generates the ion influx/efflux and further results in the membrane potential change, namely the postsynaptic potential. Postsynaptic potentials can be excitatory or inhibitory. The excitatory postsynaptic potential (EPSP) represents the postsynaptic response depolarising the membrane potential, while the inhibitory postsynaptic potential indicates a hyperpolarising response. Therefore, neurotransmitters are classified into two main groups: those that lead to EPSPs are termed as excitatory neurotransmitters, and those that lead to IPSPs are termed as inhibitory neurotransmitters. In the brain, the most common excitatory neurotransmitter is glutamate, and the most important inhibitory neurotransmitter is γ-aminobutyric

acid (GABA). An EPSP is mainly mediated by the sodium and/or calcium influx through ligand-gated cation channels, such as α-amino-3-hydroxy-5-methyl-4-isoxazolepropionic acid (AMPA) receptors, N-methyl-D-aspartic acid (NMDA) receptors and kainate receptors. The fast form IPSP is primarily from the chloride influx through the opening of $GABA_A$ receptors. The opening of potassium channels by $GABA_B$ receptors, however, contributes to the slow form IPSP.

1.4.4 Integration of synaptic inputs

EPSPs and IPSPs are local electronic potentials, without a discrete nature, which can be summated. This process is named synaptic integration (London & Hausser, 2005). A single EPSP or IPSP generally is about 1mV. To fire a neuronal action potential that can be transmitted throughout neurons, post-synaptic depolarisation must be strong enough to overcome the threshold, which is around 10mV. Therefore, spatial and temporal summation of EPSPs or IPSPs determine the magnitude and the time course of gross synaptic inputs, and in turn generate the output as an action potential firing. Two types of summations are observed, temporal and spatial summation (Bartos *et al.*, 2007). In temporal summation, continual postsynaptic potentials come closely after each other before the last potential decays; thus, the amplitude of the potential will be added into the previous one. However, the spatial summation means that the postsynaptic potentials originate from multiple synapses and arrive simultaneously at a given neuron. Thus, in spatial summation, the membrane potential of postsynaptic neuron equals the sum of EPSPs and IPSPs. Both temporal summation and spatial summation coexist and function simultaneously to steer a particular neuron to fire APs or not in response to EPSPs and IPSPs in a neuronal circuit.

1.5 Synaptic plasticity

The efficacy of synaptic transmission between neurons can be strengthened or weakened both *in vitro* and *in vivo*; this is called synaptic plasticity (Bliss & Collingridge, 1993; Bortolotto *et al.*, 1999; Kemp & Bashir, 2001; Zucker & Regehr, 2002; Whitlock *et al.*, 2006). Three types of synaptic plasticity are observed: short-term plasticity, long-term plasticity and long-term depression. Synaptic plasticity is regarded as the molecular and cellular basis for learning and memory, as information may be stored and retrieved by transforming differential spatiotemporal patterns of neural activity into synaptic changes in different locations, circuits and neurons in the brain (Bliss & Collingridge, 1993; Martin *et al.*, 2000; Holtmaat & Svoboda, 2009; Wang & Morris, 2010). The term "synaptic plasticity" was first introduced by Dr. Jerzy Konorski in the late 1940s (Konorski, 1948). The concept was subsequently refined by Dr. Donald Hebb in 1949 with a proposed mechanism known widely as Hebb's postulate (Hebb, 1949):

'When an axon of cell A is near enough to excite a cell B and repeatedly or persistently takes part in firing it, some growth process or metabolic change takes place in one or both cells such that A's efficiency, as one of the cell firing B, is increased'.

In the following sections, the three types of synaptic plasticity are illustrated.

1.5.1 Short-term plasticity

Short-term plasticity means a short-term increase or decrease of synaptic strength that lasts at most a few minutes. Depending on the patterns of synaptic strength change, it could be divided into two groups, short-term facilitation (STF) or short-term depression (STD).

In experiments, short-term facilitation (STF) has been observed upon application of a closely paired stimuli paradigm (paired pulse), with an interval of between 10ms and 300ms. The synaptic response of the second pulse can be several times stronger than the first one and it has a presynaptic mechanism (Zucker & Regehr, 2002). It originates from an increase in the release of readily releasable vesicles and the transient accumulation of presynaptic calcium, as calcium influx

triggered by the second action potential is added into the residual calcium which has not been depleted after the first pulse (Wu & Saggau, 1994).

Short-term depression (STD) also occurs in the paired pulse paradigm, and the most widely accepted mechanism for STD is the 'depletion model' (Zucker & Regehr, 2002). That means the STD is the result of a decrease in available vesicles in readily releasable pools in presynaptic terminals in response to closely paired stimuli.

1.5.2 Long-term potentiation

Long-term potentiation (LTP), a long-lasting form of synaptic strength increase, was first described in the perforant path from the entorhinal cortex into the dentate gyrus in an anaesthetised rabbit (Bliss & Gardner-Medwin, 1973; Bliss & Lomo, 1973). Subsequently, it is observed in all excitatory pathways into principal cells in the hippocampus, the neocortex, the striatum, and the cerebellum (Wilson & Racine, 1983; Calabresi *et al.*, 1992; Shibuki & Okada, 1992). LTP has also been discovered in excitatory synapses onto inhibitory interneurons in the hippocampus (Mahanty & Sah, 1998; Perez *et al.*, 2001; Kullmann & Lamsa, 2007; Lamsa *et al.*, 2007).

LTP has three distinct properties: input-specificity, associativity, and cooperativity (Bliss & Collingridge, 1993). Input-specificity means that LTP does not spread and is only found within the pathway that has been activated to express LTP. Associativity indicates that a weak input may induce LTP as long as a separate strong input simultaneously stimulates the same target neuron. Cooperativity describes the existence of a threshold of input intensity for inducing LTP. LTP can be either induced by strong tetanus stimulation in a single pathway or by the summation of several small stimuli.

In addition, LTP can be divided into NMDA receptor-dependent or NMDA receptor-independent groups, depending on whether or not the NMDA receptor antagonist can block its induction. In the hippocampus, the LTP in the Schaffer collateral-to-CA1 pyramidal cell synapses is the most studied type of the NMDA receptor-dependent group (Bliss & Collingridge, 1993). However, the LTP in the mossy fibre synapses onto CA3 pyramidal cells is representative of the NMDA

receptor-independent group (Harris & Cotman, 1986; Nicoll & Schmitz, 2005). Schaffer collateral LTP can be induced either by tetanus stimulation or theta burst stimulation, and this induction follows Hebb's postulate (Collingridge *et al.*, 1988; Kauer *et al.*, 1988; Huang *et al.*, 1992). The voltage dependent magnesium blockade of NMDA receptors in postsynaptic membrane sets the LTP threshold for cooperativity, and associativity is reflected by the requirement of removing the magnesium blockade of NMDA receptors by depolarising postsynaptic terminals by a voltage step or convergent excitatory inputs. The permeability to calcium is the key to Schaffer collateral LTP induction (Lynch *et al.*, 1983). The time course of LTP can be divided into four phases: post-tetanus potentiation (PTP), short-term potentiation (STP), early-LTP, and late-LTP (Bliss & Collingridge, 1993; Malenka & Nicoll, 1999). Post-tetanus potentiation (PTP, immediately following the tetanus stimulation) is the response of enhanced neurotransmitter release corresponding to residual calcium accumulation presynaptically during the tetanus stimulation, and is NMDA receptor-independent. Short-term potentiation (STP), which usually lasts 30-60 minutes after the tetanus stimulation, can be also acquired by a weak stimulation protocol. Early-LTP describes a synaptic strength increase that lasts under 3 hours, and has been verified as protein kinase-dependent (Malinow *et al.*, 1988; Malenka *et al.*, 1989). Late-LTP, which normally lasts beyond 3 hours, however, has been shown to be protein synthesis-dependent (Frey *et al.*, 1988).

1.5.3 Long-term depression

The opposing process to LTP, long term depression (LTD) is the long-lasting decrease of synaptic strength. This phenomenon was first reported in a hippocampal CA1 LTP study, a LTP induction unexpectedly resulted in a continuing depressed synaptic efficacy, a phenomenon later described as the "heterosynaptic LTD" by Lynch and co-workers in 1977 (Lynch *et al.*, 1977). In 1980, another report described that low frequency stimulation effectively reversed hippocampal LTP (Barrionuevo *et al.*, 1980). Both phenomena were neglected until the early 1990s, when a new form of "homosynaptic LTD" was discovered by Mark Bear's group, and this was supported by Robert Malenka's group in 1992, who showed that low frequency stimulation (LFS) of 900 stimuli at 1 Hz produced a prolonged reduction of synaptic transmission in the hippocampal CA1 region (Dudek & Bear, 1992; Mulkey & Malenka, 1992).

Homosynaptic LTD is development-dependent. One study showed that the standard low frequency stimulation protocol, 900 stimuli at 1 Hz, routinely produced LTD in hippocampal CA1 regions from 2-week-old animals, whereas LTD magnitude decreased by half in 5-week-old animals (Dudek & Bear, 1993).

LTDs are classified as NMDA receptor-dependent or mGlu receptor-dependent. The LTD induced by LFS (900 stimuli, 1Hz) in the CA1 region of hippocampus has been confirmed as NMDA receptor-dependent (Dudek & Bear, 1992; Mulkey & Malenka, 1992). NMDA receptor-dependent LTD was also found in the visual cortex (Kirkwood & Bear, 1994), the perirhinal cortex (Ziakopoulos *et al.*, 1999), and the barrel cortex (Feldman *et al.*, 1998). It has been confirmed that the induction of NMDA receptor-dependent LTD requires a rise of postsynaptic calcium concentration (Mulkey & Malenka, 1992).

The LFS-induced LTD in the hippocampal CA1 region is NMDA receptor-dependent and was proved by one report, which discovered that overexpression of embryonic dominant NR2D subunit resulted in a loss of LTD in juvenile mice (Okabe *et al.*, 1998). Also, functional knockout of the NR2B subunit in NMDA receptor prevented LFS-induced LTD, thus further supporting this hypothesis (Kutsuwada *et al.*, 1996).

The involvement of mGlu receptors in LTD was first evidenced by the discovery that the group I/II mGluR antagonist, MCPG, blocked the induction of depotentiation by the LFS protocol (900 stimuli, 1 Hz) in the CA1 region of the hippocampus (Bashir *et al.*, 1993; Bashir & Collingridge, 1994). LTD induced by low-frequency stimulation of paired-pulse at 1Hz (PP-LFS) in adult (Kemp & Bashir, 1999) and juvenile animals (Huber *et al.*, 2000) were shown to require mGluRs. Interestingly, NMDA receptor-dependent LTD induced by LFS is also present in the same synapses in the hippocampal CA1, but it has been suggested that these two forms of LTD utilise distinct induction pathways: mGluR-dependent LTD requires the calcium influx from T-type calcium channel, and protein kinase C, whereas, NMDA receptor-dependent LTD requires calcium influx through NMDA receptors (Oliet *et al.*, 1997). It has been further suggested that the requirement of NMDA receptors and mGlu receptors in induction of LTD may be mutually exclusive, as where there is a role for NMDA receptors, there is no role for mGluRs and *vice versa* (Bortolotto *et al.*, 1999; Kemp & Bashir, 2001).

1.5.4 Glutamate receptors and synaptic plasticity

In the cortex of mammalian brain, excitatory synaptic transmission is mediated primarily by glutamate-gated ion channels embedded in the postsynaptic cell membrane. Glutamate receptors contribute to the fast excitatory postsynaptic response by allowing positively charged ions to flow into the postsynaptic compartment upon binding glutamate. Different classes of receptors are named for their most potent agonists, such as AMPA (α-amino-3-hydroxy-5-methyl-4-isoxazole proprionate) receptors and NMDA (*N*-methyl-D-aspartate) receptors. In the mature brain, AMPA receptors primarily conduct sodium ions and mediate the initial and largest component of field excitatory postsynaptic potential (fEPSP), while NMDA receptors have the unique property of allowing calcium ions to flow into the postsynaptic cell in addition to sodium ions. The contribution of NMDA receptors to basal synaptic transmission is highly variable because, under resting physiological conditions, their ion pores are blocked by magnesium ions which prevent current flow. However, during periods of heightened stimulation, the amount of positive charge flowing in through AMPA receptors depolarises the postsynaptic spine sufficiently to remove the magnesium ion block and allow calcium ions to enter the postsynaptic terminal through the NMDA receptor (see figure 1.4A) (Mayer *et al.*, 1984; Nowak *et al.*, 1984). The NMDA receptor thus satisfies the requirement of Hebb's coincidence detector, with its activation requiring concurrent presynaptic glutamate release and postsynaptic depolarisation. The amount of calcium ions passing through the NMDA receptor varies depending on the magnitude of pre- and postsynaptic co-activation and ultimately determines whether synaptic connections will be strengthened or weakened (Lisman, 1985; Madison *et al.*, 1991; Malenka & Nicoll, 1999). The most commonly studied forms of LTP and LTD are NMDA receptor-dependent synaptic plasticities.

The induction of LTP requires large influxes of calcium ions in the postsynaptic terminal that trigger the activation of protein kinases, enzymes, and whose enzymatic activity can long outlast the changes in calcium ion concentration that triggered them (figure 1.4A and 1.4B). The phosphorylation of synaptic and structural substrates plays a critical role in the induction and expression of LTP (Soderling & Derkach, 2000). In addition to the phosphorylation of AMPA receptors at synapses, new AMPA receptors are also recruited to the

postsynaptic membrane (Malinow *et al.*, 2000), leading to larger amplitude fEPSPs with faster onsets, while on the presynaptic side more glutamate is released into the synaptic cleft (Bliss *et al.*, 1990a; Bliss *et al.*, 1990b; Dolphin *et al.*, 1982). Structural changes, such as the growth of new spines and the enlargement or splitting of synapses in two, have also been observed following LTP induction (Yuste & Bonhoeffer, 2001). In LTD, small increases in calcium ions arising from weak synaptic stimulation favour the activation of protein phosphatases that dephosphorylate synaptic proteins including glutamate receptors (figure 1.4B) (Mulkey *et al.*, 1994; Mulkey *et al.*, 1993). Contrary to LTP, LTD results in the removal and eventual degradation of AMPA receptors, NMDA receptors, and structural synaptic proteins (Ehlers, 2000; Heynen *et al.*, 2000; Colledge *et al.*, 2003).

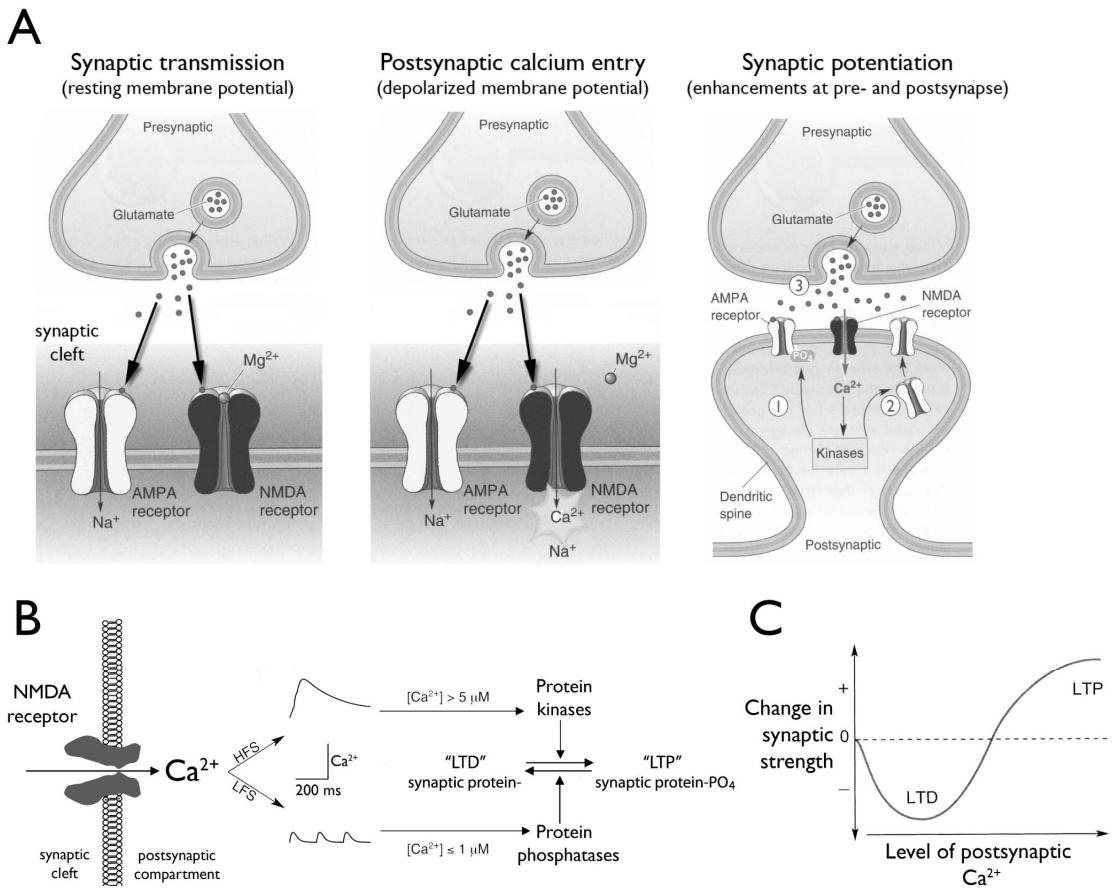

Figure 1.4 Glutamate receptors and synaptic plasticity.

(A) The NMDA receptor is mediated and activated by coincident pre- and postsynaptic activities. (B) A large increase in postsynaptic calcium, induced by HFS, favours the activation of protein kinases and results in LTP, while small, sustained Ca^{2+} elevations during LFS favour the activation of protein phosphatases, resulting in LTD. (C) Long-term

changes in synaptic strength can be explained as a function of the amount of calcium ions flowing into the postsynaptic neuron via NMDA receptors. (Adopted and modified from M. Bear, B. Connors, & M. Paradiso, *Neuroscience: Exploring the brain*, 3rd edition, © 2007, Lippincott Williams & Wilkins.)

Assessing synaptic plasticity deficits in disease animal models of neurodevelopmental disorders will be beneficial for understandings of the synaptic functional alterations in these disorders. Several synaptic plasticity studies in RTT animal models have been introduced in section 1.2.5 and were reviewed again in the introduction of Chapter 5.

1.6 Aims

There are still numerous limitations in the RTT research. Firstly, the genotype-phenotype correlations differ from species to species, and the manner in which MeCP2 modulates the neuronal functions is still obscure. Secondly, at cellular level, MeCP2 dysfunctions induced an overall higher cell packing rate, smaller soma size and deficits in axon targeting and dendrite branching (see previous sections). However, few detailed studies have compared the cellular densities or the change in distribution patterns in distinct cell types. Since a recent study has already demonstrated that selective knock-out of MeCP2 in GABAergic neurons recapitulated nearly all RTT-like phenotypes in mouse (Chao *et al.*, 2010), it is of interest to assess the alteration of cellular density and localisations in various neuronal subtypes. Thirdly, RTT can be classified as synaptopathy, and most symptoms are closely linked to synaptic dysfunction. Nevertheless, a recent electrophysiological report showed several discrepancies in the "phenotype-synaptic functions" relationship (Dani & Nelson, 2009), and it is necessary to elucidate the precise mechanism underlying RTT synaptopathy by more sensitive experimental designs. Finally, the ultimate MeCP2 research aim is primarily focused on the clinical treatment of RTT. Numerous animal drug studies and clinical trials are already underway to further assist RTT patients.

The understanding of MeCP2 molecular functions is the key to future RTT therapy development, and in this thesis, I have aimed to address three sets of principal questions relating to the effects of MeCP2 deficiency in the central nervous system,

1. How do the gross signs of the *Mecp2-stop* phenotype develop postnatally? Do distinct symptoms progress in different ways from each other?

2. How does the absence of functional MeCP2 affect neuronal density? Does the absence differentially affect different subtypes of neurons?

3. How is synaptic plasticity affected in the *Mecp2-stop* brain? Is there a relationship between synaptic plasticity deficits and the progression of neurological signs? Can these synaptic plasticity deficits be amended or reversed by pharmacological modulations?

2 Material and Methods

2.1 The timeline of experiments

All the studies in the current thesis used *Mecp2*^{tm2bird} mouse, in which the first generation was originally obtained from Prof. Adrian Bird's laboratory at the University of Edinburgh as a gift. The original mouse at the University of Edinburgh was purchased from Jackson Laboratories (Maine, USA; stock number 006849). In the following sections and chapters, *Mecp2*^{tm2bird} mice are referred to as *Mecp2-stop* mice. The *Mecp2-stop* mice were introduced from the University of Edinburgh, and the mouse colony was bred and maintained in the animal unit at the University of Glasgow. Figure 2.1 illustrates the timeline of all the experiments in this thesis. All the offspring from the *Mecp2-stop* mice colony were weaned at the age of 3 weeks and the genotyping was done at the same time (see results in Chapter 3). In order to maintain the *Mecp2-stop* mice colony, heterozygous females (*Mecp2*$^{stop/+}$) were preserved for further mating with wild type (WT) Balb/c mice introduced from Harlan Laboratories (Shardlow, UK). WT females from the *Mecp2-stop* colony were humanely culled, while both WT and hemizygous (*Mecp2*$^{stop/y}$) males were selected for future experimental use. The phenotyping was performed weekly for every hemizygous *Mecp2-stop* mouse from the time of weaning to death, as labelled in the yellow block in figure 2.1 (see results in Chapter 3).

For the immunohistochemistry studies (see results in Chapter 4), both "symptomatic" *Mecp2*$^{stop/y}$ mice and their WT littermates were used. The definition of "symptomatic" mice refers to the fact that the sum symptom score reached 5 or above in the phenotyping test (see section 2.5 for detailed description). Generally, *Mecp2*$^{stop/y}$ mice reached symptom scores of 5 at around 10 to 15 weeks, as illustrated by the selection phase (the red block) in figure 2.1.

With regard to the electrophysiology studies (see results in Chapter 5), synaptic plasticity (long-term potentiation) was assessed using the symptomatic *Mecp2*$^{stop/y}$ mice and their WT littermates (as in the immunohistochemistry studies). However, synaptic plasticity saturation was evaluated in mild symptomatic (score 2-4) *Mecp2*$^{stop/y}$ mice, symptomatic (score 5 or above) *Mecp2*$^{stop/y}$ mice and their age-matched WT littermates. Finally, the *in vivo*

chronic pharmacological treatment (Memantine treatment, see also section 2.8 for detailed information) on both *Mecp2*$^{stop/y}$ mice and WT littermates was applied from week 5 to week 8 (the blue block in figure 2.1). In later sections, all the detailed materials and methods are listed.

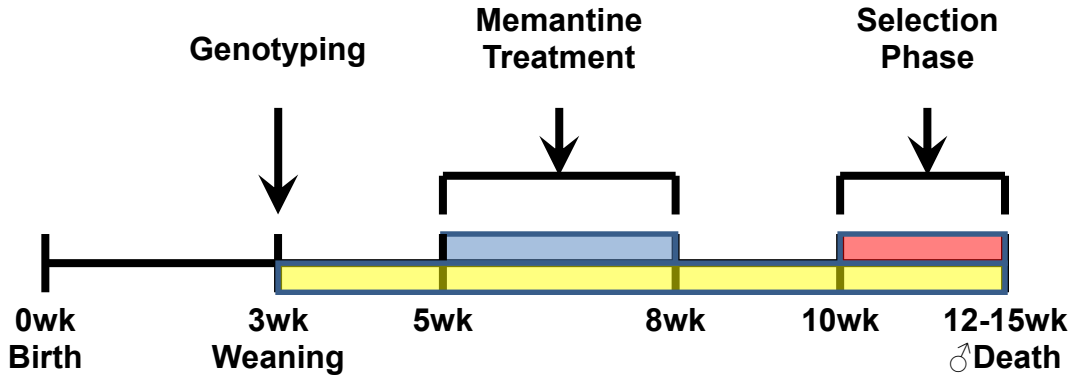

Figure 2.1 Illustration of the timeline of experiments.

After litters were weaned, ear samples were collected for genotyping (data shown in Chapter 3). *Mecp2*$^{stop/y}$ and their littermates were paired for future experimental use, and *Mecp2*$^{stop/+}$ were selected for breeding. The yellow block represents the phenotype study (data shown in Chapter 3), which started immediately after genotyping as a weekly scoring assessment, and ended before mice were culled or death. For the immunohistochemistry study (data shown in Chapter 4), symptomatic mice were used after the symptom score reached five or more (represented as the selection phase in the red block), and their WT littermates were also used for comparison. For the synaptic plasticity study in acute brain slices (data shown in Chapter 5), symptomatic mice and their WT littermates were selected using the same criteria as above in the immunohistochemistry study, while in the *in vivo* chronic memantine treatment study (data shown in Chapter 5), *Mecp2*$^{stop/y}$ and their littermates were treated with memantine from 5 to 8wks (represented by the blue block).

2.2 General materials

All the chemicals below without specified origins were supplied from Merck Ltd. (BDH laboratories, UK) or Sigma-Aldrich Company Ltd. (Sigma, UK).

2.2.1 Solutions

0.1M PB: Solution A: $NaH_2PO(2H_2O)$ 37.44 g in 1200 ml H_2O; Solution B: Na_2HPO_4 84.90 g in 3000 ml H_2O; Add 1120 ml of solution A to 2880 ml of solution B and mix well. Adjust pH to 7.4 with either HCl or NaOH. Add 3000 ml distilled water to the final solution.

0.3M PBS: 0.2 M phosphate buffer 100 ml, Distilled water 1900 ml & NaCl 36 g.
1kb+ ladder: 60ng/µl 1kb ladder (Invitrogen, UK), 1x DNA loading dye in 1x TBE.

1x Artificial cerebrospinal fluid (ACSF): NaCl 124mM (VWR International, UK), KCl 3mM (VWR International, UK), $NaHCO_3$ 26mM (Fischer Scientific, UK), $NaH_2PO_4 \cdot 2H_2O$ 1.25mM (Sigma, UK), $MgSO_4 \cdot 7H_2O$ 1mM (VWR International, UK), $CaCl_2$ 2mM (BDH, UK), and D(+)-Glucose $C_6H_{12}O_8$ 10mM (VWR International, UK) dissolved in 1 litre distilled water.

1x TBE: 90mM Trizma base, 90mM orthoboric acid, 2mM EDTA.

5x DNA loading dye: 0.5% (w/v) SDS, 0.25% (w/v) xylene cyanol, 0.25% (w/v) bromophenol blue, 1.5% (w/v) Ficoll®400, in 3x TBE.

Ethidium Bromide: Stock solution: 10mg/ml in H_2O.

TE buffer: 10mM Tris-HCl pH 8.0, 1mM EDTA pH 8.0.

2.2.2 Enzymes

Enzymes and suppliers are listed in Table 2.1

Table 2.1 Enzymes

Enzymes	Supplier	Remarks
Dnareleasy™	Anachem, UK	Enzyme for cell digestion (DNA extraction)
Thermostart high performance PCR mixture	Fisher Scientific, UK	PCR reaction mixtures (ready-mixed for PCR)

2.2.3 Oligonucleotide primers

All oligonucleotide primers were obtained from Sigma Genosys Ltd (Haverhill, UK). The primer sequence and the targeted alleles for each oligonucleotide are listed in Table 2.2

Table 2.2 Oligonucleotide primers

Primer name	Nucleotide Sequence 5'-3'	For detection	Product size
P5	TGGTAAAGACCCATGTGACCCAAG	WT *Mecp2* allele	416bp
P7	GGCTTGCCACATGACAAGAC	WT *Mecp2* allele	416bp
NeoF	GTCATCTCACCTTGCTCCTGCC	*STOP Mecp2* allele	470bp
NeoR	GAAGGCGATAGAAGGCGATGCG	*STOP Mecp2* allele	470bp

2.2.4 Antibodies

Primary antibodies used are listed in Table 2.3

Table 2.3 Primary antibodies

Antibodies	Species raised	Working dilution	Supplier	References
Somatostatin	Rabbit	1:2000	Millipore, UK	Elde *et al.,* 1978
Parvalbumin	Mouse	1:5000	Swant, UK	Celio & Heizmann *et al.,* 1981
Calbindin	Mouse	1:5000	Swant, UK	Garcia-Segura *et al.,* 1984
Calretinin	Mouse	1:5000	Swant, UK	Rogers, 1987
MeCP2	Rabbit	1:500	Millipore, UK	Guy *et al.,* 2001
NeuN	Mouse	1:500	Millipore, UK	Mullen *et al.,* 1992

Secondary antibodies used are listed in Table 2.4

Table 2.4 Secondary antibodies

Antibodies	Species against	Working dilution	Supplier
Alexa-488	Mouse	1:500	Jackson Laboratories, USA
Alexa-488	Rabbit	1:500	Jackson Laboratories, USA
Alexa-546	Mouse	1:500	Jackson Laboratories, USA
Alexa-546	Rabbit	1:500	Jackson Laboratories, USA

2.3 *Mecp2-stop* animal model

2.3.1 Design of the Mecp2-stop model

Originally, the *Mecp2-stop* mouse was designed by Prof Adrian Bird's team at the University of Edinburgh, Edinburgh, UK. The endogenous *Mecp2* allele was silenced by a targeted *NEO-STOP* cassette (Guy *et al.*, 2007) as illustrated in figure 2.2. The *NEO-STOP* cassette was inserted inside intron 2 to generate truncated mRNA (or incomplete mRNA) during transcription. The truncated or incomplete mRNA was not then translated; therefore null production of MeCP2 was observed in the *Mecp2-stop* model. The breeding strategy of the *Mecp2-stop* colony is described in later sections.

Figure 2.2 Design of the *Mecp2-stop* model.

In the *Mecp2* allele, a *NEO-STOP* cassette was inserted inside intron 2. Incomplete or truncated *Mecp2* mRNA was not then translated, and generated a functional knock-out phenotype by null production of the MeCP2.

2.3.2 Breeding strategy and animal husbandry of the Mecp2-stop colony

A local *Mecp2-stop* colony at University of Glasgow was established by breeding heterozygous *Mecp2*$^{stop/+}$ females (C57BL/6 background, fully congenic) with WT males (Balb/c background) purchased from Harlan laboratories (Shardlow, UK). The reason for back-cross with Balb/c background was because *Mecp2*$^{stop/+}$ females of C57BL/6 background normally neglected to feed offspring and had a smaller litter size. After back-cross with WT males of Balb/c background, this concern was largely improved. All mice used in the current experiments were hemizygous *Mecp2*$^{stop/y}$ males and WT male littermates resulting from a breeding

scheme involving at least 6 generations of back-cross from a congenic C57BL/6 background onto a BALB/c background. Figure 2.3 shows all the possible genotypes of the *Mecp2-stop* offspring. Four distinct combinations of genotypes and genders were observed, heterozygous *Mecp2*$^{stop/+}$ females, hemizygous *Mecp2*$^{stop/y}$ males, WT females and WT males. The offspring genotype was determined by PCR reactions (see results in Chapter 3). Mice were housed in groups of 1-3, maintained on a 12-hour light/dark cycle and provided with food and water ad libitum. Experiments were carried out in accordance with the European Communities Council Directive (86/609/EEC) and a project license with local ethical approval under the UK Scientific Procedures Act (1986).

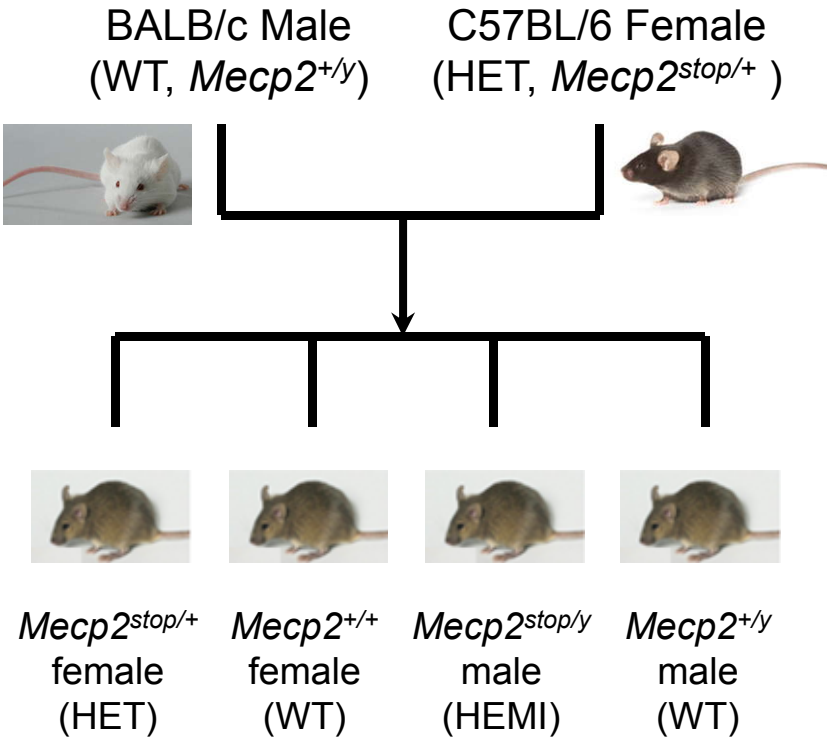

Figure 2.3 Breeding scheme of the *Mecp2-stop* colony.

The *Mecp2-stop* colony was established by breeding heterozygous (HET) *Mecp2*$^{stop/+}$ females (C57BL/6 background) with WT males (Balb/c background). Four distinct combinations of genotypes and genders were observed, heterozygous *Mecp2*$^{stop/+}$ females, hemizygous *Mecp2*$^{stop/y}$ males (HEMI), WT females (*Mecp2*$^{+/+}$) and WT males (*Mecp2*$^{+/y}$). The heterozygous females (*Mecp2*$^{stop/+}$) were preserved for further breeding, WT females (*Mecp2*$^{+/+}$) were culled humanely, while hemizygous males (*Mecp2*$^{stop/y}$) and WT males (*Mecp2*$^{+/y}$) were selected for experimental use.

2.4 Genotyping

2.4.1 PCR protocols for genotyping of the Mecp2-stop mice

Standard PCR reactions were carried out in a volume of 25µl using 1x Thermostart PCR mixture (Epsom, UK) with each primer at a concentration of 1µM. The primer set P5/P7 was designed to detect the WT *Mecp2* allele, and the primer set NeoF/NeoR was designed to detect the *STOP Mecp2* allele (see table 2.3). The template concentration varied between 20-100ng of extracted mouse genomic DNA. The mouse genomic DNA was extracted using the Dnareleasy™ (Anachem, UK) to digest ear/tail samples at 75°C for 5 minutes followed by 96°C for 2 minutes. All PCR amplifications were carried out in a GeneAmp thermal cycler (PCR system 9700; Applied Biosystems, UK). The reaction had an initial heating step at 95°C to activate the polymerase in the Thermostart PCR mixture and a post cycling extension step at 72°C for 10 minutes. Reactions were thermally cycled as follows:

Thermostart *Taq* polymerase activation: 94°C for 15 minutes

35 cycles: 94°C for 45sec

61°C for 1 minute

72°C for 1 minute

Final extension: 72°C for 10 minutes

PCR products were separated according to their size by agarose gel electrophoresis. Solutions of 0.8% (w/v) agarose in 200ml of TBE were prepared in a microwave. When the TBE solution had cooled to approximately 40°C, ethidium bromide was added to a final concentration of 200ng/ml. Gels were cast in a horizontal tray. DNA samples were mixed with 1x DNA loading dye and electrophoresed for periods of time from 45 minutes to one hour at 120V. An aliquot of a DNA size ladder (around 500ng) was also electrophoresed and used as a size marker. Separated DNA samples were visualised using an UV transilluminator (UV-TM-40; Upland, USA; wavelength 254nm) and photographed

by Canon digital camera (PC1192; Japan). PCR products for the P5/P7 primer set are 416bp, and PCR products for the NeoF/NeoR primer set are 470bp.

2.5 Phenotyping

2.5.1 Phenotyping protocols of the Mecp2-stop mice

After weaning, *Mecp2-stop* mice were scored weekly for a number of RTT-like signs as described by Guy *et al*. 2007 (Guy *et al.*, 2007). A comparison of human RTT signs and RTT-like phenotypes in *Mecp2*-null mouse models are listed in table 2.5. In Guy *et al*. 2007's report, they selected six cardinal RTT-like features for assessment of symptoms progress and the assessment was carried out weekly to generate a semi-quantitative measure of phenotype status (Guy *et al.*, 2007). Each of six observable features including mobility, gait, hindlimb clasping, tremor*, breathing* and general condition* were scored on a 0 (no signs), 1 (mild signs) or 2 (severe signs) scale, and scores for each feature were added to yield a composite symptom score between 0 and 12. The detailed information of each scoring category is listed in section 2.5.2. This score was also used to determine when animals should be subjected to humane culling. Any animal scoring 2 for any of the categories indicated* were routinely culled.

Table 2.5 Comparisons of human RTT symptoms and RTT-like phenotypes in *Mecp2*-null mice models

Symptoms	Human	*Mecp2*-null models
Early normal development	√ (infant stage)	√ (before adult stage)
Motor defects	√	√
Ataxia	√	√
Hypoactivity	√	√
Hand stereotypies	√	√
Breathing dysrhythmias	√	√
Reduced social reactions	√	√
Impaired learning	√	√

2.5.2 Detailed information of each scoring category

Scoring descriptions are as below, and all the scorings were performed every Friday morning (9-10AM) under room temperature in the animal procedure room (on the laboratory bench) within the animal unit at the University of Glasgow.

1. Mobility: The mouse was observed on bench and when handled gently.

Score 0 = as wild-type.

Score 1 = reduced movement, extended freezing periods.

Score 2 = no spontaneous movement.

2. Gait:

Score 0 = as wild-type.

Score 1 = hind legs are spread wider than wild-type when walking or running with reduced pelvic elevation, resulting in a “waddling” gait.

Score 2 = more severe abnormalities: tremor when feet are lifted, walks backwards or 'bunny hops' by lifting both rear feet at once.

3. Hindlimb clasping: The mouse was observed when suspended by base of the tail. The hindlimb clasping representative pictures are illustrated in figure 2.4.

Score 0 = legs splayed outwards.

Score 1 = hindlimbs are drawn into the midline (without touching trunk) or one leg is drawn into the trunk.

Score 2 = both legs are pulled into the midline tightly or touching body.

4. Tremor: Mouse observed while standing.

Score 0 = no tremor.

Score 1 = intermittent mild tremor.

Score 2 = continuous or violent tremor.

5. Breathing: Observed while animal is standing still.

Score 0 = normal breathing.

Score 1 = short periods of rapid breathing or pauses in breathing.

Score 2 = very irregular breathing - gasping or panting.

6. General condition: Mouse observed for indicators of general well-being such as coat condition, eyes, body stance.

Score 0 = clean shiny coat, clear eyes, normal stance.

Score 1 = eyes dull, coat dull/ungroomed, somewhat hunched stance.

Score 2 = eyes crusted or narrowed, piloerection, hunched posture.

(A) **(B)**

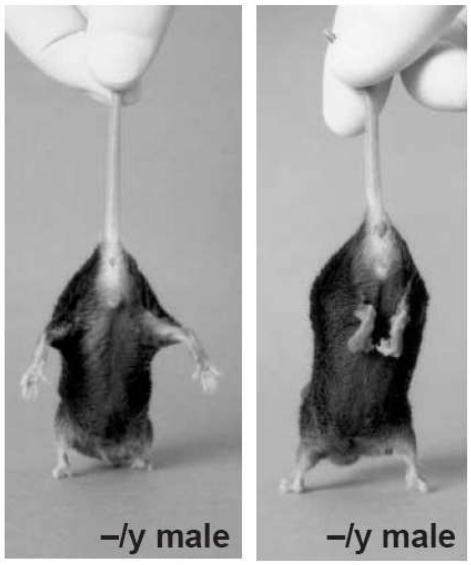

Figure 2.4 Representative pictures of the hindlimb clasping scoring.

For the hindlimb clasping scoring, the mouse was observed when suspended by the tip of the tail. (A) At early stages (normally less than five weeks), the hindlimbs stretched out widely during observations, and the reaction was similar to that of WT littermates (score=0). (B) However, at later stages (normally after ten weeks), the hindlimbs were found to be withdrawn, and constantly in contact with the body (score=2). Adopted and modified from Guy *et al.*, 2001 (Guy *et al.*, 2001).

2.5.3 The selection of symptomatic *Mecp2*$^{stop/y}$ mice

In this thesis, "symptomatic" *Mecp2*$^{stop/y}$ mice were widely used in various experiments. The hemizygous male mice (*Mecp2*$^{stop/y}$ genotype) used in the current study developed overt RTT-like signs during postnatal development that mirrored those reported by Guy *et al*. 2007 (Guy *et al.*, 2007). In order to select appropriate time points for the immunohistochemistry (see Chapter 4) and electrophysiological experiments (see Chapter 5), the onset and the progression of observable phenotypes were monitored by adopting the semi-quantitative scoring system described in section 2.5.1. Once the sum symptom score reached 5 or above, *Mecp2*$^{stop/y}$ mice were considered to be sufficiently "symptomatic" and selected with the age-matched WT littermates for further experimental use (see "selection phase" in figure 2.1).

2.6 Immunohistochemistry methods

2.6.1 Preparation of immunohistochemistry experiments

A range of neurochemical markers that enable discrimination between discrete populations of cortical interneurons, including somatostatin (SOM), parvalbumin (PV), calbindin (CB) and calretinin (CR), were examined in the hippocampus and neocortex (see primary antibodies and secondary antibodies in table 2.3 and table 2.4). NeuN was also examined to evaluate the neuronal density change in the neocortex of hemizygous *Mecp2-stop* mice (Herculano-Houzel & Lent, 2005).

The animals were deeply anaesthetised with sodium pentobarbital at 100 mg/kg body weight (Merial Animal Health Ltd., Harlow, UK). After animals were fully anesthetised, all four limbs were fixed with No.23G needles (BD Microlance, UK) on a wood or a polystyrene plate. The chest was opened immediately with dissecting scissors. Superior and inferior vena cava were clamped by a haemostatic forceps and a No.19G needle (BD Microlance, UK) was inserted into the right atrium of heart. After the No.19G needle was fixed by another haemostatic forceps and connected to a 100ml syringe setting on the syringe pump (BD Microlance, UK), the mouse was perfused transcardially with 5-10ml normal saline, followed by 60ml 4.0% paraformaldehyde in the 0.1M PB at a rate of 5-6 ml/min continuously. When mice were completely fixed (which was recognised by the rigid state of the tail and four limbs), brains were removed using a No.22 scalpel (Swann Morton Ltd., Sheffield, UK) from the skull. Brains were then immersed in 4.0% paraformaldehyde in 0.1M PB at room temperature for three hours and transferred to 0.1M PB overnight at 4^{o}C. On the second day, brains were embedded in 3% agarose (w/v) and cut coronally into 50μm-thick serial sections on a Vibratome (Series 1000; Technical Products International, St. Louis, MO). Serial sections were collected and stored in 0.1 M PB. After rinsing three times in 0.3M PBS, for ten minutes each, the brain sections were incubated with primary antibodies that contained 0.3% Triton X-100 in 0.1M PB for 3 days at 4^{o}C. The sections were again rinsed three times, for ten minutes each, in 0.3M PBS, to wash out excess primary antibodies. Sections were then incubated with secondary antibodies that contained 0.3% Triton X-100 in 0.1M PB for three hours at room temperature. Finally, they were rinsed three times in 0.3M PBS, mounted on glass slides, covered by coverslips in an anti-fade medium

containing DAPI (Vectashield; Vector Laboratories, Burlingame, CA, USA) and stored at -20ºC. All the brain sections were then examined with a confocal laser-scanning microscope (CLSM; MRC-1000; Bio-Rad, Herts, UK).

All the brain coronary sections were scanned with a confocal laser scanning microscope equipped with a Krypton-Argon laser (Bio-Rad, UK) through an oil-immersion 40x lens with a zoom of 1 and a z-separation of 0.5μm or 1μm. Scans were saved in the format of raw images (Bio-Rad PIC files) and viewed using Image J software (version 1.44; National Institutes of Health, USA). Maximum intensity projections were made from these image stacks and saved in TIFF format.

2.6.2 Quantification of cortical cells

For cortical cell counting, the primary somatosensory cortex of a hemizygous *Mecp2-stop* mouse was selected. After they were immunostained with neurochemical markers (see section 2.6.1), coronal brain sections located at Bregma -2.80mm to -3.60mm were chosen. As illustrated in figure 2.5, for each of the selected brain section, the intermediodorsal thalamic nucleus (IMD) was regarded as the central point, and an oblique line (35-40^{o} deviation from the vertical axis) was drawn from this centre. The line normally crossed through the hippocampal CA2 and CA3 regions and reached the somatosensory cortex area at the outer surface of brain section. As described in Chapter 1, the somatosensory cortex is layered from I to VI (from the outermost to the innermost layers). Under microscopic examination, layer V of the somatosensory cortex was identified, and the image stack was obtained by using a confocal laser-scanning microscope (Bio-Rad, UK) through an oil-immersion 40x lens with a zoom of 1 and a z-separation of 1 μm. For either side of the coronal brain section, one to three adjacent areas located at the somatosensory cortex layer V were selected for the confocal scanning (see figure 2.5). Generally, one image stack contained 21 to 31 images (20 to 30μm thickness).

Image stacks were saved in the format of raw images (Bio-Rad PIC files) and analysed using Image J software (National Institutes of Health, USA). The cortical cell counting was performed by using the disector method. First, the probe that is used to count is called the counting frame (see figure 2.6(A)). The

counting frame is an interesting probe since it is asymmetrical and extends to infinity. The red lines border the rejection region and are known as the rejection lines. The green lines pass through the acceptance region and are the acceptance lines. The rejection and acceptance regions cover everywhere. The border between these two regions extends to infinity.

The disector method is used to count objects in three dimensions. The disector method uses the counting frame to count objects in two adjacent sections. In fact, the term disector comes from the composition of the terms *di* for two and *section*. The two sections must be close enough so that it is possible to infer what lies between the two sections. This makes it possible to use the disector method to sample volume.

The two sections are referred to by unique terms. One is called the reference section and the other is called the lookup section. Particles are selected in the reference section and counting is done in the lookup section. If a particle appears in the reference section but not the lookup section, then the particle is counted. This ensures that a unique point, i.e., the top, of the particle is counted. Therefore, the disector method results in unbiased estimates of cell number in a fixed volume built by adjacent image stacks. (Sterio, 1984)

As illustrated in figure 2.6(B)&(C), incomplete or partial cells attached to the border of the image stack were counted at one end but not the other, and this principle was applied to the x, y and z axes. The image stack was opened in Image J (National Institutes of Health, USA) and the counting was completed manually to avoid overlapped counting of the same cell in adjacent planes of image stacks. For cell density measurement, the density was generated by dividing the cell count of the image stack by its own volume.

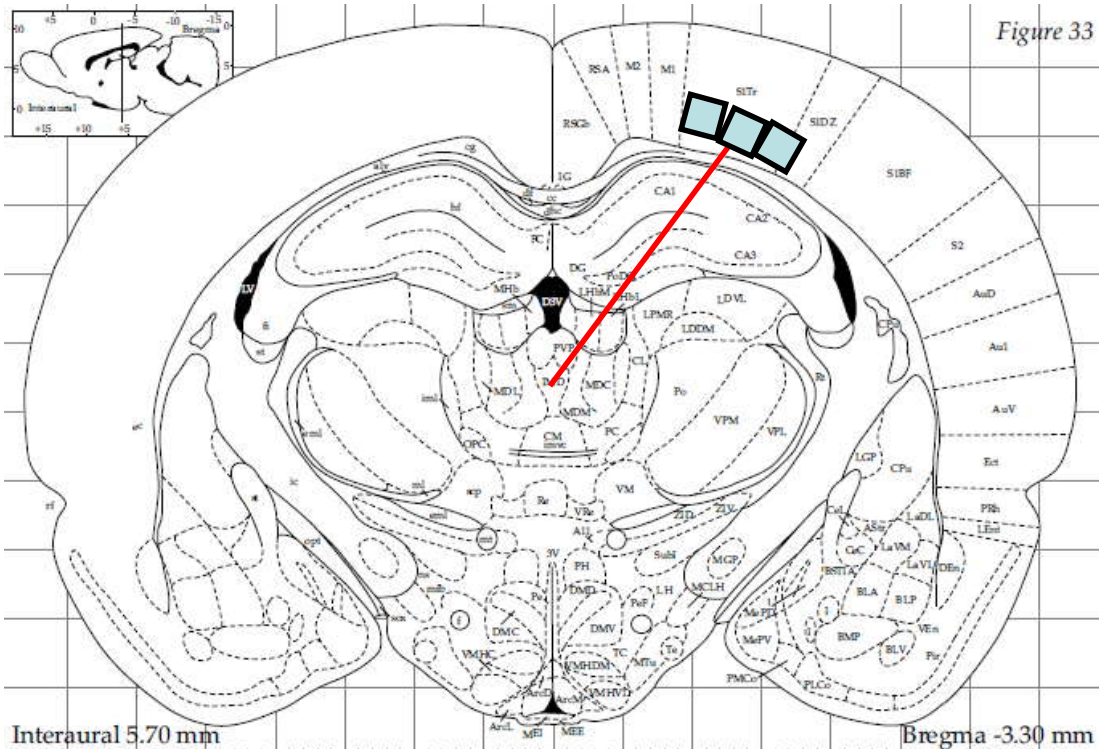

Figure 2.5 Localisation of the somatosensory cortex.

In the coronal brain sections at Bregma -3.30mm, an oblique line (35-40^{o} deviation from the vertical axis) was drawn from the intermediodorsal thalamic nucleus (IMD). This line normally passed through hippocampal CA1 and CA2 regions and reached somatosensory cortex at the superficial region of brain section. The blue square boxes indicate the selected areas for the cortical cell counting studies.

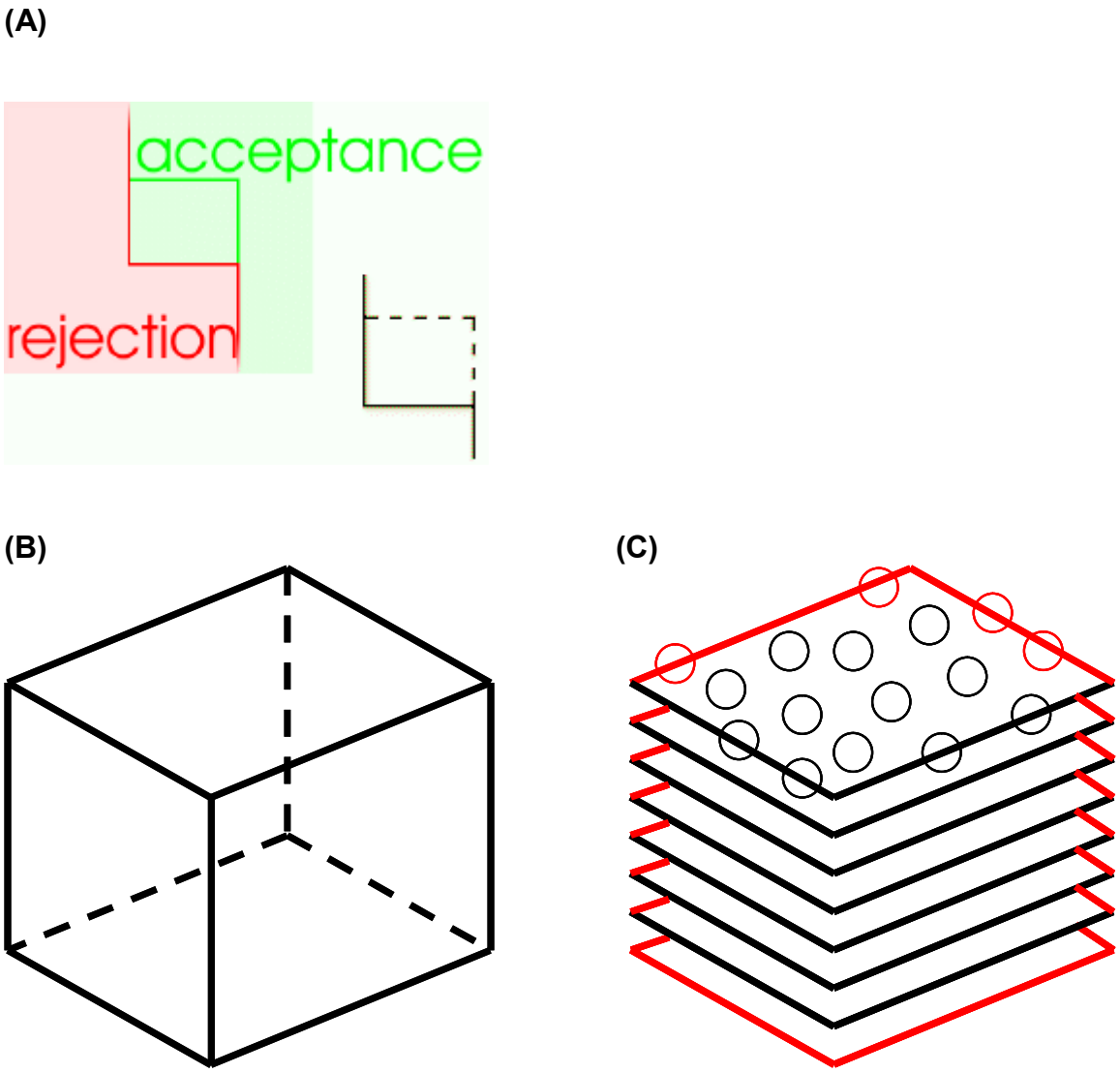

Figure 2.6 Disector counting method.

(A) The counting frame, showing acceptance (green lines) and rejection regions (red lines). The confocal image stack (B) consisted of several two-dimensional images (C). The disector counting method was applied when incomplete or partial cells (labelled as circles) attached to the border of the image stack; cells were counted at one end but not the other. As illustrated here, incomplete or partial cells attached the red border were excluded for counting, while those attached the black border were considered as one intact cell. Following the same principle, incomplete or partial cells at the top plane were counted while those at the bottom plane were excluded.

2.7 Electrophysiology methods

2.7.1 Preparation of brain slices

Symptomatic hemizygous (*Mecp2*$^{stop/y}$ genotype) male (see section 2.5.3 for the selection criteria) and their WT littermates were culled by cervical dislocation, followed by decapitation in accordance with UK Home Office Schedule 1 guidelines. After decapitation, the brain was removed quickly from the skull and immersed in ice-cold (0-4^{o}C) oxygenated (95% O_2, 5% CO_2) 1x artificial cerebrospinal fluid (ACSF) solution. The brain was further hemisected and each part was glued to the stage of a vibrating microtome (see figure 2.7; Campden Instruments Ltd., UK).

As illustrated in figure 2.7, parasagittal hippocampal slices (400μm thick) were prepared and transferred to an interface holding chamber in a humidified and oxygen-enriched (95% O_2, 5% CO_2, maintained at 32°C) atmosphere for at least one hour to enable recording, as described (McNair *et al.*, 2006).

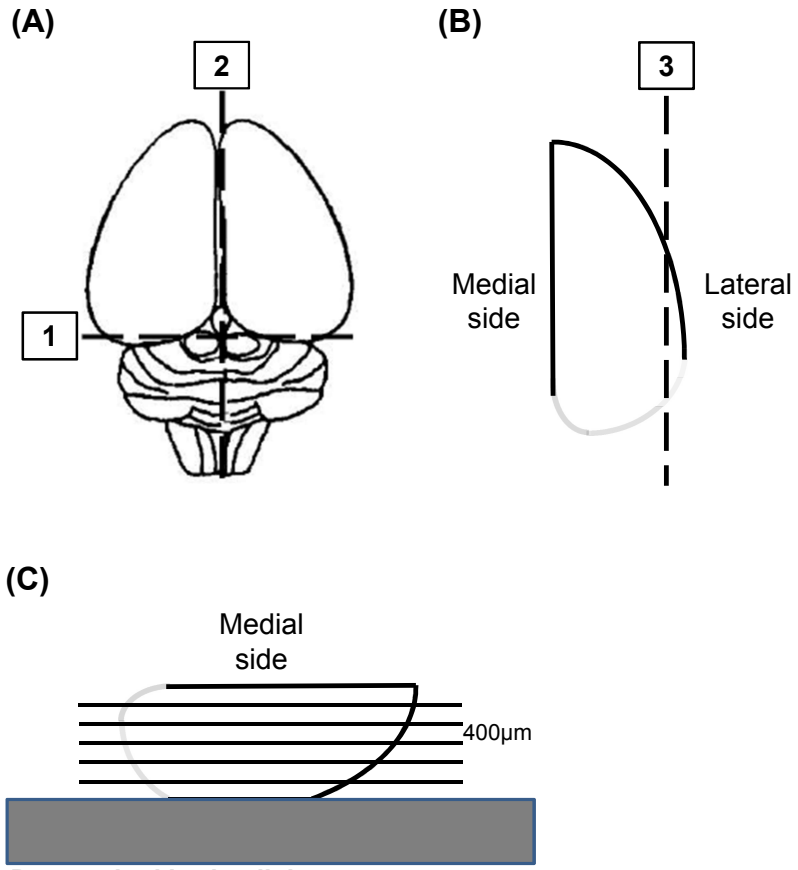

Figure 2.7 Parasagittal brain slicing.

(A) After removal of the brain from the skull, the cerebellum was separated from the cerebrum (as shown in "1") using a scalpel blade. Secondly, the cerebrum was divided into two hemispheres (as shown in "2"). (B) A portion of the lateral side of each hemisphere was cut (as shown in "3") to allow the hemisphere to be glued onto the plastic board (coloured grey in (C)). (C) The parasagittal brain slicing started from the medial side of the hemisphere to the lateral side and the thickness setting on the vibrating microtome (Campden Instruments Ltd., UK) was 400µm.

2.7.2 Equipment used for extracellular recording

Transverse brain slices were transferred into a humidified and oxygen-enriched (95% O_2, 5% CO_2) atmosphere interface recording chamber maintained at 32°C and perfused by 1x ACSF oxygenated by 95% O_2 and 5% CO_2 at a rate of 6-8 ml/min powered by a peristaltic pump (Minipuls 3; Gilson, France). Figure 2.8 shows the equipment used for the extracellular recording. An interface recording chamber (HAAS-type; Berlin), a binocular dissecting microscope (Zeiss, Germany), a stimulating micromanipulator (Narishige, Japan), a recording micromanipulator (Leica, Germany) and a lamp were secured on an anti-vibration table (Intracel, UK). Moreover, an amplifier (AxoClamp 2B; Axon instruments, USA), a digitizer (Digidata 1320A; Axon instruments), a 50Hz line noise eliminator (Hum Bug; Quest Scientific), an instrumental amplifier (model

440; Brown precision) and a desktop were secured into a rig. Stimulating current was delivered through a bipolar tungsten stimulating electrode of 3.5MΩ resistance (World Precision Instruments, USA) using an isolated constant current stimulator (model D52A; Digitimer Ltd., UK). The current range was 0-30mA and the pulse duration was 0.1ms. Recording electrodes were made from standard walled (1.2mm O.D. x 0.69mm I.D.) borosilicate glass capillaries (Harvard Apparatus, UK) pulled on a Flaming/Brown micropipette puller (model P-87; Sutter Instrument Co., USA). The electrodes (1-5MΩ) were filled with ACSF solution and were connected via a silver chloride pellet-containing electrode holder to a headstage (HS2A; Axon Instruments).

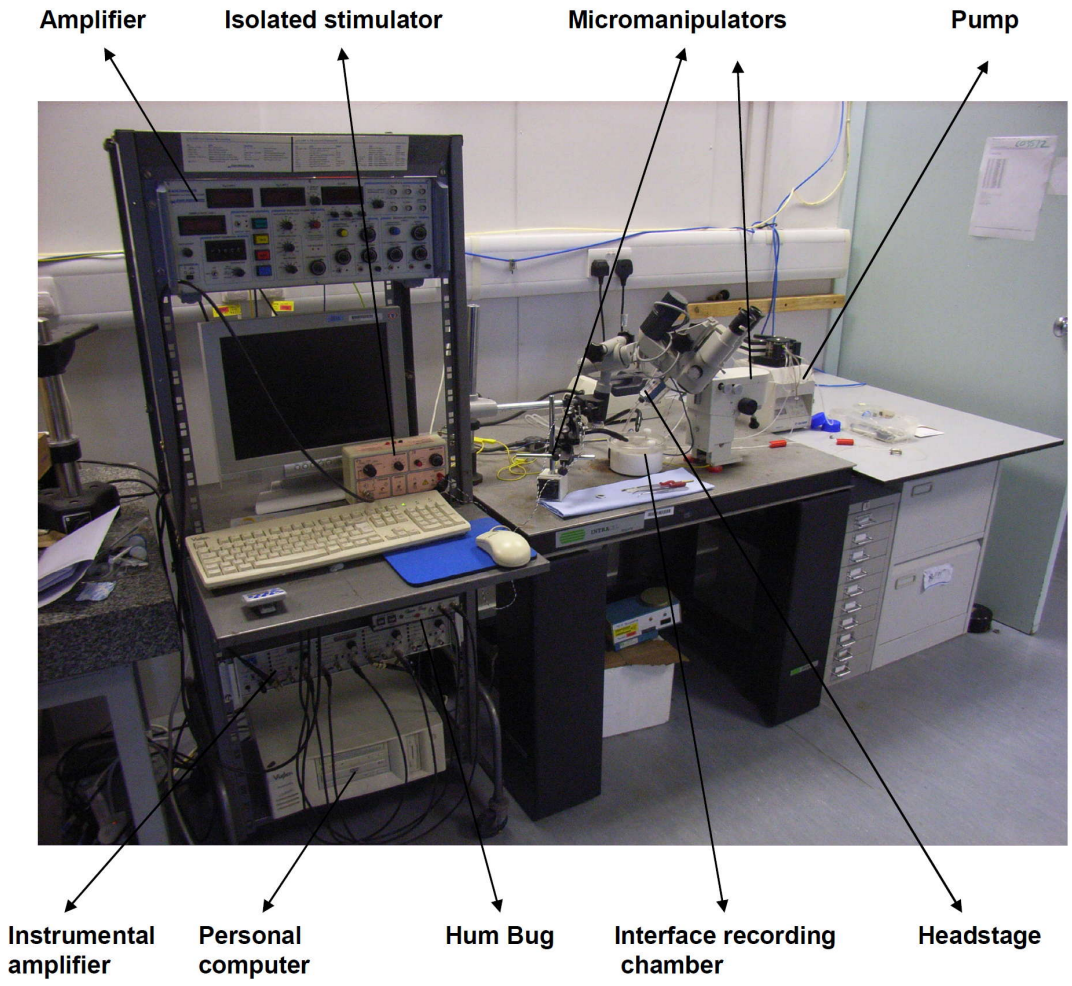

Figure 2.8 Image of the electrophysiology experimental setup.

The electrophysiology experiments were performed using this setup. The equipment has been labelled in the figure. This image was taken by a previous PhD student, Jian Gan.

Pre-amplification (x100) was carried out by an AxoClamp 2B amplifier (Axon instruments, USA) set to current clamp mode. Further amplification (x20) and filtering (1Hz HP-1KHz LP) was carried out using a Brownlee instrumentation amplifier (model 440; Brownlee Precision, USA), giving a total amplification of x2000. A Hum Bug 50/60Hz noise eliminator (Quest Scientific, UK) was used to eliminate 50Hz line frequency noise where necessary. Data were captured by Digidata 1320A analogue-to-digital acquisition board (Axon Instruments) and transferred directly to the desktop (Viglen Pentium 4) at a sampling rate of 10 KHz.

2.7.3 Extracellular recording protocols

After at least one hour equilibration time for hippocampal slices, a single stimulating electrode and a single recording electrode were placed on either side of the stratum radiatum in the CA1 region of hippocampal slice to stimulate the Schaffer collateral pathway (see figure 2.9). Small stimulating current pulses (current range 0-30mA; pulse duration 0.5ms) were administered to test for the presence of field excitatory postsynaptic potentials (fEPSP) responses. Once synaptic potentials were observed, input-output (I/O) curve was obtained by gradually increasing stimulating current and monitoring fEPSP responses. The stimulating current which gave half the maximum fEPSP response was then applied for the remainder of experiment. Measurements of synaptic responses were monitored in terms of the initial slope of fEPSP (Figure 2.10). The window for slope measurement was typically in the range of 2 to 6 ms following stimulation.

Field EPSPs were evoked at the frequency of 0.05 Hz in the stratum radiatum of the hippocampal CA1 region. Paired-pulse facilitation (PPF) was investigated using a 50ms intersimulus interval. A high-frequency stimulation paradigm of 100Hz high frequency stimulation (HFS) for one second was used to induce long-term potentiation (LTP). Synaptic efficacy was monitored for at least 20 minutes before LTP induction by recording fEPSP responses every 20s (traces were averaged for every minute interval). Slices that did not exhibit stable fEPSP

slopes (more than 5% amplitude change) during the initial 20 minutes baseline recording were excluded from the study.

(A)

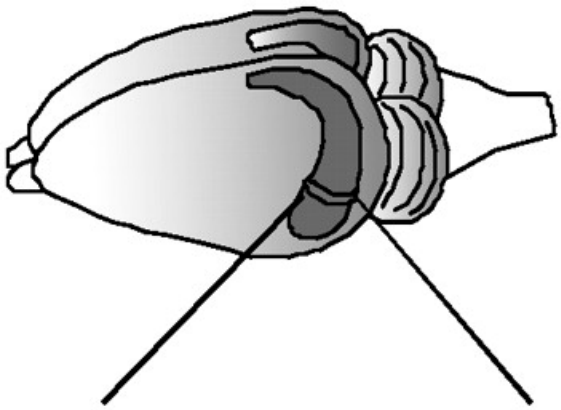

(B)

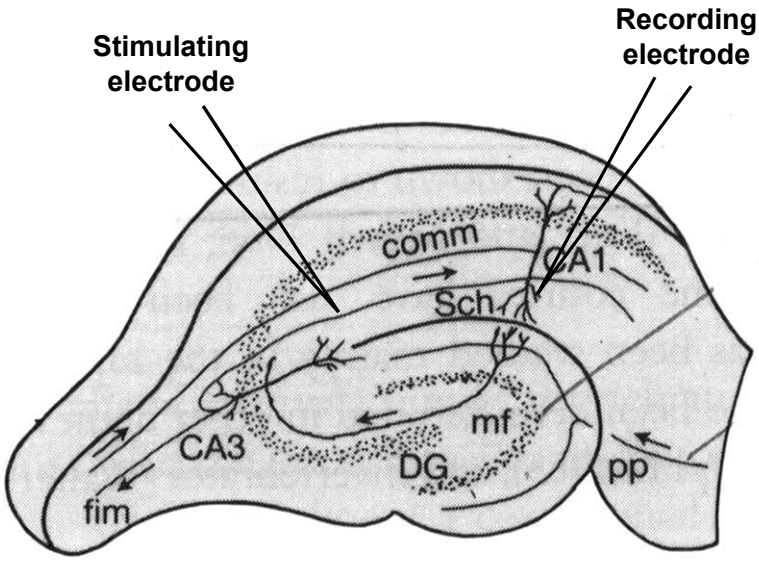

Figure 2.9 Extracellular recording at the hippocampal CA1 region.

(A) For extracellular recording at the hippocampal CA1 region, acute hippocampal slices were used. (B) Illustration of a hippocampal slice from (A). On the hippocampal CA1 region, stimulating and recording electrodes were placed at either side of the CA1 region to stimulate the Schaffer collateral (Sch) pathway. Abbreviations: commissure (comm), fimbria (fim), dentate gyrus (DG), Mossy fibre (mf), perforant path (pp). Source: http://graulab.tamu.edu/J-Grau/Psyc606/Outlines/ComplexStim-Neurobio.html

Figure 2.10 Recording of the field excitatory postsynaptic potential (fEPSP).

Example of a fEPSP recorded in the stratum radiatum of the mouse hippocampal CA1 region. The arrow indicates the time of stimulation for fEPSP. The red dashed line indicates slope measurement for the fEPSP trace.

2.7.4 Electrophysiology data analysis

All data from extracellular recordings in acute hippocampal slices were analysed online and fEPSP slopes re-analysed offline using the software packages WinLTP (Anderson & Collingridge, 2007) and Excel 2003 (Microsoft, USA). Paired-pulse facilitation (PPF) was calculated as the amplitude ratio of second to first response for each paired stimulation event (see figure 2.11). Post-tetanic potentiation (PTP) was calculated as the mean of the first three slope data points following HFS. LTP was measured at 40-60 minutes post-HFS in the one-hour LTP experiments, and at 12-15 minutes post-HFS in the LTP saturation experiments. Data were gathered from recordings made from 1-3 slices per mouse brain and were expressed as mean±SEM of all the slices. All data were graphically illustrated using GraphPad Prism 5.0 (GraphPad Software, USA). WT mice used as controls were age-matched to their respective experimental (i.e. symptomatic or pre-symptomatic) groups.

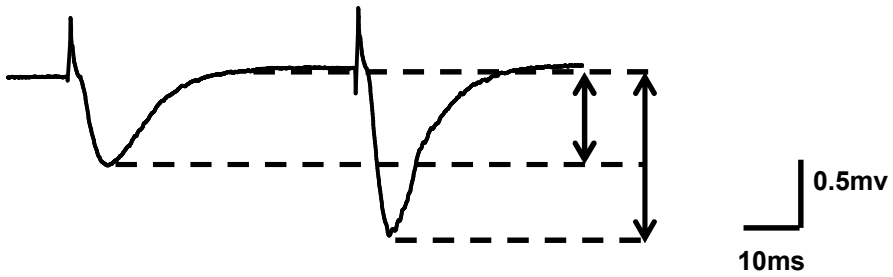

Figure 2.11 Measurement of the pair-pulse facilitation (PPF).

As illustrated, paired stimulations (50ms interval) were applied for the generation of paired fEPSPs. The second fEPSP had a higher response (amplitude) than the first one due to elevated presynaptic calcium concentrations. Paired-pulse facilitation (PPF) was calculated as the amplitude ratio of second to first response for each paired stimulation event.

2.7.5 Statistical analysis of electrophysiological data

Data from the PPF, PTP and LTP experiments were compared by repeated-measures ANOVA with Tukey's post-hoc analysis (Minitab version 10) and a *p* value of less than 0.05 was taken as indicating statistical significance.

2.8 Drug application in *Mecp2-stop* mice

2.8.1 Memantine application

For the memantine treatment experiment in acute slices (see Chapter 5), 1mg/ml memantine stock was made by dissolving memantine hydrochloride (Tocris Bioscience, Bristol, UK) in 1x ACSF. This was subsequently added to the slice perfusion medium (ACSF) at 1μM final concentration and pumped into the bath containing the slices being recorded. Recordings were commenced 30–60 min after the slices first became exposed to memantine. For the chronic *in vivo* memantine treatment study (see results in Chapter 5), memantine hydrochloride was dissolved in sterile water at a final perfusate concentration of 3mg/ml (Diehl *et al.*, 2001). Dosing was administered orally by gavage at a dose of 30mg/kg. Mice were dosed daily over a four-week period. The choice of doses for the drug was based on those found to be effective in previous studies, with *in vitro* at 1μM (Frankiewicz & Parsons, 1999), *in vivo* at 30mg/kg/day (Minkeviciene *et al.*, 2004).

3 Genotype phenotype correlations in *Mecp2-stop* mice

3.1 Introduction

Over 95% of the classical RTT pathogenesis originates from *MECP2* mutations (Neul *et al.*, 2008), and the *Mecp2*-mutant mouse model recapitulates most RTT symptoms and serves as a good model for investigating MeCP2 functions (Calfa *et al.*, 2011) (see table 2.5 in chapter 2). *Mecp2*-mutant mouse has a late onset of phenotypes (as in RTT patients), and it is generally not possible to differentiate them from their WT littermates based on gross phenotypic assessments at early postnatal stages (Calfa *et al.*, 2011). In this thesis, I used the *Mecp2-stop* model, and three possible genotypes (WT, $Mecp2^{stop/+}$ and $Mecp2^{stop/y}$) of offspring were generated (Guy *et al.*, 2007). In order to set breeding colonies and select animals for further experimental use, it was essential to identify genotypes. Therefore, the aim in this chapter was to confirm the genotypes of the *Mecp2-stop* mouse colony established in Glasgow. This was done by applying two sets of PCR reactions (one for detection of the WT allele, and the other for detection of the mutant allele). The second aim was to map out the progression of symptoms as the RTT-like phenotype developed. For this, I adopted the scoring system that was published by Guy *et al.*, 2007 for the phenotype recording of the *Mecp2-stop* mice (Guy *et al.*, 2007). Since the progression of symptoms has never been analysed in detail in hemizygous *Mecp2-stop* mice, both the sum symptom score and the score of each subcategory (mobility, gait disturbance, hindlimb clasping, tremor, breathing abnormality, and general conditions) were recorded and analysed.

3.2 Confirmation of genotypes in *Mecp2-stop* mouse colony

3.2.1 Confirmation of genotypes in Mecp2-stop mouse colony by PCR

The *Mecp2-stop* mouse model was designed by Prof. Adrian Bird's team at the University of Edinburgh with a *STOP* cassette inserted into intron 2 (see Chapter 2 for the detailed design). This design led to a truncated mRNA production and generated a MeCP2 protein-null phenotype. In order to detect both the WT and mutant alleles in the *Mecp2-stop* mice, the primers designed by Guy *et al*. 2007 were adopted to generate and amplify a 416bp product (from primers P5/P7 reaction; to detect the WT allele) and a 470bp product (from primers NeoF/NeoR reaction; to detect the mutant allele), respectively (Guy *et al.*, 2007) (see figure 3.1). Tissue samples were collected from *Mecp2-stop* mice and the DNA from each sample was extracted. The extracted DNA was diluted and prepared for PCR reactions. PCR products were loaded onto an agarose gel for electrophoreses. The scheme for interpretation of genotype results is given in table 3.1. Representative PCR results are shown in figure 3.2. For each DNA sample, two PCR reactions were performed; the first lane was loaded with the PCR product from P5/P7 primers reaction and the second lane was loaded with the PCR product from NeoF/NeoR primers reaction. As illustrated in figure 3.2, the tenth and eleventh lanes were typically representative of the WT genotype result (positive only in the primers P5/P7 reaction), and the sixteenth and seventeenth lanes were from the hemizygous *Mecp2*$^{stop/y}$ DNA sample, only presenting positive in the primers NeoF/NeoR reaction. Once genotypes had been confirmed, heterozygous females were preserved for breeding and maintenance of the *Mecp2-stop* colony, and WT females were culled humanely. Both WT and hemizygous males, were selected for further experimental use (immunohistochemistry or electrophysiology studies) and were recorded weekly for symptom progression. In later sections, the observation of symptom progress of the *Mecp2*$^{stop/y}$ mice is illustrated.

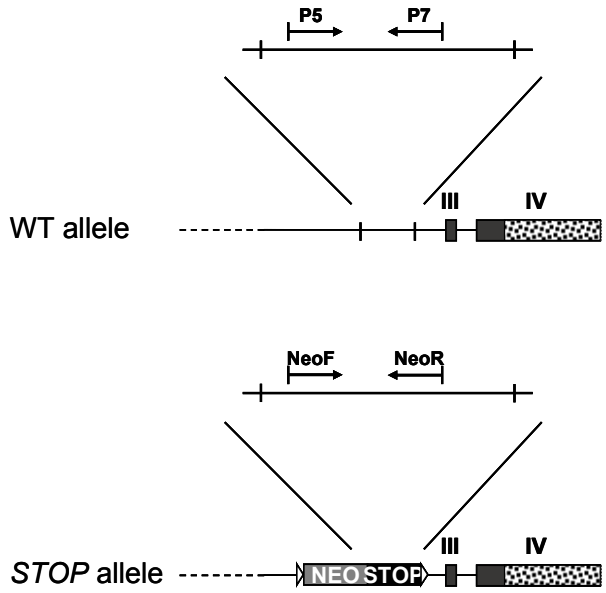

Figure 3.1 Illustration of the *Mecp2-stop* mice design

The upper diagram shows the *Mecp2* gene of the WT allele, and the lower diagram shows the insertion of a *neo-stop* cassette into intron 2 of the *Mecp2* gene of the *STOP* allele. The primer set P5/P7 was designed to amplify a 416bp PCR product in the WT allele, while the primer set NeoF/NeoR was designed to amplify a 470bp PCR product in the *STOP* allele.

Table 3.1 *Mecp2-stop* mice genotype patterns

	Genotype	P5/P7	NeoF/NeoR	Lanes in fig. 3.2
Heterozygous female	*Mecp2*$^{stop/+}$	Positive	Positive	6/7, 8/9,12/13, 26/27, 28/29
WT female	*Mecp2*$^{+/+}$	Positive	Negative	10/11, 14/15
Hemizygous male	*Mecp2*$^{stop/y}$	Negative	Positive	16/17, 18/19
WT male	*Mecp2*$^{+/y}$	Positive	Negative	20/21, 22/23, 24/25

(A)

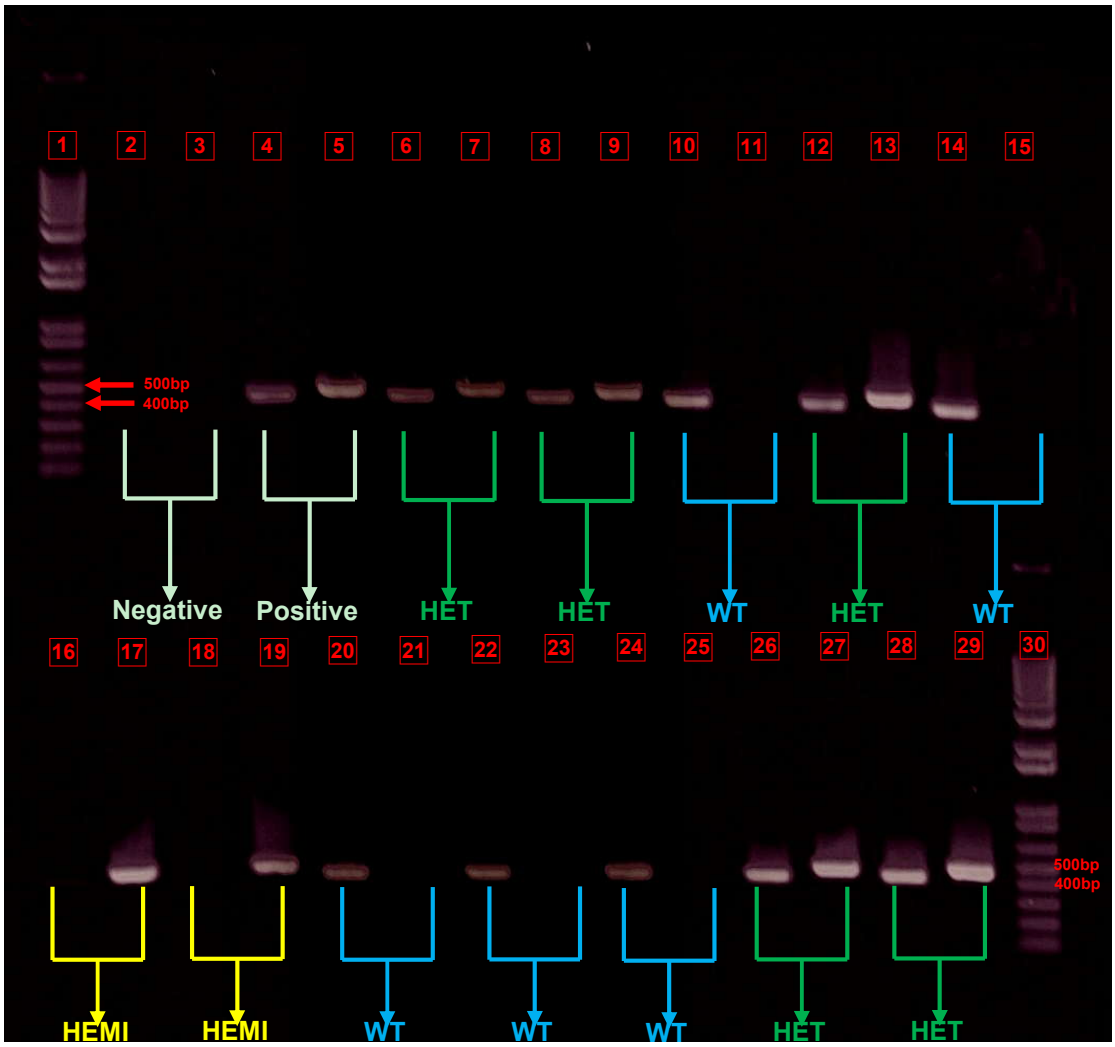

Figure 3.2 Genotyping data of the *Mecp2-stop* mouse model

(A) Three different genotypes (WT, *Mecp2*$^{stop/+}$ and *Mecp2*$^{stop/y}$) were distinguished by the PCR test. 1kb+ DNA ladder was loaded in lane 1 and lane 30. For each animal DNA sample, the first lane was for the WT allele detection (416bp), and the second lane was for the mutant allele detection (470bp). Lanes 2 and 3 were no DNA controls, and lanes 4 and 5 were positive controls (previously confirmed heterozygous female DNA in the PCR reaction).

3.2.2 Western blot and immunohistochemistry verifications of lack of MeCP2 production in the hemizygous Mecp2-stop mice

In the *Mecp2-stop* model design, a *STOP* cassette was inserted into intron 2 leading to a functional knock-out of *Mecp2*. In order to confirm that MeCP2 has not been generated in detectable amounts in hemizygous *Mecp2-stop* brains, tissues from hemizygous *Mecp2-stop* mice were assessed by western blot and immunohistochemistry. Coronal brain slices from one-month-old *Mecp2*$^{stop/y}$ mice and their age-matched WT littermates were used in both types of experiments. As shown in figure 3.3, western blot analysis (performed by Ms Faye McLeod; WT: *n*=2, *Mecp2-stop*: *n*=2) confirmed the absence of a detectable 75kDa MeCP2 band in protein extracts from the brains of hemizygous *Mecp2*$^{stop/y}$ mice. This conclusion was in line with the absence of detectable MeCP2 within the hippocampus as revealed by immunohistochemistry studies (performed by myself; WT: *n*=2, *Mecp2-stop*: *n*=2; see figure 3.3). In contrast, in WT mice a strong MeCP2 signal was detected from a similar amount of protein in the western analysis and strong expression was apparent in the cell nuclei in the hippocampal formation including all principal cells of the hippocampus (not shown) and dentate gyrus. Therefore, the functional silencing of MeCP2 in the *Mecp2-stop* model was proved to be robust.

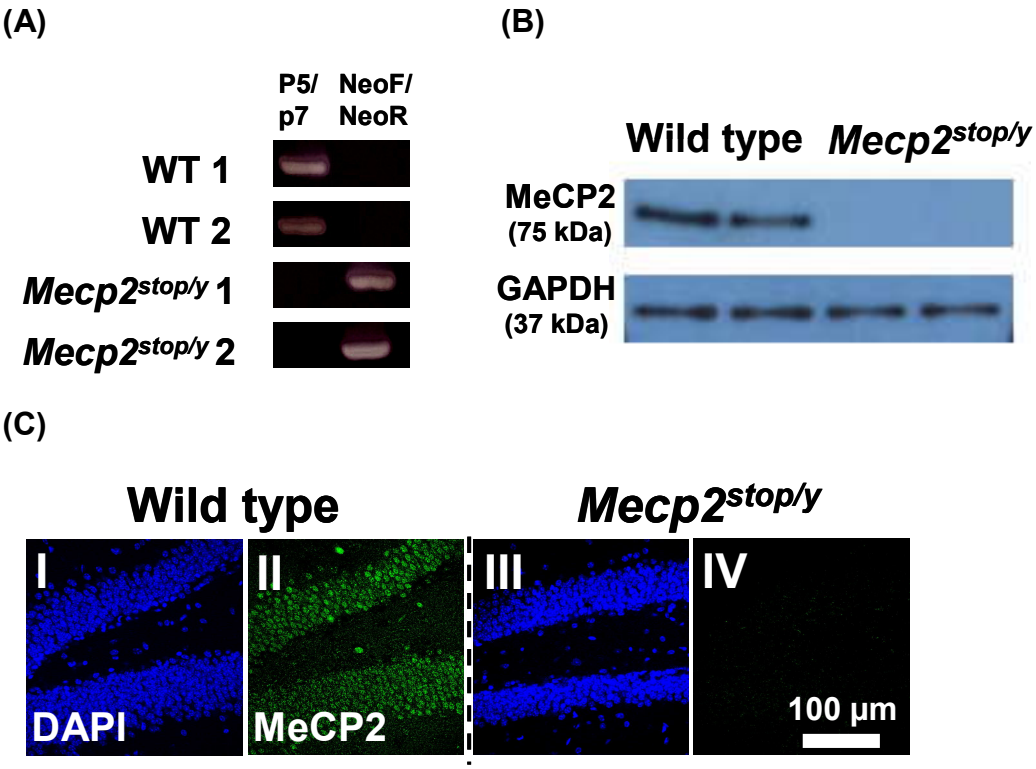

Figure 3.3 Robust silencing of MeCP2 expression in the *Mecp2-stop* mouse model

(A) Genotyping results from two WT and two hemizygous *Mecp2-stop* mice used in the western blot and immunohistochemistry experiments. (B) Western blot of protein extract from hippocampus of WT and hemizygous male mice. Samples from each of two mice were loaded in adjacent lanes. GAPDH (37 kDa) detection was carried out as a loading control. (Data collected and provided by Ms Faye McLeod) (C) Fluorescence micrographs of dentate gyrus from WT (I, II) and from hemizygous (III, IV) male mice immunostained for MeCP2 (II, IV) and co-stained with DAPI (I, III) to reveal nuclei. In the *Mecp2-stop* model, only DAPI stained nuclei were identified, while no signals were detected in the MeCP2 staining.

3.3 Phenotype scoring of *Mecp2-stop* mice

3.3.1 Progression of sum symptom score in hemizygous Mecp2-stop mice

The phenotype progression of hemizygous *Mecp2-stop* mice was recorded by adopting the scoring method described by Guy *et al.* 2007 (Guy *et al.*, 2007). Six categories of symptoms were scored (mobility, gait, hindlimb clasping, tremor, breathing, and general condition) using a semi-quantitative method (see Chapter 2 for detailed methods). All the *Mecp2-stop* mice and their WT littermates were documented weekly for symptom scoring, and once the symptom score reached five or more, the *Mecp2-stop* animal and its age-matched WT littermate were selected and processed for immunohistochemistry (see in Chapter 4) or electrophysiological (see in Chapter 5) experiments. Figure 3.4 presents the progression of sum symptom score in hemizygous *Mecp2-stop* mice and their WT littermates. Symptom onset was generally recorded from the fifth week to the seventh week, and always before the tenth week. After the tenth postnatal week, symptoms progressed rapidly to reach a score of five or more (as the defined as "symptomatic" in this thesis).

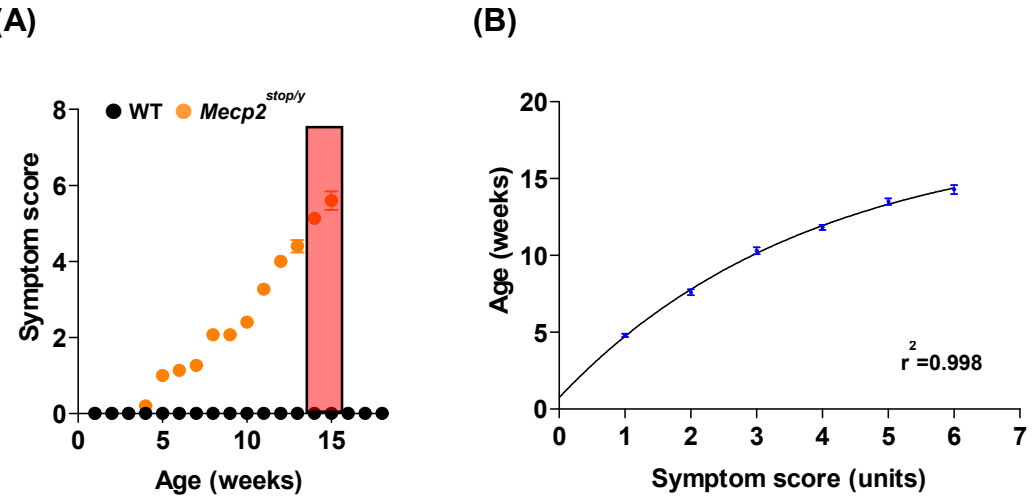

Figure 3.4 Symptoms progression in *Mecp2-stop* mice

(A) Time plot showing onset and progression of phenotypic signs in *Mecp2-stop* mice (*n*=15). Scores for WT mice (*n*=10) were also plotted for comparison. The curve for the hemizygous mice was censored at the top end due to the humane culling policy in operation. The red semi-transparent block indicates the selection phase (symptomatic animals) for immunohistochemistry or electrophysiological experiments. (B) Using nonlinear regression method, the symptoms versus age plot fits a one-phase exponential curve.

3.3.2 Progression of symptom score in each specific category of hemizygous Mecp2-stop mice

As mentioned in previous sections, the sum score system consisted of six distinct categories: motor dysfunction, gait disturbance, hindlimb clasping, tremor, breathing abnormality, and abnormal general conditions. These categories represent key aspects of the RTT-like phenotype and the scoring system was tailored to the specific constellations of features and was adopted in order to give a score that encompassed the key salient features, that characterise the *Mecp2-stop* phenotype. However, I also went on to assess each of the observed measures individually. The symptom progression of each distinct category was documented weekly.

The progression of symptom scores in each individual category of hemizygous *Mecp2-stop* mice were plotted in figure 3.5. As illustrated in figure 3.5, the mobility score of *Mecp2-stop* mice (n=7) had a mean onset of 7.58 ± 0.36 weeks and mean maximal score of 1.67 ± 0.33 units. The gait score of *Mecp2-stop* mice had a mean onset of 7.87 ± 0.68 weeks and mean maximal score of 1.33 ± 0.33 units. The hindlimb clasping score of *Mecp2-stop* mice had a mean onset of 8.58 ± 0.81 weeks, and the mean maximal score was 1 ± 0 units. The tremor score of *Mecp2-stop* mice had a mean onset of 8.01 ± 0.68 weeks, and the mean maximal score was 1 ± 0 units. The breathing score of *Mecp2-stop* mice had a mean onset of 11.58 ± 0.52 weeks, and the mean maximal score was 0.33 ± 0.33 units. The last was the general condition score; the mean onset was 10.72 ± 0.72 weeks, and the mean maximal score was 0.67 ± 0.67 units. The tremor, breathing and general condition data never reached a score of two due to the censoring criteria (indicated by ★ sign in figure 3.5). In summary, motor dysfunction, gait disturbance, hindlimb clasping, and tremor all had an earlier onset, while breathing abnormality and abnormal general conditions occurred later with severer phenotypes developed (see figure 3.6 & 3.7).

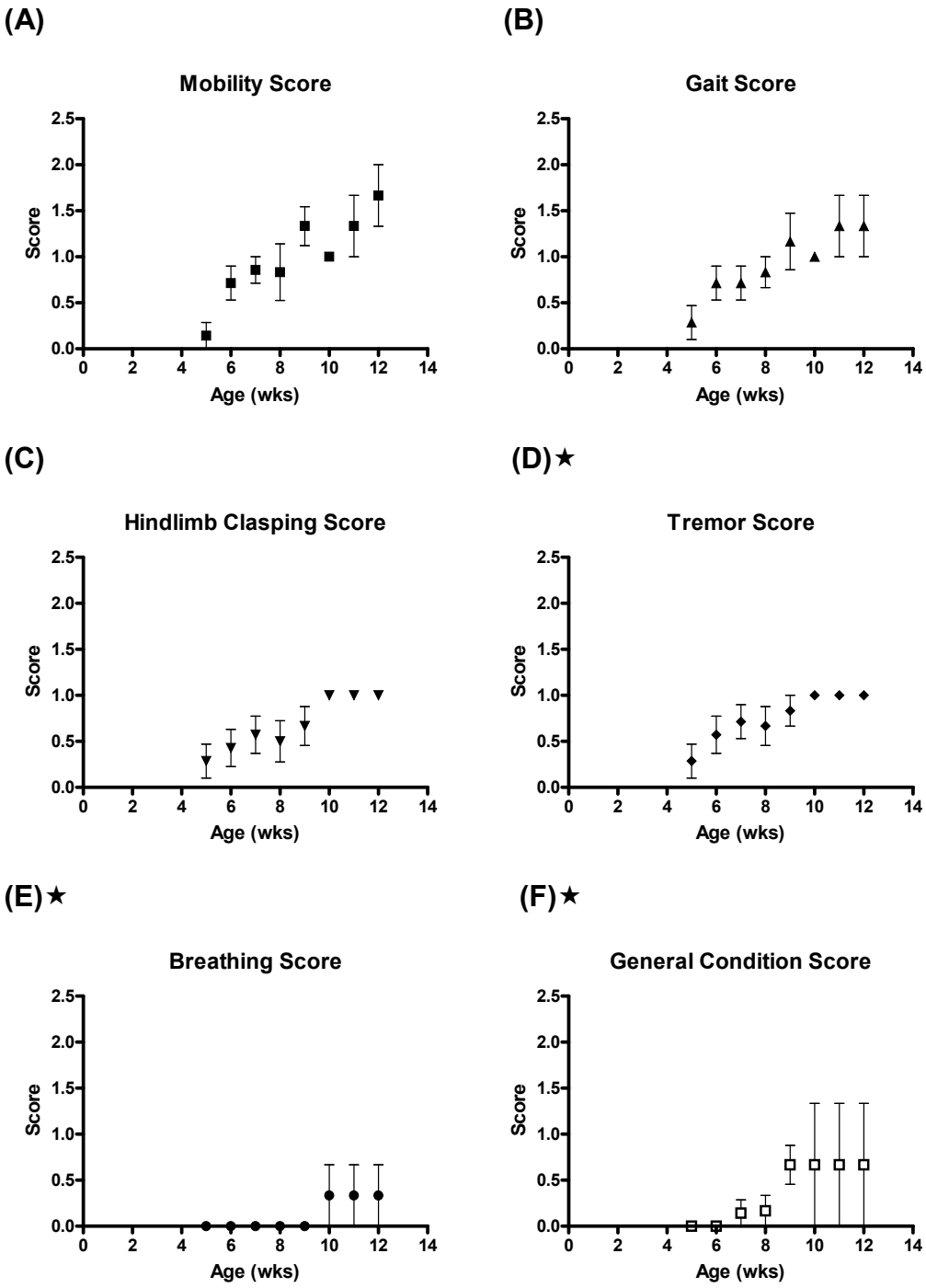

Figure 3.5 The progression of symptom score in each individual category.

(A)-(F) The progression of symptom score in each individual category was plotted as mean ± SEM units. The star sign (★) indicates the criterion that an *Mecp2-stop* mouse was selected for experiments or culled once score reached two in any of the tremor, breathing or general condition groups.

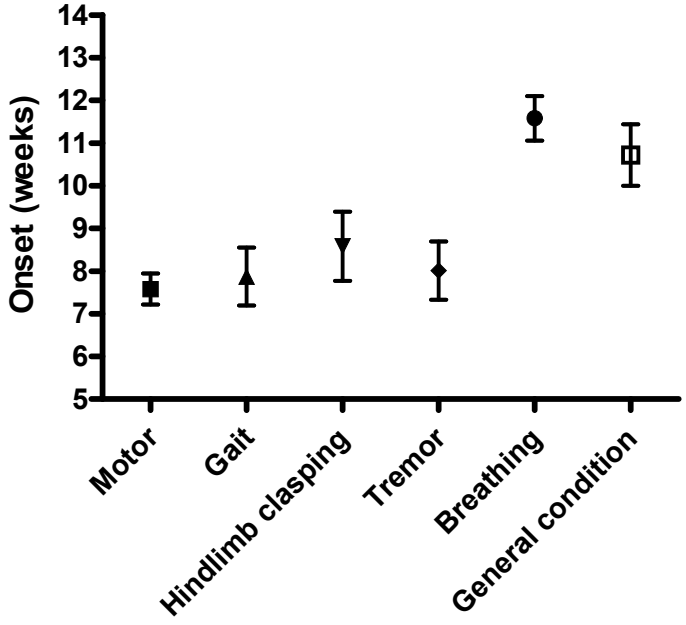

Figure 3.6 The onset of symptom score in each individual category.

The symptom onset of each individual category was plotted as mean ± SEM wks.

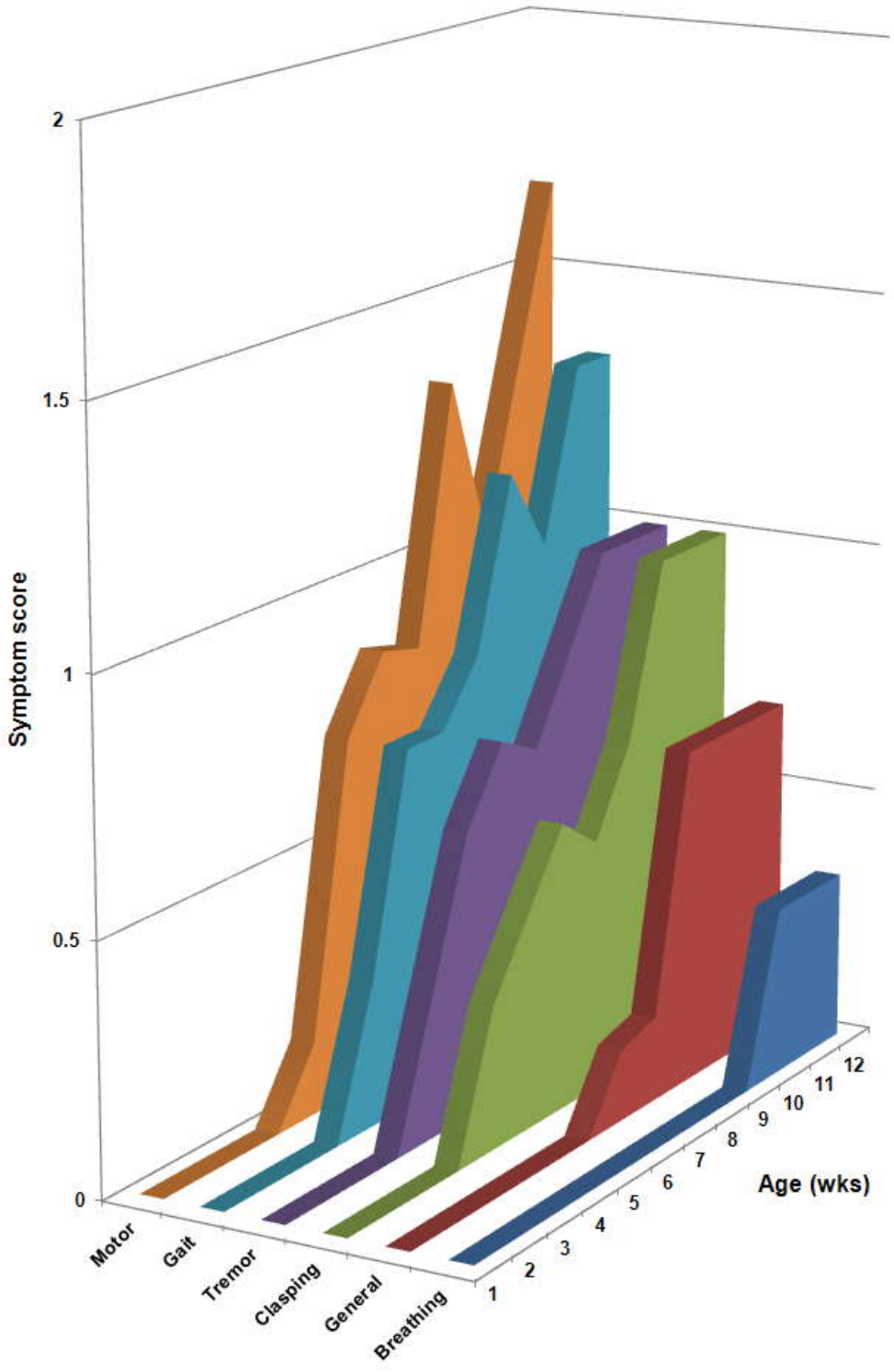

Figure 3.7 Summary of score progression for each symptom measure. All symptom score data were plotted as weekly score means.

3.4 Survival analysis of hemizygous *Mecp2-stop* mice

Both progression of symptoms and the shortened period of survival were characteristic features of phenotypes in MeCP2 functional knock-out mice. A previous study (Guy *et al.*, 2001) reported that MeCP2 functional knock-out mice had a shorter life span compared to WT mice. Reactivation of MeCP2 in MeCP2 functional knock-out mice was proved to be capable of prolonging the life span and alleviating symptoms at adult stages (Guy *et al.*, 2007). The aim here was to assess the normal life span of *Mecp2-stop* mice. *Mecp2-stop* mice (*n*=10) and their WT littermates (*n*=8) were caged under identical conditions in the Animal Unit at the University of Glasgow (see Chapter 2) The incidence of sudden or unexpected death before 2 month old was low (less than 1%) under the care of experienced animal unit staff. Animals were monitored on a daily basis for obvious signs of distress. Symptom scores were recorded at weekly intervals, and any *Mecp2-stop* mouse that scored two in the tremor, breathing or the general condition category was humanely culled and reported as death. As presented in figure 3.8, the distribution of *Mecp2-stop* mice survival ranged from 70 days (10wk) to 110 days (15.7wk).

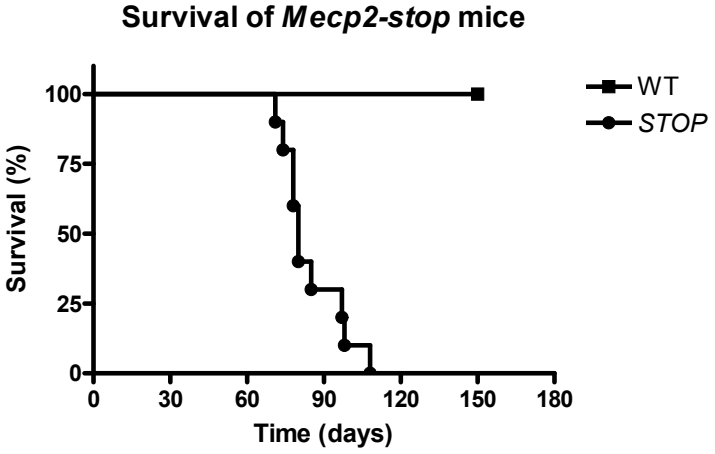

Figure 3.8 Survival of hemizygous *Mecp2-stop* mice

***Mecp2-stop* mice (*n*=10) and their WT littermates (*n*=8) were assessed for the normal life span. Both groups were caged under identical conditions described in chapter 2. Survival was recorded on a daily basis for obvious signs of distress. Any *Mecp2-stop* mouse that was given a score of two in any of the tremor, breathing or general condition categories was humanely culled and reported as death. The distribution of *Mecp2-stop* mice survival ranged from 70 days (10wk) to 110 days (15.7wk).**

3.5 Discussion

Before the application of *Mecp2-stop* animals in immunohistochemistry (see Chapter 4) or electrophysiological experiments (see Chapter 5), it was essential to confirm the genotypes of the colony we established in Glasgow. The primers designed by Guy *et al*. 2007 (Guy *et al.*, 2007) were adopted in the PCR experiments to confirm the genotypes of *Mecp2-stop* animals. The PCR results showed unambiguous evidence of all three different genotypes (WT, *Mecp2*$^{stop/+}$ and *Mecp2*$^{stop/y}$). However, the PCR results were solely the functional knock-out evidence at the gene level, the null production of MeCP2 still needed to be verified at the protein level. The western blot and immunostaining assessments for brain slices from *Mecp2-stop* mice provided further robust evidence and confirmed the functional knock-out of MeCP2 in hemizygous *Mecp2*$^{stop/y}$ mice.

RTT-like phenotype development serves as a feature of the *Mecp2-stop* mouse model. On average, *Mecp2*$^{stop/y}$ mice began to display symptoms around week 7, and the severity increased gradually. After postnatal week 10, symptoms aggravated rapidly and induced inevitable death at around week 12 to 15, while their WT littermates always scored zero all the time. The symptom score system was adopted from Guy *et al*. (Guy *et al.*, 2007). Previous study has described the sum symptom score as a good indicator for categorising suitable *Mecp2-stop* animals into mild symptomatic (score= 2-4) and symptomatic (score= 5 or more) groups (Guy *et al.*, 2007). In this thesis, I adopted an identical symptom score system for the selection of *Mecp2-stop* mice for experimental use.

The individual category of the symptom score represented key aspects of the RTT-like phenotype and the score system was tailored to the specific constellations of features. The analyses from distinct symptom categories showed that impaired mobility and gait disturbance consistently occurred earlier (the mean onset of impaired mobility was 7.58 ± 0.36 weeks and the mean onset of gait disturbance was 7.87 ± 0.68 weeks), followed by tremor (8.01 ± 0.68 weeks) and hindlimb clasping (8.58 ± 0.81 weeks), and the last two to occur were abnormal general conditions (10.72 ± 0.72 weeks) and irregular breathing (11.58 ± 0.52 weeks). Regarding the maximal score of each category, the highest was the impaired mobility (1.67 ± 0.33 units) and the lowest was the breathing (0.33 ± 0.33 units). From the analyses of individual symptom progression, the

mobility score appeared to be the best indicator since it always started earliest and reached the highest maximal score when *Mecp2-stop* mice became symptomatic. In contrast, both the breathing and general condition scores seemed to contribute less to the sum symptom score. In RTT patients, the clinical signs begin with hypotonia, microcephaly, and later develop into respiratory abnormalities (Chahrour & Zoghbi, 2007). Therefore, it is not surprising that the breathing score in *Mecp2-stop* mice always had a late onset. Both the breathing and general condition scores may not be the most suitable indicators of the phenotype development and the experimental animal selection of *Mecp2-stop* mice. However, the order of symptom onsets in *Mecp2-stop* mice was similar to that of human RTT patients, and this indicated the *Mecp2-stop* animal was a good model for investigating the pathogenesis of Rett syndrome by recapitulating most of the clinical features of RTT.

During weeks 12 to 15, the variance in the progression of each distinct symptom score showed huge differences. The breathing and the general condition scores showed great standard errors while in the hindlimb clasping and the tremor scores, no standard errors were shown. This was possibly due to the diminished number of *Mecps2-stop* mice since some died or were culled.

4 Immunohistochemistry

4.1 Introduction

RTT mouse models provide potent resources for investigating the genotype–phenotype pathway. In Chapter 3, I examined the phenotype progression in the *Mecp2-stop* male mice. However, the underlying alterations to neuronal network behaviour that lead to the clinical symptoms are still poorly understood. Amongst the prominent clinical features of RTT are abnormal EEG patterns and a predisposition to epilepsy (Chahrour & Zoghbi, 2007). Most RTT patients have seizures, ranging from benign focal partial convulsions to generalised intractable epilepsies (Jian *et al.*, 2006). Molecular changes that occur during epileptogenesis are not yet clarified and could be attributed to cell death, reorganisation of neural networks, alterations in the release of neurotransmitters, etc (Herman, 2006). These changes cause neuronal networks to become hyperexcitable, and may lead to seizures.

Recent laboratory studies have observed the hyperexcitable state within cortical and hippocampal circuits in RTT mouse models (Dani *et al.*, 2005; Nelson *et al.*, 2006; Zhang *et al.*, 2008; Wood & Shepherd, 2010). The crucial mechanism that underlies hyperexcitability might be due to the loss or dysfunction of inhibitory neurons. Interestingly, one recent report showed that functional knock-out of MeCP2 selectively in inhibitory neurons could recapitulate most of the RTT-like symptoms in mice, including seizure disorder and hyperexcitable discharging patterns in EEG recordings (Chao *et al.*, 2010). A previous study has also demonstrated that lack of MeCP2 disrupted the development and function of inhibitory neuronal circuits (Zhang *et al.*, 2010). In summary, MeCP2 is regarded as critical to the development and functions of inhibitory neuronal networks.

In the mammalian brain, inhibitory neurons can be further classified into distinct subgroups by various protein markers (Druga, 2009). Although the pivotal function of inhibitory neurons may underlie the pathogenesis of seizures in RTT patients, few studies have focused on the role of MeCP2 in the development and functioning of inhibitory neurons, and they have particularly rarely focused on the alterations of distinct subgroups of inhibitory neurons.

The aim of the work presented in this chapter was to assess the possible alterations in cell density and distribution pattern of each subtype of inhibitory neurons. In this chapter, I first assessed the cell densities of the cortex in both symptomatic *Mecp2-stop* and WT brains to obtain the correcting factor for the standardisation of cell density of each subtype of inhibitory neurons. Secondly, the cell density of each subgroup of inhibitory neurons in the symptomatic *Mecp2-stop* and WT cortices was assessed and standardised by the correcting factor. Thirdly, the distribution pattern of distinct neuronal subtypes in the symptomatic *Mecp2-stop* hippocampus was characterised and compared with that of the WT hippocampus.

4.2 Macroscopic structure of the symptomatic *Mecp2-stop* mouse cortex

The cortical thickness of both symptomatic *Mecp2-stop* (score 5 or more) and WT mice were assessed microscopically. The cortical thickness measurement was accomplished in the primary motor cortex (coronal section ranges from Bregma -0.1 to 0.74mm) and primary somatosensory cortex (coronal section ranges from Bregma 2.8 to 3.6mm) in both symptomatic *Mecp2-stop* and WT brains. Figure 4.1(A) presents the measurement of cortical thickness in the primary motor cortex at Bregma 0.2mm. As shown in figure 4.1(B)&(C), the cortical thickness of primary motor cortex in symptomatic *Mecp2-stop* mouse was significantly thinner than that of age-matched WT mouse (data was shown as mean ± SEM; WT= 1493 ± 58.58 μm, n=4 animals; symptomatic *Mecp2-stop*= 1292 ± 72.47 μm, n=4 animals; p<0.001; data collected and analysed by Dr Rosie Spike). This data was comparable with the cortical thickness data of the primary somatosensory cortex of symptomatic *Mecp2-stop* mice. As illustrated in figure 4.1(D), the cortical thickness of the primary somatosensory cortex in symptomatic *Mecp2-stop* mice was also significantly thinner than that of WT mice (data was shown as mean ± SEM; WT= 1189 ± 53.3 μm, n=5 animals; symptomatic *Mecp2-stop*= 1062 ± 68.33 μm, n=4 animals; p<0.001; data collected and analysed by myself). All these data together indicated that the cortex of symptomatic *Mecp2-stop* mouse is thinner than that of WT mouse.

A

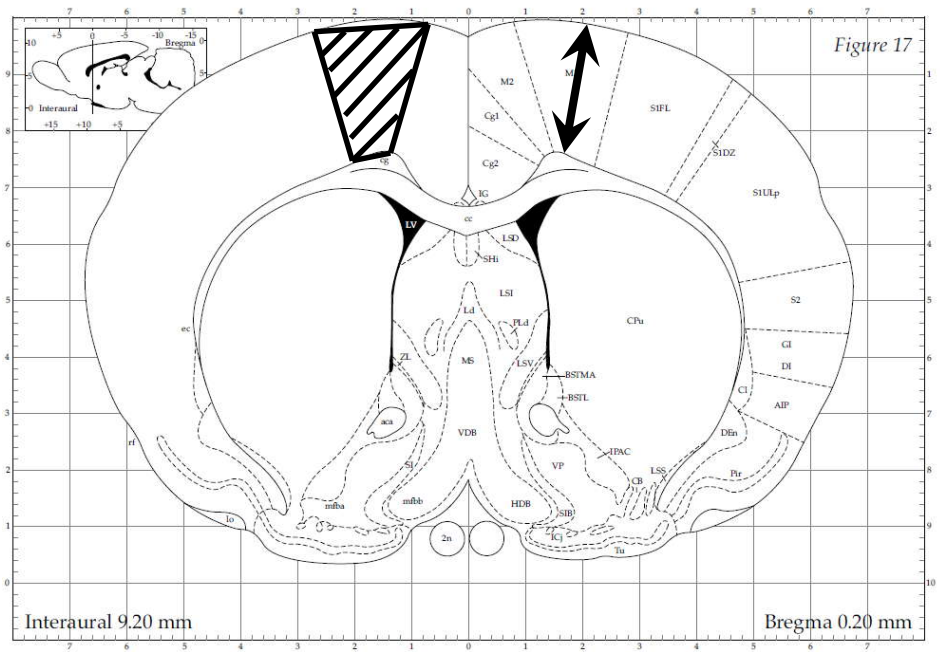
Figure 17
Bregma
Interaural
M2
M1
Cg1
Cg2
S1FL
S1DZ
S1ULp
S2
RG
cc
LV
LSD
SHi
LSI
Ld
PLd
CPu
ec
ZL
MS
LSV
BSTMA
BSTL
aca
VDB
IPAC
VP
LSS
CB
Pir
DEn
AIP
DI
GI
Cl
rf
SI
mfba
mfbb
HDB
SIB
2n
ICj
Tu
Io
Interaural 9.20 mm
Bregma 0.20 mm

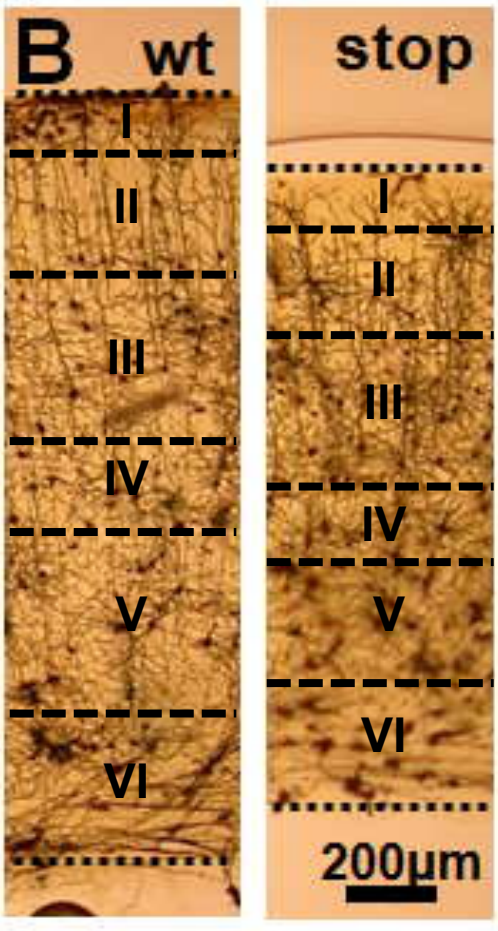
B wt
stop
I
II
III
IV
V
VI
200µm

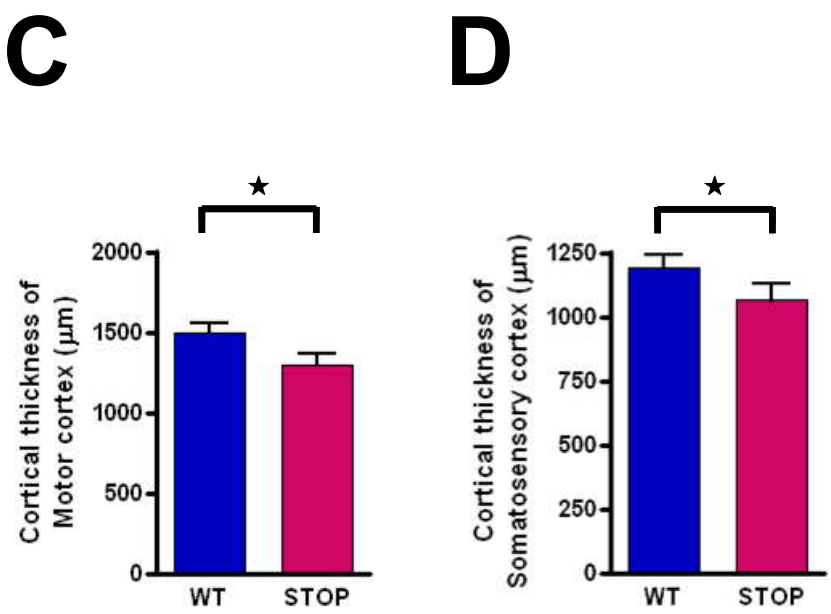

Figure 4.1 The cortical thickness of symptomatic *Mecp2-stop* mice was thinner in WT mice.

(A) Illustration of measurement of cortical thickness in primary motor cortex of mouse. (B) Representative micrographs for cortical thickness measurement of primary motor cortex in both symptomatic *Mecp2-stop* and WT brains. (C) Comparison of cortical thickness of primary motor cortex in both symptomatic *Mecp2-stop* and WT brains. (D) Comparison of cortical thickness of primary somatosensory cortex in both symptomatic *Mecp2-stop* and WT brains. All data presented as mean ± SEM.

4.3 Cortical cell density quantifications in the somatosensory cortex in *Mecp2-stop* mice

4.3.1 Cell densities in layer five of the somatosensory cortex in symptomatic Mecp2-stop mice

As detailed in chapter 2, the cell quantification work in the following sections was carried out on brains from symptomatic *Mecp2-stop* mice and their WT littermates. The brains were fixed with paraformaldehyde prior to immunostaining and image analysis. In order to assess the cortical cell density, DAPI-positive cell densities in the somatosensory cortex layer five of both symptomatic *Mecp2-stop* mice and age-matched WT littermates were examined. The cortical layer five was chosen because it is the main output layer of the cortex, and because it is easy to recognise even without counterstaining. In particular, the large pyramidal cells in cortical layer five of the primary somatosensory cortex in *Mecp2*-null mice have been reported to have reduced spontaneous firing at both early postnatal developmental stages by using whole-cell patch-clamp recordings (Dani *et al.*, 2005).

As presented in figure 4.2(A)-(C), all the brain sections used in this chapter were co-stained with DAPI and NeuN markers. The cell density quantification was carried out in image stacks by applying disector methods manually (see details in Chapter 2). As shown in figure 4.2(D), the DAPI positive cell density in somatosensory cortex layer five of symptomatic *Mecp2-stop* mice was 1.28 times greater than that of WT littermates (data shown as mean ± SEM; WT= 271851.3 ± 6845.7 cells/mm^3, n=10 from 5 animals; *Mecp2-stop*= 348671.6 ± 9014.2 cells/mm^3, n=10 from 4 animals; p<0.0001).

In the rodent cortical layer five, neurons constitute 70-80% of the cell population (Bass *et al.*, 1971). In order to evaluate whether neuronal density was also different in the symptomatic *Mecp2-stop* mouse brain, NeuN-positive cell densities in the somatosensory cortex layer five of both symptomatic *Mecp2-stop* and WT mice were analysed. NeuN is a neuronal nuclear antigen and was detected in most neuronal types within the mouse brain; therefore NeuN is recognised as a neuronal marker (Herculano-Houzel & Lent, 2005). As shown in figure 4.2(D), NeuN-positive cell density was 1.41 times greater than that of WT

(data shown as mean ± SEM; WT= 206620.2 ± 7254.2 cells/mm^3, *n*=10 from 5 animals; *Mecp2-stop*= 290504.5 ± 9600.8 cells/mm^3, *n*=10 from 4 animals; *p*<0.0001).

Since the DAPI and NeuN positive cell count were quantified from the same regions of brain sections, NeuN-positive cell percentage of the total cortical population in layer five of somatosensory cortex was calculated. As illustrated in figure 4.2(E)&(F), NeuN-positive percentage in layer five of somatosensory cortex had no statistical difference between *Mecp2-stop* and WT groups (data shown as mean ± SEM; WT(NeuN)= 76 ± 2.67%, WT(non-NeuN)=24 ± 2.43%, *n*=10 from 5 animals; *Mecp2-stop*(NeuN)= 83.3 ± 2.75%, *Mecp2-stop*(non-NeuN)=16.7 ± 2.53%, *n*=10 from 4 animals; Chi-Square test, *p*=0.0726). Although a trend towards a higher proportion of neurons in symptomatic *Mecp2-stop* mice existed, these results have demonstrated that the NeuN-positive cell density in the symptomatic *Mecp2-stop* mouse brain is elevated, compared to WT mice, and is roughly proportional to the total cortical cell density alteration.

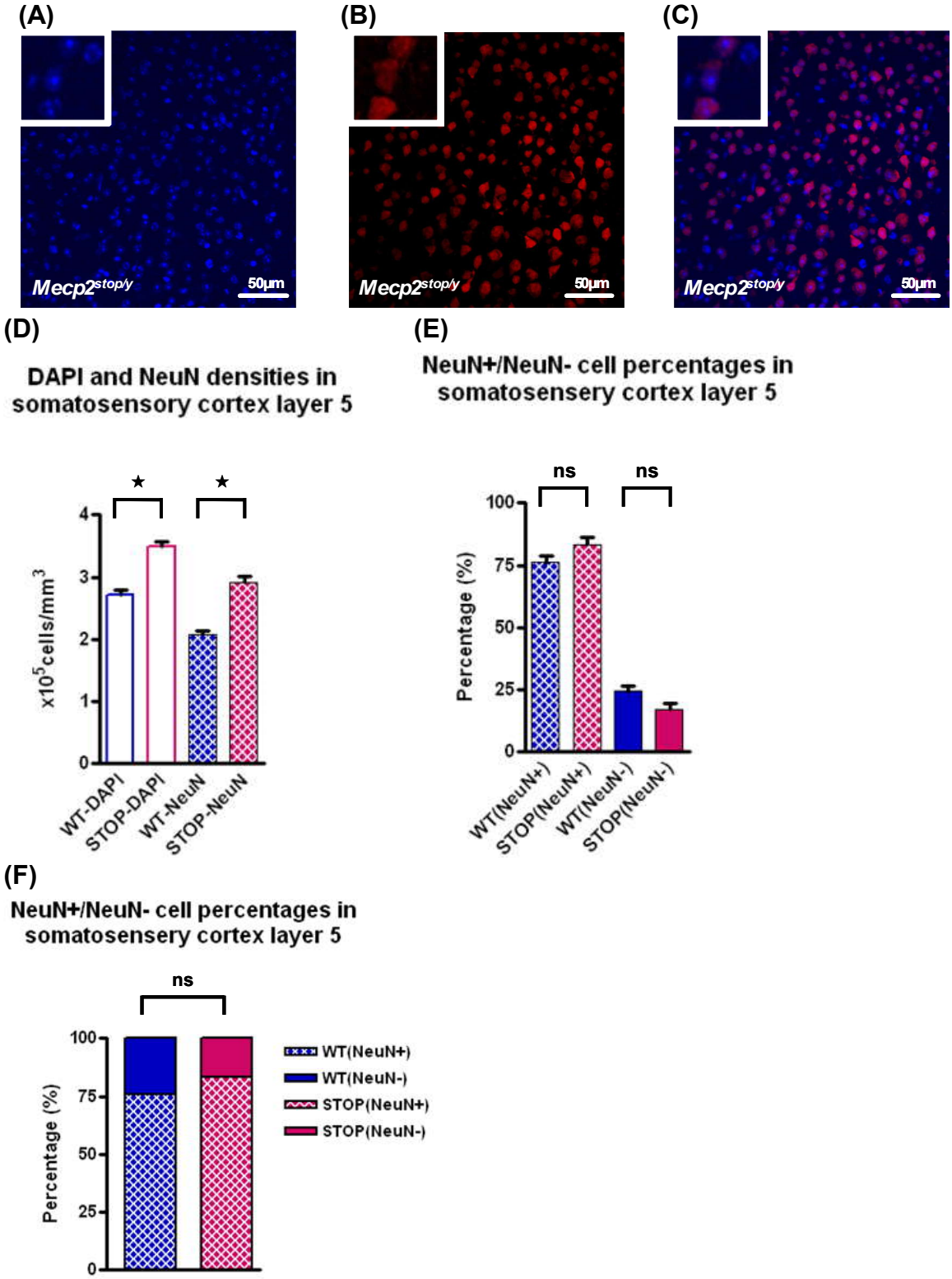

Figure 4.2 Cell densities elevated with remaining NeuN-positive percentage in layer five of somatosensory cortex in symptomatic *Mecp2-stop* mice.

(A)-(C) Confocal images of DAPI-positive and NeuN-positive cells. DAPI is coloured blue while NeuN is coloured red. High power insets from (A)-(C) are shown at upper left corners. (D) DAPI-positive and NeuN-positive cortical cell densities in symptomatic *Mecp2-stop* mice and their WT littermates. (D)&(E) The percentage of NeuN-positive and NeuN-negative cells in layer five of somatosensory cortex in both symptomatic *Mecp2-stop* and WT cortices.

4.3.2 Categorisation of inhibitory interneurons in the somatosensory cortex layer V by the expression of calcium-binding proteins

Neurons releasing excitatory neurotransmitters are regarded as excitatory neurons and neurons releasing inhibitory neurotransmitters are regarded as inhibitory neurons. Recently, functional knock-out of MeCP2 selectively in inhibitory neurons was reported to recapitulate most of the RTT-like symptoms in mice (Chao *et al.*, 2010). Inhibitory neurons comprise subgroups of neurons with distinct electrical and anatomical properties. In the mammalian cortex, inhibitory neurons can be further classified into distinct subtypes on the basis of protein markers; parvalbumin (PV), somatostatin (SOM), calretinin (CR) and calbindin (CB). In the following sections, these protein markers (as illustrated in figure 4.3) were examined to assess whether the cell density of different inhibitory neuron subtypes was altered in the somatosensory cortex of symptomatic *Mecp2-stop* mice.

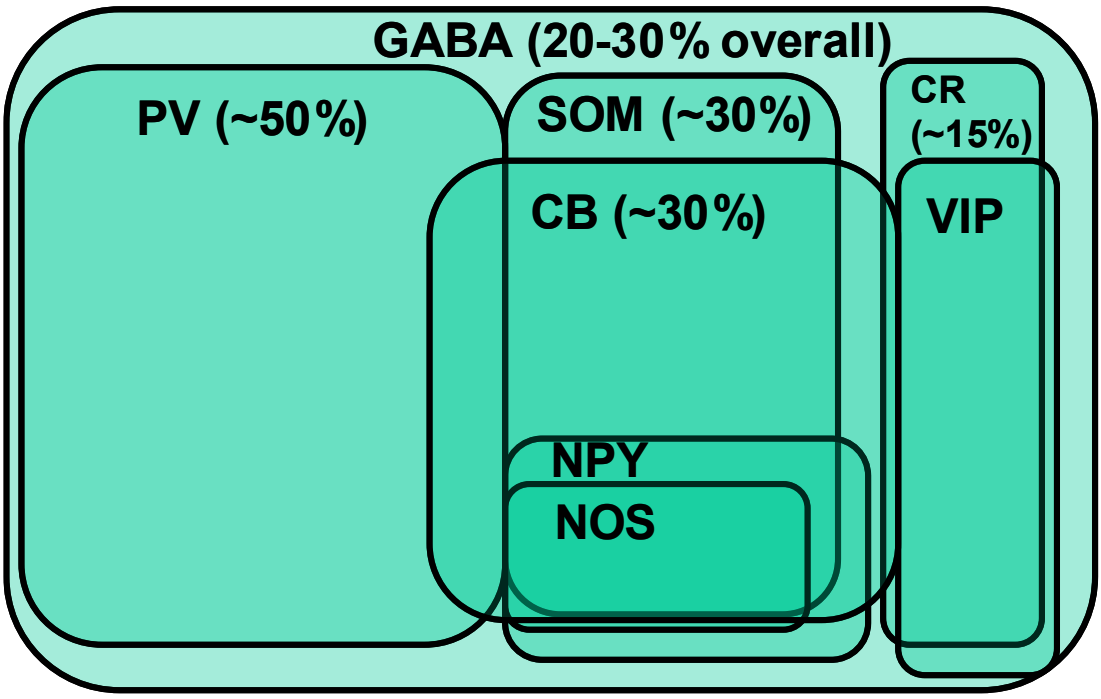

Figure 4.3 The percentage of distinct inhibitory neurons in rodent cortical layers V & VI.

In order to discriminate distinct subtypes of inhibitory neurons (GABAergic neurons), different protein markers were applied. In rodent cortical layers V & VI, PV positive cells comprise ~50% of all inhibitory neurons, while SOM positive cells comprise ~30%, CR positive cells comprise ~15%, and CB positive cells comprise ~30% (most CB positive cells were recognised by more than one protein marker). Therefore, more than 95% of inhibitory neurons could be recognised by staining with one or more of these four markers (PV, SOM, CR and CR). Adopted and modified from Kubota *et al.*, 1994 (Kubota *et al.*, 1994).

4.3.3 Parvalbumin (PV) positive cell density in layer five of the somatosensory cortex in symptomatic Mecp2-stop mice

The cell density of PV positive neurons in layer five of the somatosensory cortex was quantified in confocal image stacks by manual counting with the disector principle (see Chapter 2). As shown in figure 4.4(B), the raw PV positive cell density in the somatosensory cortex layer five of symptomatic *Mecp2-stop* mice was significantly increased compared to WT mice (data shown as mean ± SEM; WT= 38516.3 ± 1497.5 cells/mm^3, *n*=30 regions from 5 animals; *Mecp2-stop*= 51756.9 ± 2791.3 cells/mm^3, *n*=24 regions from 4 animals; *p*<0.0001). In section 4.3.1, the total cortical cell density (DAPI-positive cell density) in layer five of somatosensory cortex in symptomatic *Mecp2-stop* mice was shown to be 1.28 times greater than that of WT mice (the *Mecp2-stop*/WT DAPI correcting factor= 1.28). In order to calibrate the effect of higher cell density in the *Mecp2-stop* mouse brain, the raw PV positive density was standardised by the *Mecp2-stop*/WT DAPI correcting factor. The DAPI-standardised PV positive cell density equals to the raw PV positive cell density divided by the *Mecp2-stop*/WT DAPI correcting factor. As presented in figure 4.4(B), after calibration with the *Mecp2-stop*/WT DAPI correcting factor, there was no difference between *Mecp2-stop* and WT groups (data shown as mean ± SEM; WT= 38516.3 ± 1497.5 cells/mm^3, *n*=30 regions from 5 animals; *Mecp2-stop*= 40353.7 ± 2176.3 cells/mm^3, *n*=24 regions from 4 animals; *p*=0.48).

In this chapter, I also applied the *Mecp2-stop*/WT NeuN correcting factor to calibrate the raw cell density. In section 4.3.1, the total neuronal cell density (NeuN-positive cell density) in layer five of the somatosensory cortex in symptomatic *Mecp2-stop* mice was shown to be 1.41 times greater than that of WT mice (the *Mecp2-stop*/WT NeuN correcting factor = 1.41). The NeuN-standardised PV positive cell density is equal to the raw PV positive cell density divided by the *Mecp2-stop*/WT NeuN correcting factor. As shown in figure 4.4(B), after calibration with the *Mecp2-stop*/WT NeuN correcting factor, there was no difference between *Mecp2-stop* and WT groups (data shown as mean ± SEM; WT= 38516.3 ± 1497.5 cells/mm^3, *n*=30 regions from 5 animals; *Mecp2-stop*= 36811.9 ± 1985.3 cells/mm^3, *n*=24 regions from 4 animals; *p*=0.49).

(A) (B)

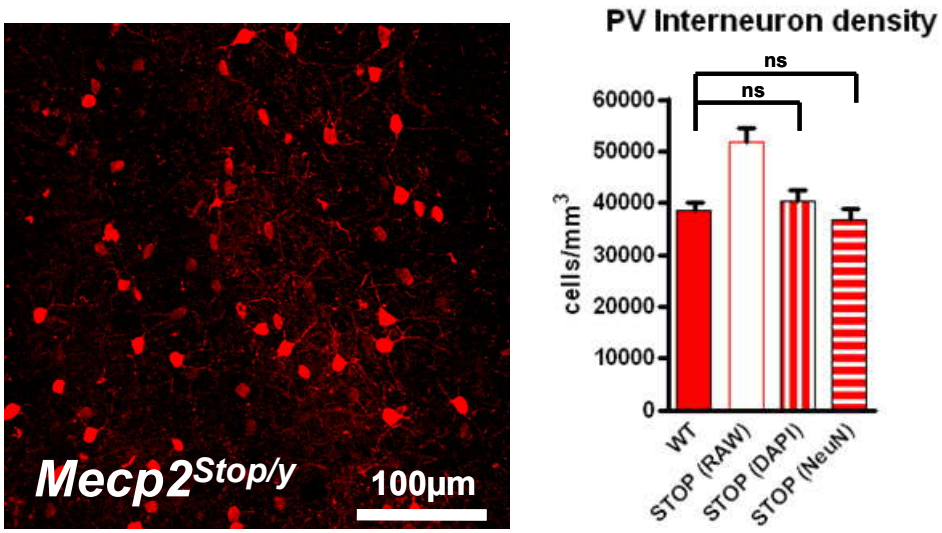

Figure 4.4 Parvalbumin (PV)-positive cell density in layer five of the somatosensory cortex layer five in symptomatic *Mecp2-stop* mice.

(A) Representative micrograph of PV-positive cells in layer five of the somatosensory cortex in symptomatic *Mecp2-stop* brains. PV-positive cells are coloured red. (B) The PV-positive cell density in symptomatic *Mecp2-stop* (raw data and after calibrations) and WT mice. All data shown as mean ± SEM.

4.3.4 Somatostatin (SOM) positive cell density in layer five of the somatosensory cortex in symptomatic Mecp2-stop mice

I next examined the cell density of SOM immunopositive neurons in layer five of the somatosensory cortex in symptomatic *Mecp2-stop* mice. As shown in figure 4.5(B), the raw SOM positive cell density in layer five of the somatosensory cortex showed no difference between *Mecp2-stop* and WT groups (data shown as mean ± SEM; WT= 20381.3 ± 1381.7 cells/mm^3, *n*=30 regions from 5 animals; *Mecp2-stop* = 23559.1 ± 1018.6 cells/mm^3, *n*=24 regions from 4 animals; *p*=0.08). After calibration with the *Mecp2-stop*/WT DAPI correcting factor, there was no difference between *Mecp2-stop* and WT groups (data shown as mean ± SEM; WT= 20381.3 ± 1381.7 cells/mm^3, *n*=30 regions from 5 animals; *Mecp2-stop*= 18368.5 ± 794.2 cells/mm^3, *n*=24 regions from 4 animals; *p*=0.2544). Interestingly, after calibration with the *Mecp2-stop*/WT NeuN correcting factor, the NeuN-standardised SOM positive cell density in layer five of the somatosensory cortex in symptomatic *Mecp2-stop* mice was significantly decreased compared to that of WT mice (data shown as mean ± SEM; WT= 20381.3 ± 1381.7 cells/mm^3, *n*=30 regions from 5 animals; *Mecp2-stop*= 16756.3 ± 724.5 cells/mm^3, *n*=24 regions from 4 animals; *p*=0.04).

(A) **(B)**

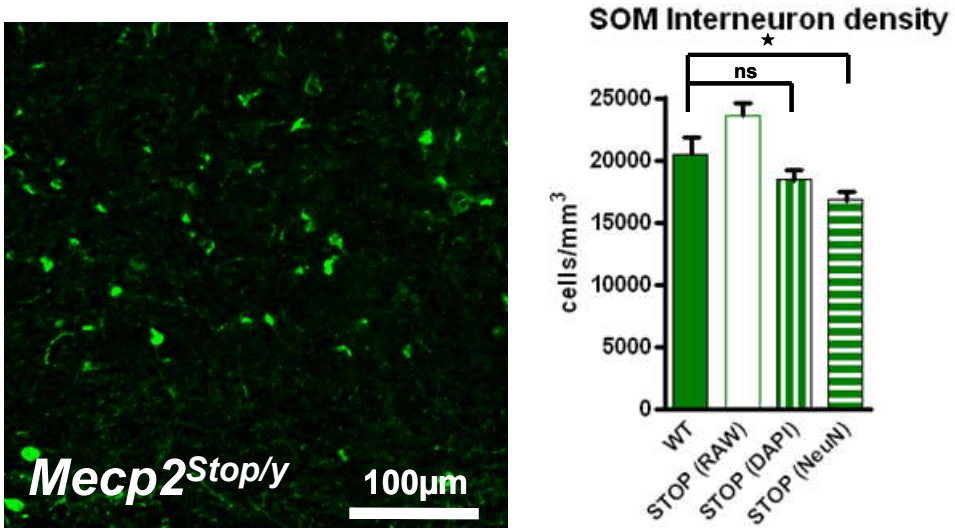

Figure 4.5 Altered cell density of somatostatin (SOM) positive neurons in the somatosensory cortex in symptomatic *Mecp2-stop* after the NeuN correcting factor calibration.

(A) Representative micrograph of SOM-positive cells in layer five of the somatosensory cortex in symptomatic *Mecp2-stop* brains. SOM-positive cells are coloured green. (B) The SOM-positive cell density in symptomatic *Mecp2-stop* (raw data and after calibrations) and WT mice. All data shown as mean ± SEM.

4.3.5 Calretinin (CR) positive cell density in layer five of the somatosensory cortex in symptomatic Mecp2-stop mice

The cell density of CR immunopositive neurons in layer five of the somatosensory cortex in symptomatic *Mecp2-stop* mice was also assessed. As shown in figure 4.6(B), the raw CR positive cell density in layer five of the somatosensory cortex showed no difference between *Mecp2-stop* and WT groups (data shown as mean ± SEM; WT= 9944.1 ± 978.5 cells/mm^3, *n*=30 regions from 5 animals; *Mecp2-stop* = 9971.5 ± 687.4 cells/mm^3, *n*=24 regions from 4 animals; *p*=0.98). After calibration with the *Mecp2-stop*/WT DAPI correcting factor, the DAPI-standardised CR positive cell density in layer five of the somatosensory cortex in symptomatic *Mecp2-stop* mice was significantly decreased compared to that of WT mice (data shown as mean ± SEM; WT= 9944.1 ± 978.5 cells/mm^3, *n*=30 regions from 5 animals; *Mecp2-stop*= 7774.6 ± 535.9 cells/mm^3, *n*=24 regions from 4 animals; *p*=0.04). The same decrease was also observed after calibration with the *Mecp2-stop*/WT NeuN correcting factor. The NeuN-standardised CR positive cell density in layer five of the somatosensory cortex in symptomatic *Mecp2-stop* mice was significantly decreased compared to that of WT mice (data shown as mean ± SEM; WT= 9944.1 ± 978.5 cells/mm^3, *n*=30 regions from 5 animals; *Mecp2-stop*= 7092.2 ± 488.9 cells/mm^3, *n*=24 regions from 4 animals; *p*=0.02).

(A) **(B)**

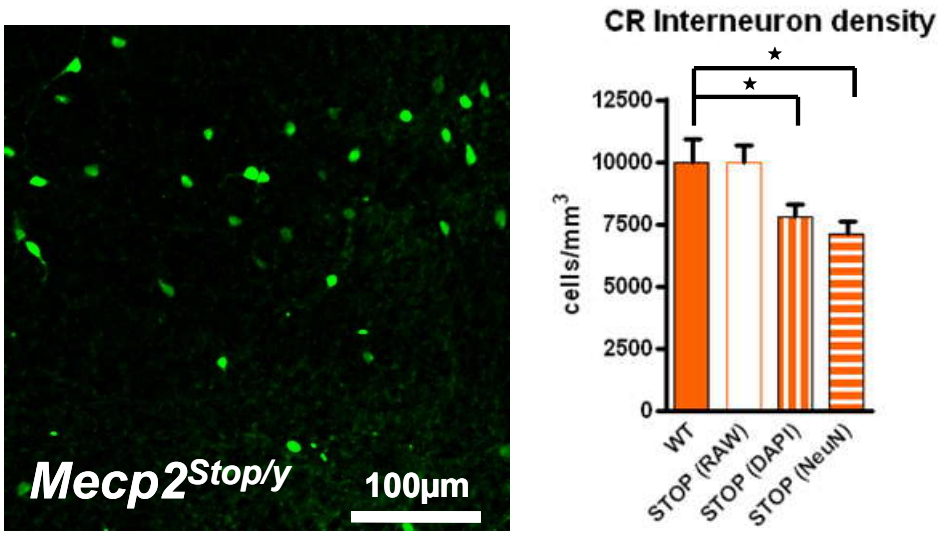

Figure 4.6 Altered cell densities of calretinin (CR) positive neurons in symptomatic *Mecp2-stop* somatosensory cortex after DAPI or NeuN correcting factor calibrations.

(A) Representative micrograph of CR-positive cells in layer five of the somatosensory cortex in symptomatic *Mecp2-stop* brains. CR-positive cells are coloured green. (B) The CR-

positive cell density in symptomatic *Mecp2-stop* (raw data and after calibrations) and WT mice. All data shown as mean ± SEM.

4.3.6 Calbindin (CB) positive cell density in layer five of the somatosensory cortex in symptomatic Mecp2-stop mice

The cell density of CB immunopositive neurons in layer five of the somatosensory cortex in symptomatic *Mecp2-stop* mice was assessed. As shown in figure 4.7(B), the raw CB positive cell density in layer five of the somatosensory cortex showed no difference between *Mecp2-stop* and WT groups (data shown as mean ± SEM; WT= 26435.5 ± 1632.2 cells/mm^3, *n*=30 regions from 5 animals; *Mecp2-stop* = 31010.3 ±1829.9 cells/mm^3, *n*=24 regions from 4 animals; *p*=0.07). After standardisation with the *Mecp2-stop*/WT DAPI correcting factor, the DAPI-standardised CB positive cell density in layer five of the somatosensory cortex showed no difference between symptomatic *Mecp2-stop* and WT groups (data shown as mean ± SEM; WT= 26435.5 ± 1632.2 cells/mm^3, *n*=30 regions from 5 animals; *Mecp2-stop*= 24178 ±1426.7 cells/mm^3, *n*=24 regions from 4 animals; *p*=0.32). After calibration with the *Mecp2-stop*/WT NeuN correcting factor, the NeuN-standardised CB positive cell density in layer five of the somatosensory cortex showed no difference between *Mecp2-stop* and WT groups (data shown as mean ± SEM; WT= 26435.5 ± 1632.2 cells/mm^3, *n*=30 regions from 5 animals; *Mecp2-stop*= 22056 ±1301.5 cells/mm^3, *n*=24 regions from 4 animals; *p*=0.053).

(A) **(B)**

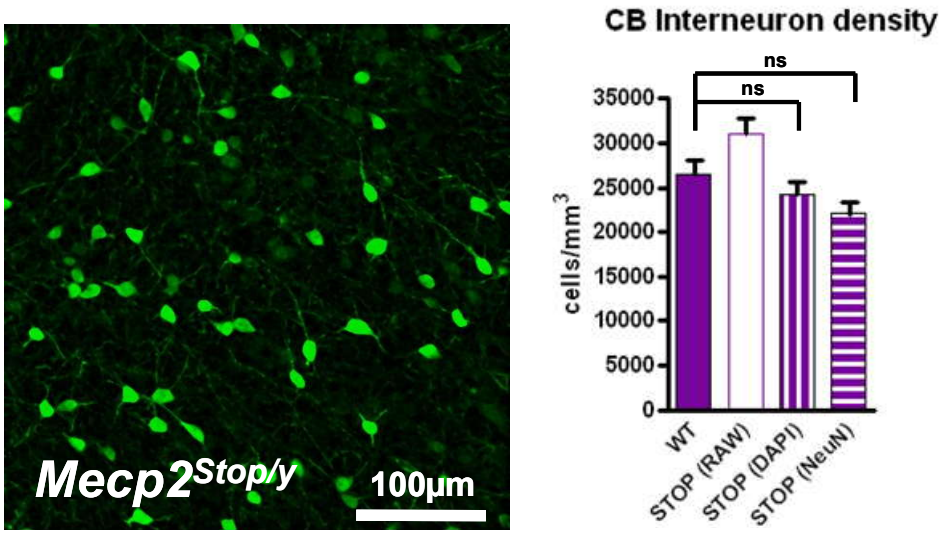

Figure 4.7 The cell density of calbindin (CB) positive neurons remained no change in layer five of somatosensory cortex in symptomatic *Mecp2-stop* mice.

(A) Representative micrograph of CB-positive cells in layer five of the somatosensory cortex in symptomatic *Mecp2-stop* brains. CB-positive cells are coloured green. (B) The CB-positive cell density in symptomatic *Mecp2-stop* (raw data and after calibrations) and WT mice. All data shown as mean ± SEM.

4.4 Morphological analyses in the hippocampus in symptomatic *Mecp2-stop* mice

After assessing the cell density change of inhibitory neuronal subtypes in layer five of the somatosensory cortex in symptomatic *Mecp2-stop* mice, I further examined the distribution pattern of inhibitory neuronal subtypes in the hippocampus. The hippocampus was chosen because its structure and neuronal circuits are already well-investigated and can provide an excellent platform for recognising alterations in distribution pattern of distinct neuronal subtypes (see section 1.3.4).

4.4.1 PV and SOM positive cell distribution patterns in the hippocampus in symptomatic Mecp2-stop mice

As detailed in Chapter 2, the morphological work in the following sections was carried out on brains from symptomatic *Mecp2-stop* mice and their WT littermates. The brains were fixed with paraformaldehyde prior to immunostaining and image analysis. First I examined brain sections co-stained with both parvalbumin (PV) and somatostatin (SOM) protein markers.

As illustrated in figure 4.8, brain sections from both symptomatic *Mecp2-stop* and WT mice revealed identical distribution patterns in hippocampal CA1 regions under microscopic examinations. Since most hippocampal PV positive cells are inhibitory neurons which directly target to the pyramidal cells located at the stratum pyramidale layer (sp), one obvious red band that represented PV positive neuronal innervations was clearly detected in the sp layers in both images (see in figure 4.8(B)-(G)).

(A)

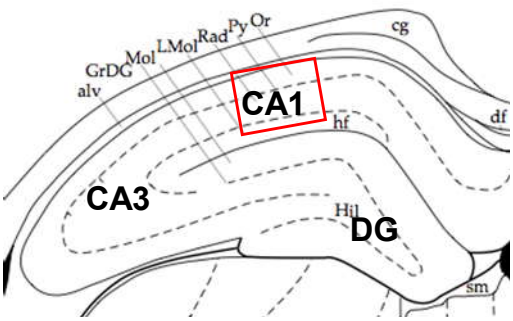

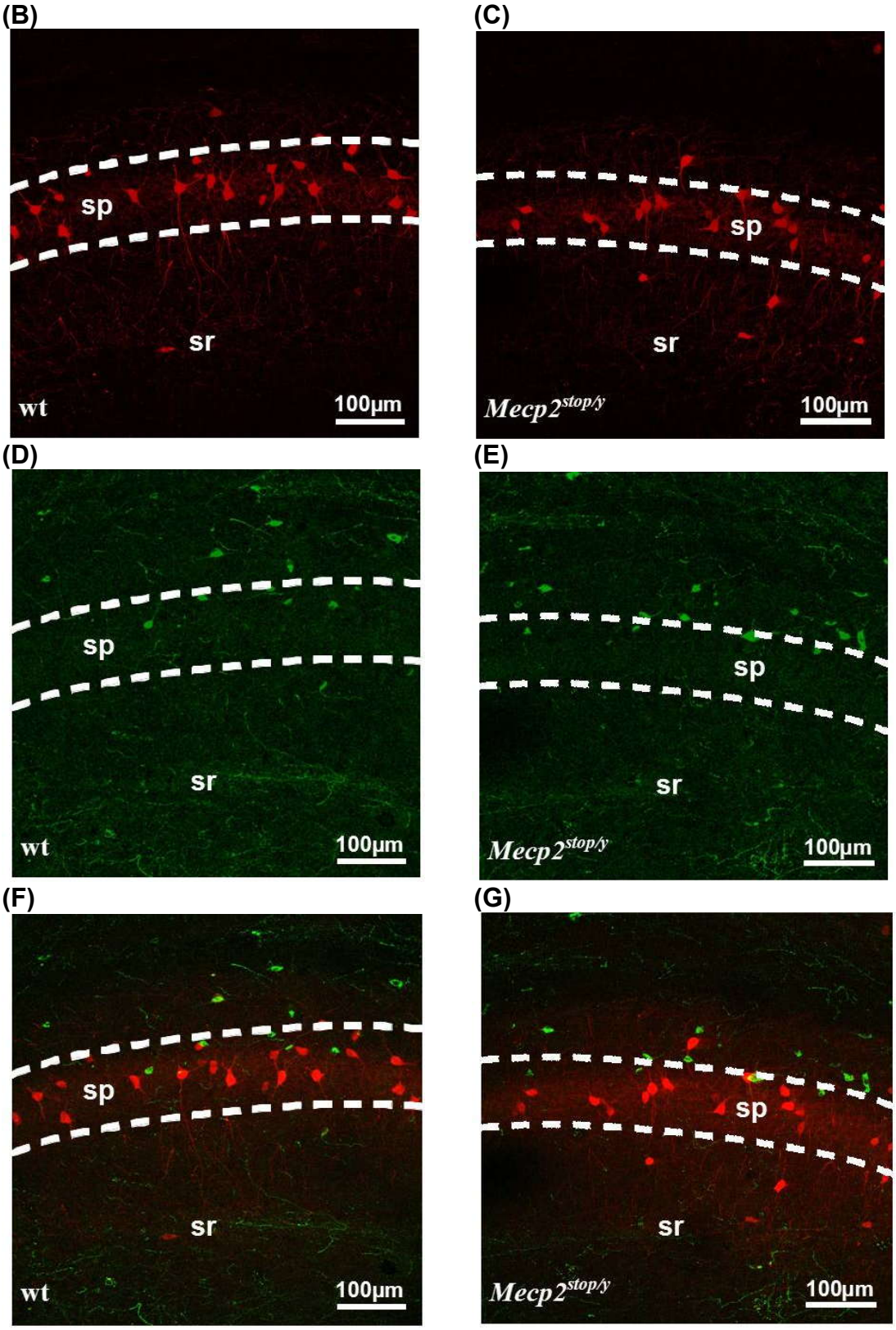

Figure 4.8 PV-positive cells in the hippocampal CA1 region of symptomatic *Mecp2-Stop* mice had an identical distribution pattern to that of WT mice.

(A) Illustration of demonstrative areas in (B)-(G) in hippocampal CA1 regions. (B),(D)&(F) Under confocal microscopic examinations, PV positive cells were stained red while SOM positive cells were stained green. The figure represents the PV positive distribution pattern in the WT CA1 region. Most PV positive cells were located in the stratum pyramidale (sp) and targeted pyramidal cells in the same sp layer (red band). (C),(E)&(G) Confocal images show identical distribution patterns in symptomatic *Mecp2-stop* mice brains. Similarly, PV positive innervations are visible in the sp layer and show the same distribution pattern.

Figure 4.9 further reveals the innervation pattern of PV positive cells in the sp layer of CA1 region in the hippocampus. In both symptomatic *Mecp2-stop* and WT hippocampi, PV positive cells (coloured red) project axons to form string-like innervations around proximal pyramidal cells (coloured blue with DAPI stain).

With regard to the SOM immunopositive neurons, shown in figure 4.10, these cells in the hippocampal CA1 region of symptomatic *Mecp2-stop* mice were located in the stratum oriens layer (so) and sent out innervations through the stratum radiatum layer (sr) to reach the stratum lacunosum-moleculare layer (slm) and form a green band in the slm layer. This identical distribution pattern has been reported previously in normal WT rodents (Jinno & Kosaka, 2006).

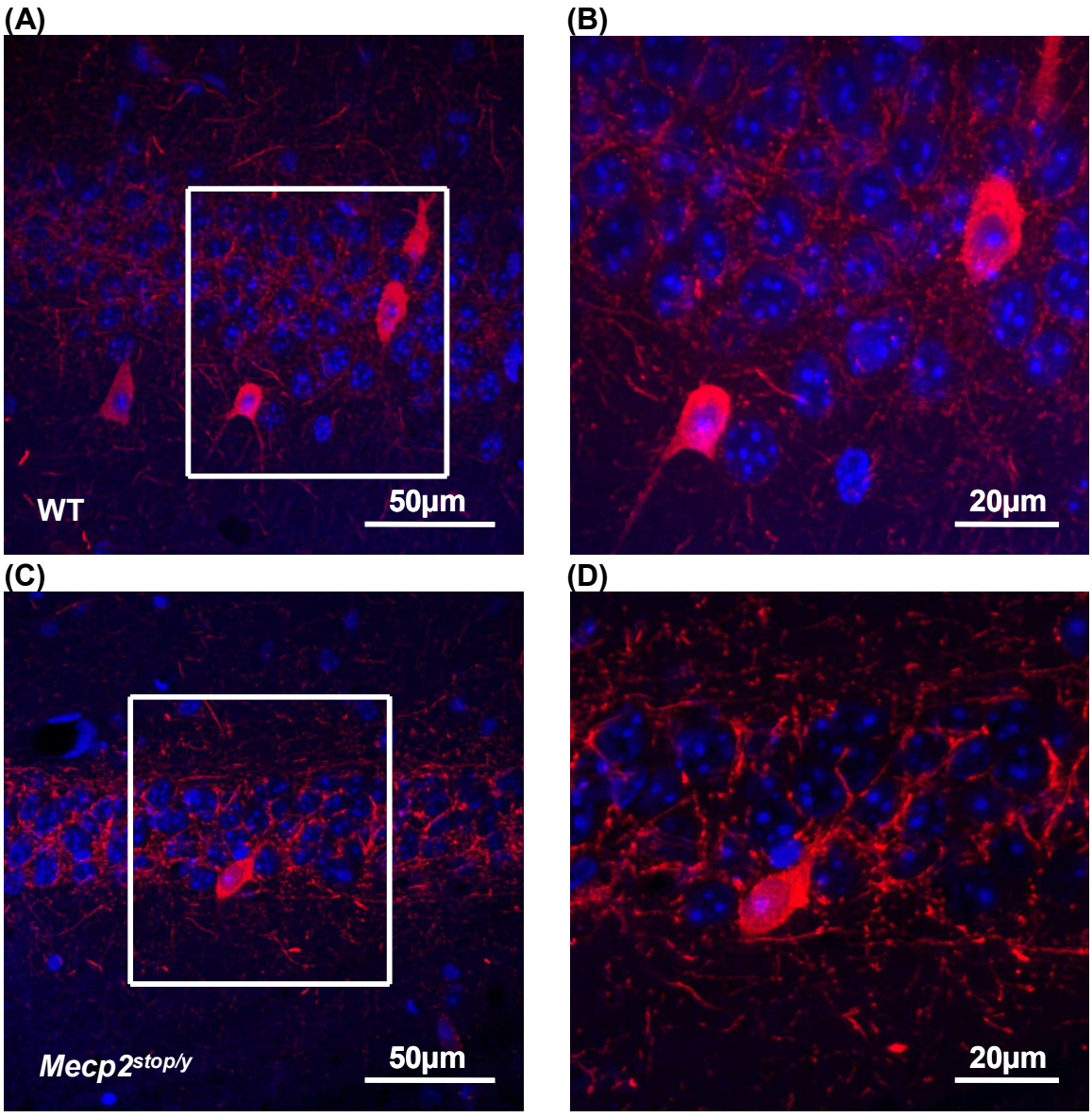

Figure 4.9 PV positive cells in stratum pyramidale at CA1 regions of symptomatic *Mecp2-stop* and WT mice showed an identical distribution pattern.

Under the confocal microscopic examinations, PV positive cells are coloured red while DAPI positive cells are coloured blue. The white boxes in (A)&(C) label the same regions which

are further magnified to be micrographs as (B)&(D) to show more detailed PV positive cell distribution pattern.

(A)

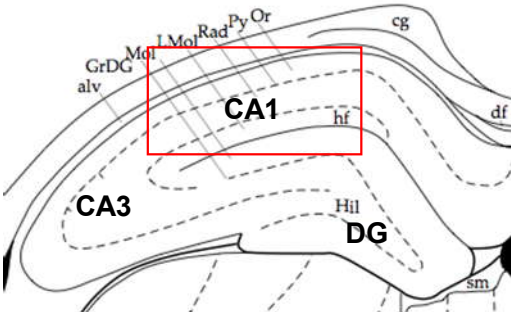

(B) **(C)** **(D)**

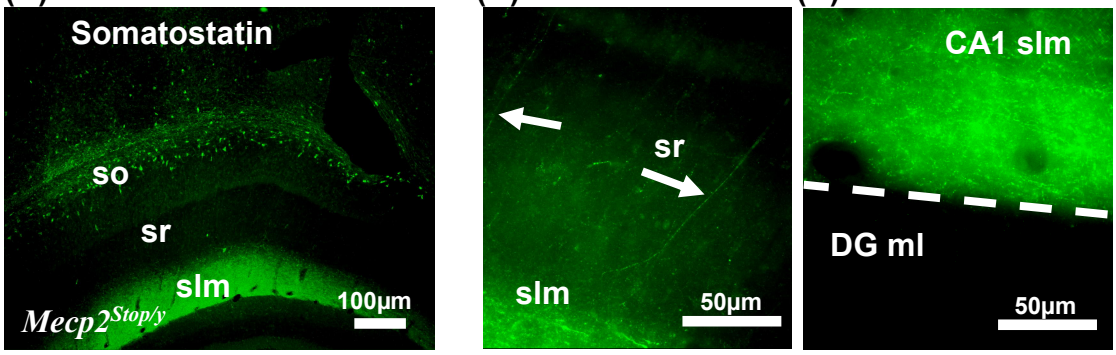

Figure 4.10 SOM positive cells in hippocampal CA1 regions of symptomatic *Mecp2-stop* mice had an identical distribution pattern as that of WT mice.

(A) Illustration of demonstrative areas in (B),(C)&(D) in hippocampal CA1 regions. Under the confocal microscopic examinations, SOM positive areas are coloured green. Figure (B) shows the SOM positive distribution pattern of symptomatic *Mecp2-stop* mice in the hippocampal CA1 region at lower magnification. Demonstrating the same distribution pattern as that of WT mice, most SOM positive cells were located at the stratum oriens layer (so) and sent out innervations through the stratum radiatum layer (sr) to reach the stratum lacunosum-moleculare layer (slm). Figure (C) was magnified from figure (B) and several string-like projections (as indicated by arrows) were visible inside the sr layer and linked from the so layer to the slm layer. Figure (D) shows that the green band formed by SOM positive projections was limited in the slm layer and not beyond the molecular layer (ml) of dentate gyrus.

4.4.2 CR positive cell distribution pattern in the hippocampus in symptomatic Mecp2-stop mice

I next examined the cell distribution pattern of calretinin (CR) immunopositive neurons in the hippocampus. Under the confocal microscopic examination, the CR positive cell (mossy cells) displayed green colour and was clearly recognised at the hippocampal dentate gyrus region (DG). As shown in (B), (C) of figure 4.11, the mossy cell at the hippocampal DG region was CR positive and located inside the hilus of dentate gyrus. Mossy cells projected innervations to pass through the granule cell layer and form a visible green band in the inner molecular layer. An identical distribution pattern of mossy cells was observed in the hippocampi in both symptomatic *Mecp2-stop* and WT mice. The confocal images at hippocampal DG regions were further magnified as (D), (E) of figure 4.11. In these higher power magnified images, the projections which connected the hilus and the inner molecular layer of DG were observed clearly in both the symptomatic *Mecp2-stop* and WT groups.

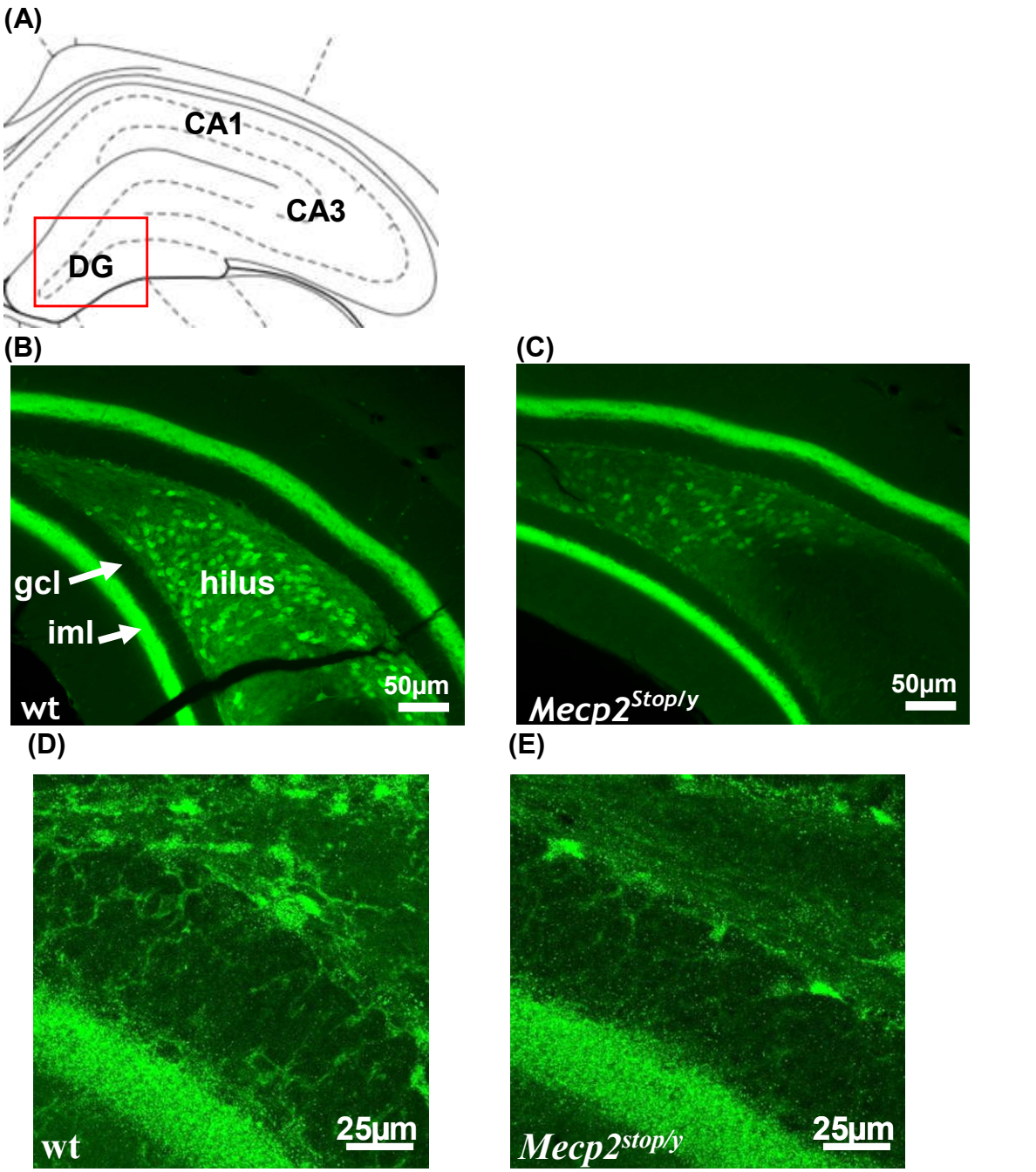

Figure 4.11 CR positive cells in the hippocampal dentate gyrus of the symptomatic *Mecp2-stop* mouse has an identical distribution pattern to that of WT mice.

(A) Illustration of demonstrative areas in (B)&(C) in hippocampal DG regions. Under confocal microscopic examinations, CR positive areas are coloured green. (B) At low power magnification, CR positive cells (mossy cells) were located in the hilus of dentate gyrus (DG) in WT mice brains. Mossy cells inside the DG hilus sent out projections through the granular cell layer (gcl) to reach the inner molecular layer (iml) and form a bright green band in the inner granular cell layer (iml). (C) In the hippocampus of symptomatic *Mecp2-stop* mice, the distribution pattern was the same as that of WT mice. At higher power magnification (D&E), the connections between the DG hilus and the iml layer were observed clearly in both genotype groups.

4.4.3 CB positive cell distribution pattern in the hippocampus in symptomatic Mecp2-stop mice

The distribution pattern of the calbindin (CB) immunopositive neurons in the hippocampus was also assessed. The CB positive cells showed a green colour under the confocal microscopic examination. A subpopulation of hippocampal pyramidal cell shares the CB antigen (the signal is weaker than that of CB positive inhibitory neurons) with CB positive inhibitory neurons. As illustrated in figure 4.12(B), a green band in the stratum pyramidale layer (sp) of WT hippocampal CA1 region was observed. The hippocampus of symptomatic *Mecp2-stop* mouse correspondingly presented an identical distribution pattern (see figure 4.12(C)). In the layer of stratum lacunosum-moleculare (under the stratum radiatum layer), CB positive cells were mainly inhibitory neurons and the cell density was rather lower. In the stratum lacunosum-moleculare layer of hippocampal CA1 regions from both genotype groups, CB positive neurons were observed (indicated by arrows in figure 4.12 (D)&(E)).

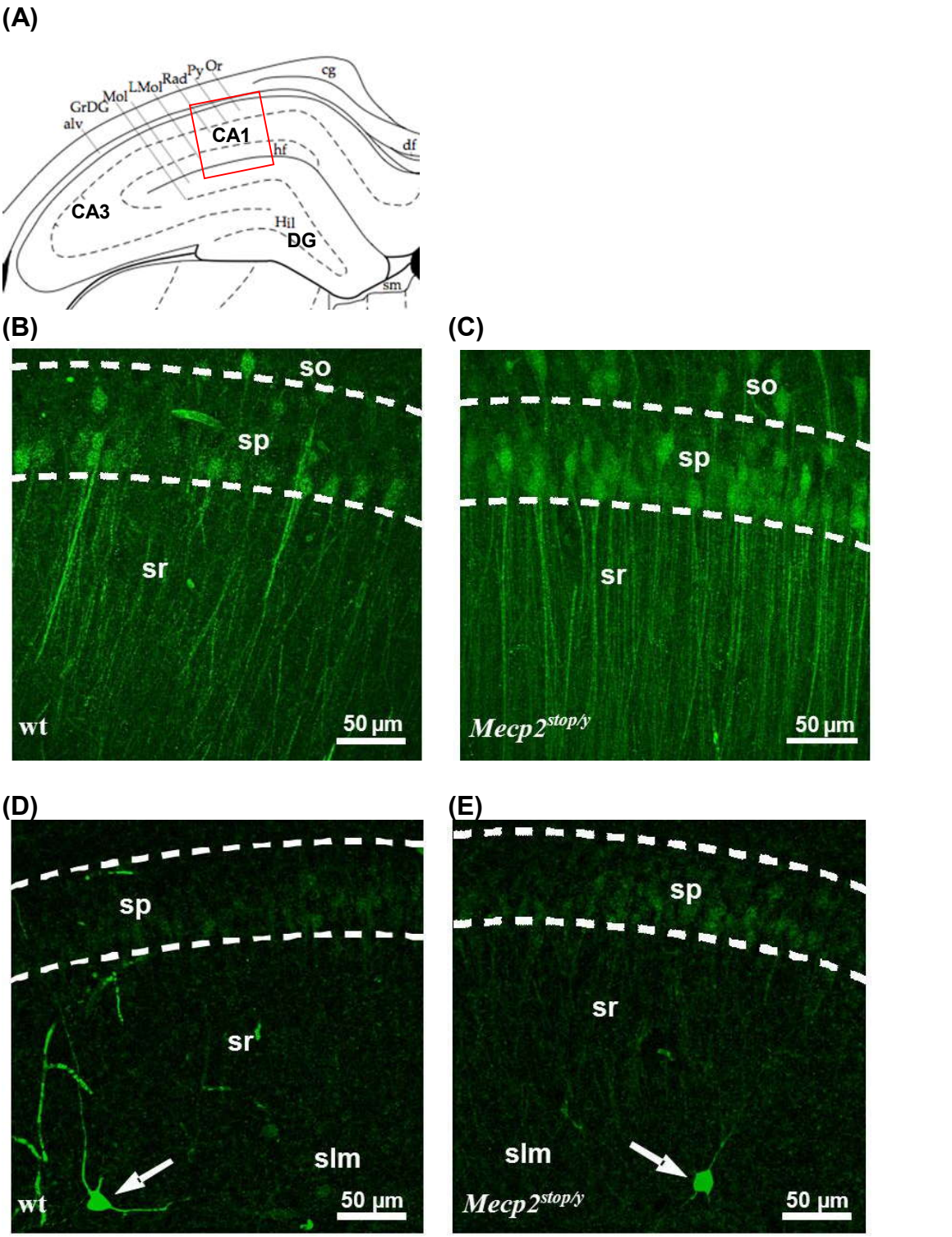

Figure 4.12 CB-positive cell in the hippocampal CA1 region of the symptomatic *Mecp2-stop* mouse has an identical distribution pattern to that of WT mice.

(A) Illustration of demonstrative areas in (B)-(E) in hippocampal CA1 regions. Under the confocal microscopic examinations, CB positive areas are coloured green. The CB marker was shared by a subpopulation of pyramidal cells (the signal is weaker than that of CB positive inhibitory neurons) and CB positive inhibitory neurons. Figure (B) was photographed at the stratum pyramidale layer of WT hippocampal CA1 region and showed that a subgroup of the pyramidal cells were weakly immunopositive. Under the stratum pyramidale layer, few scattered green cells were the CB positive inhibitory neurons (as indicated by arrows in D). Figure (C) was photographed at the stratum pyramidale layer of hippocampal CA1 region from symptomatic *Mecp2-stop* mice and showed an identical distribution pattern to that of WT mice. (D)&(E) Under higher power magnification, a subgroup of pyramidal cells was weakly stained in the sp layer and few CB positive

inhibitory neurons were scattered in the sIm layer of the CA1 region from both symptomatic *Mecp2-stop* and WT mice hippocampi.

4.5 Discussion

In this chapter, all the results can be grouped into three main parts. First, in the cortical thickness measurement, the symptomatic *Mecp2-stop* mouse had a reduced cortical thickness in the primary somatosensory cortex, approximately 89% of the WT cortex. The cortical thickness serves as a one-dimensional indicator, while the change of brain volume needs to be assessed by a three-dimensional measurement. If the reduced percentage was equal in all the three dimensions, the brain volume of symptomatic *Mecp2-stop* mice would have shrunk to 70.4% (89%x89%x89%) of that of WT mice. This prediction was later verified by the DAPI density change in symptomatic *Mecp2-stop* mice brains. The *Mecp2*/WT DAPI correcting factor was 1.28; if there was no cell loss in the symptomatic *Mecp2-stop* cortex, this higher cell density might be due to the smaller volume (1/1.28= 78%). Both the assumptions of the brain volume change were quite close (70.4% vs. 78%), and were in line with previous reports showing that *Mecp2*-null mice had a smaller brain volume (Reiss *et al.*, 1993).

The smaller brain volume was not only restricted in the *Mecp2*-null models, but was also observed in RTT patients. In previous clinical reports of RTT patients, the head circumference growth pattern differed from that of normal children (Hagberg *et al.*, 2000). Within the first six months, RTT patients had a normal head circumference growth speed. However, the head circumference growth speed decelerated from around eight to ten months old, and eventually RTT patients had a smaller brain compared to that of age-matched children.

The second part of the results was the altered cell density in the symptomatic *Mecp2-stop* cortex. The total cortical cell density in the somatosensory cortex of *Mecp2-stop* mice was elevated (the *Mecp2*/WT DAPI correcting factor was 1.28). Previous reports have shown no obvious cell loss or death in the *Mecp2*-null models or RTT brains (Chen *et al.*, 2001; Armstrong, 2005; Taneja *et al.*, 2009). The reduced cortical thickness proved in this chapter also suggested symptomatic *Mecp2-stop* mice had a smaller brain volume. Therefore, the elevated total cortical cell density may be due to the brain volume effect. This conclusion was further supported by the increased neuronal density in the

symptomatic *Mecp2-stop* cortex (the *Mecp2*/WT NeuN correcting factor was 1.41) without significant shifting of the neuron/non-neuron ratio in symptomatic *Mecp2-stop* mice brains.

One of the aims of Chapter 4 was to assess the alteration of inhibitory cortical neurons in the symptomatic *Mecp2-stop* brain, since recent study has shown that functional knock-out of MeCP2 selectively in inhibitory neurons recapitulated most RTT-like symptoms in mice, particularly the hyperexcitable state of neuronal networks. In this chapter, four protein markers (PV, SOM, CR, and CB) were applied to discriminate distinct subtypes of inhibitory neurons. As illustrated in figure 4.3, in the rodent cortical layer five, more than 95% of inhibitory neurons can be recognised by labelling with one or more of these markers (Kubota *et al.*, 1994). Therefore, the immunolabelling method was adopted to quantify the cell density alteration of distinct subtypes of inhibitory neurons in the symptomatic *Mecp2-stop* cortex.

Since both the DAPI and NeuN positive cell densities of the symptomatic *Mecp2-stop* cortex increased without significant shifting of the neuron/non-neuron ratio, the raw density of distinct subtypes of inhibitory neurons in symptomatic *Mecp2-stop* mice was standardised for further comparison to that in WT mice. After calibration with the *Mecp2*/WT NeuN correcting, all the four subtypes had a lower cellular density (see figure 4.13). However, only CR and SOM positive cell densities of symptomatic *Mecp2-stop* mice were significantly different from that of WT mice, while the change in both PV and CB positive cell densities showed no statistical difference. This data indicated certain inhibitory neuron reduced in symptomatic *Mecp2-stop* mouse brains, but the mechanism by which this occurred is unclear, and requires further investigation. However, the density change of inhibitory neurons can still serve as an indicator of MeCP2 dysfunction in various RTT animal studies.

With regard to the symptomatic (score 5 or more) heterozygous (*Mecp2*$^{stop/+}$ genotype) females, different subtypes of inhibitory neurons seemed to have significant skewing in the lack of MeCP2. As shown in figure 4.14 (data collected and analysed by Dr Rosie Spike), the skewing phenomenon of subtypes of inhibitory neurons was observed in symptomatic *Mecp2*$^{stop/+}$ brains. Theoretically, all cells in the heterozygous brain have an equal possibility of being either

MeCP2 positive or negative. Half of the cortical neurons (NeuN positive cells) were MeCP2 negative, while less than 50% of cells in each subtype of inhibitory neuron were MeCP2 negative (skewing phenomenon). The reason may be either because MeCP2 is essential for inhibitory neuronal development process (lack of MeCP2 hinders the neurogenesis of inhibitory neurons) or because MeCP2 is critical in maintaining inhibitory neuronal populations (lack of MeCP2 makes inhibitory neurons more vulnerable). What role MeCP2 plays in inhibitory neurons is still not yet clarified; however, this result supported our conclusion that MeCP2 is important to inhibitory neurons.

The third part of the results was generated from the morphological work in the hippocampus of symptomatic *Mecp2-stop* mice. Four protein markers (PV, SOM, CR, and CB) were applied in the morphological work for detecting the distribution patterns of distinct subtypes of cortical neurons in the hippocampus in symptomatic *Mecp2-stop* mice. Interestingly, no obvious difference was observed in the distribution pattern of four distinct subtypes of neurons in the symptomatic *Mecp2-stop* hippocampus. The hippocampus serves as an excellent platform for anatomical studies since the neuronal circuits and structures are already well-investigated. However, the results of the morphological work could only provide limited information since the distribution patterns might be altered in other regions of the symptomatic *Mecp2-stop* brain. Therefore, more future anatomical studies are still required to investigate the influence of MeCP2 on distribution patterns of distinct subtypes of cortical neurons in the brain.

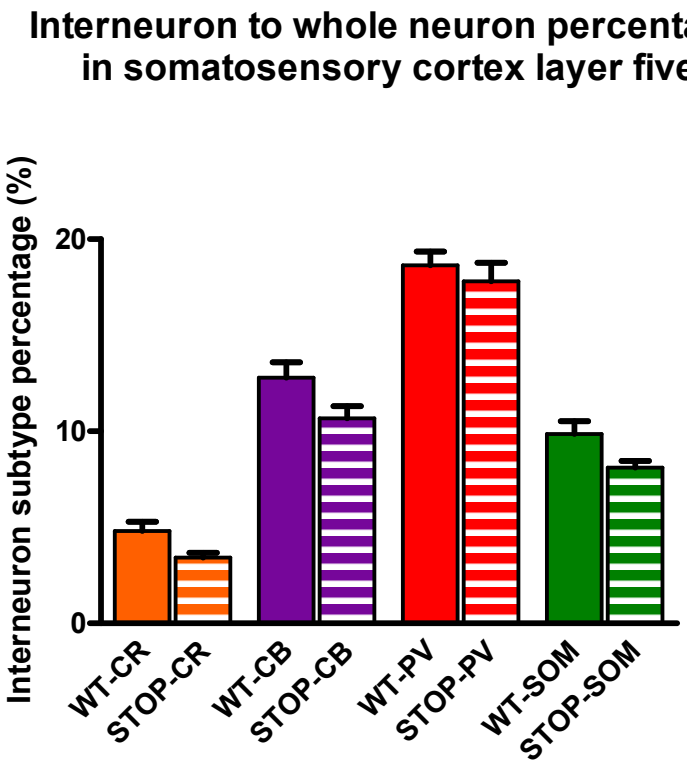

Figure 4.13 Altered interneuronal percentages in symptomatic *Mecp2-stop* mice cortex.

The CR and SOM positive cell densities were significantly reduced after calibrations by the *Mecp2*/WT NeuN correcting factor while the PV and CB positive cell densities were not significantly altered in the symptomatic *Mecp2-stop* mouse brain.

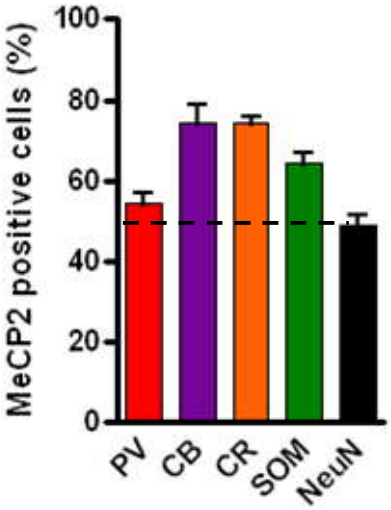

Figure 4.14 Skewing of interneuronal MeCP2 expression in symptomatic heterozygous *Mecp2*$^{Stop/+}$ mice cortex.

Theoretically, all cells in the heterozygous (*Mecp2*$^{stop/+}$) brain have an equal possibility to be either MeCP2 positive or negative. Half of the cortical neurons (NeuN+) were MeCP2 negative; however, all four subtypes of interneurons had a skewing effect, causing there to be more MeCP2 positive neurons than MeCP2 negative ones. (Data collected and provided by Dr Rosie Spike)

5 Electrophysiology

5.1 Introduction

In Chapter 3, the symptom progression in *Mecp2-stop* mice was investigated and characterised. The severity of *Mecp2-stop* mice phenotype was found to steadily increase in an age-dependent manner. It thus appeared that the neurological deficits may accumulate throughout postnatal developmental stages. In order to assess possible modifiers in the neuroanatomical differences between symptomatic *Mecp2-stop* mice and their WT littermates, the distribution patterns and cell density of distinct neuron subtypes were investigated in the hippocampus and somatosensory cortex. The results of experiments in Chapter 4 showed that distribution patterns of neuronal subtypes and their patterns of connectivity were not visibly changed, but the neuronal density of specific subtypes was altered. To probe potential changes of the synaptic level, I switched from an anatomical to physiological approach and focused my studies on the hippocampus.

In previous studies, subtle changes have been reported in neuronal electrical properties at the cellular level (Dani *et al.*, 2005; Taneja *et al.*, 2009; Kline *et al.*, 2010) but more overt changes in synaptic levels have been reported, including reduced synaptic plasticity (Asaka *et al.*, 2006; Moretti *et al.*, 2006; Guy *et al.*, 2007; Nelson *et al.*, 2008) and changes in basal inhibitory and excitatory synaptic transmission (Dani *et al.*, 2005; Medrihan *et al.*, 2008; Nelson *et al.*, 2008; D'Cruz *et al.*, 2010; Kline *et al.*, 2010; Maliszewska-Cyna *et al.*, 2010). Anatomical studies have also shown changes in synaptic connectivity and neuronal structure (Armstrong *et al.*, 1995; Belichenko *et al.*, 1997; Armstrong *et al.*, 1998; Armstrong, 2005; Chao *et al.*, 2007), whilst at the network level there were changes in network excitability (Zhang *et al.*, 2008; D'Cruz *et al.*, 2010). There is increasing evidence that MeCP2 is an important regulator of neuronal plasticity and that synaptopathy is a major component of the Rett phenotype (Gadalla *et al.*, 2011).

The aim of this chapter was to characterise hippocampal synaptic plasticity in the *Mecp2-stop* mouse model of RTT and to investigate the potential for pharmacological manipulation of plasticity deficits. In order to assess the

possible deficits at synaptic levels in symptomatic *Mecp2-stop* mice, different aspects of synaptic plasticity were investigated in this chapter. These include short-term plasticity, long-term plasticity and the saturation properties of synaptic plasticity. In addition, I also assessed the effectiveness of the Alzheimer disease drug memantine in reversing potential *Mecp2-stop* related plasticity deficits.

5.2 Assessment of the basal synaptic transmission in *Mecp2-stop* hippocampus

In the synaptic plasticity assessment, I focused on the Schaffer collateral to CA1 synapse. Evoked fEPSPs were recorded using extracellular field potentiation recording electrodes in the CA1 region of the hippocampus. At the beginning of the long-term potentiation (LTP) experiments, the input-output (I/O) curve was generated by increasing stimulus intensity and recording the respective field excitatory post-synaptic potential (fEPSP) magnitude to assess whether any difference existed in the basal synaptic transmission. Brain slices were obtained from four different mouse groups for comparison, including the symptomatic *Mecp2-stop* group, the pre-symptomatic *Mecp2-stop* group, and their age-matched WT control groups.

The comparison of the I/O curves between two different age WT mouse groups was plotted as shown in figure 5.1. The two WT groups were selected as the age-matched littermates of either symptomatic *Mecp2-stop* mice (age ranging from 12 to 15 weeks) or pre-symptomatic *Mecp2-stop* mice (age ranging from 4-5 weeks). As illustrated in figure 5.1, the stimulus intensity plot shows the fEPSP slope (mean ± SEM; WT at 4-5 wks= 6 slices from 4 animals; WT at 12-15 wks= 10 slices from 9 animals) in response to increasing stimulus strength for two WT group samples. No difference was observed in the I/O curves from two distinct age WT groups (p= 0.89, repeated-measures ANOVA). Therefore, there was no age-dependent difference in the basal synaptic transmission of WT brain slices.

As illustrated in figure 5.2, the stimulus intensity plot shows the fEPSP slope (mean ± SEM; WT= 16 slices from 13 animals; pre-symptomatic *Mecp2-stop*= 6 slices from 4 animals; symptomatic *Mecp2-stop*= 10 slices from 8 animals) in response to increasing stimulus strength for wild-type and *Mecp2-stop* samples.

Hemizygous males were used at two developmental time points, pre-symptomatic (severity score below two, blue symbols), and symptomatic (mean severity score 5.3 ± 0.2; generally at between 12 and 15 wk of age, orange symbols). Assessment of evoked synaptic transmission at the Schaffer-collateral-to-CA1 pyramidal cell synapse using conventional field recording revealed no significant differences between genotype or phenotype groups with respect to the baseline fEPSP slope (p= 0.42, repeated-measures ANOVA).

Multiple factors should be considered before making any comparison between brain slices from different animals, such as differences in the preparation process, differences in the electrode placement, the slice thickness, the slice cutting angle, *etc*. Before the comparison of fEPSPs from different brain slices, the pre-synaptic fibre volley assessment was generally adopted to evaluate whether this variability existed. As illustrated in figure 5.3, immediately after the stimulus (indicated by the arrows), a small field response that precedes the post-synaptic potential and correlates with the number of pre-synaptic afferents activated by the stimulation pulse is the pre-synaptic fibre volley. In my study, I also applied the pre-synaptic fibre volley assessment to investigate the possible difference originating from distinct brain slices. Since the pre-synaptic fibre volley response is proportional to the stimulation strength, the input current was always set to induce the half-maximum amplitude recorded in the previous I/O curve test of each brain slice. As shown in figure 5.3, two groups of brain slices were used in the pre-synaptic fibre volley experiment, one was from WT mice and the other from *Mecp2-stop* mice (all age ranged from 12 to 15 weeks). The pre-synaptic fibre volley data showed no difference in brain slices of WT and *Mecp2-stop* mice (WT= 0.028 ± 0.009mV, n=30 slices from 13 animals; *Mecp2-stop*= 0.033 ± 0.003mV, n=30 slices from 12 animals; p= 0.61).

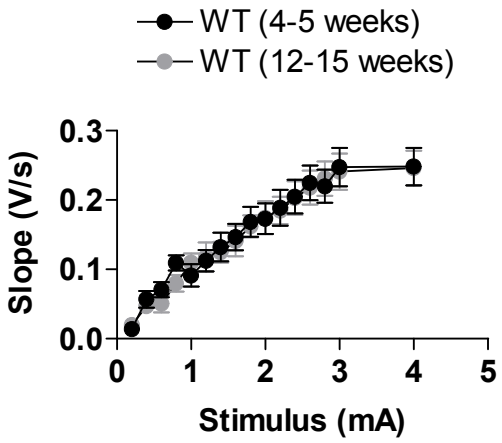

Figure 5.1 Comparison of Input-output curves between two different age WT mice groups.

Stimulus intensity plot showing fEPSP slope (mean±SEM; WT at 4-5 wks= 6 slices from 4 animals; WT at 12-15 wks= 10 slices from 9 animals) in response to increasing stimulus strength for two different age WT mice samples. Males were used at two developmental time points, one matched the age of pre-symptomatic *Mecp2-stop* mice (generally range between 4 and 5wk of age, black symbols), and the other matched age of symptomatic *Mecp2-stop* mice (generally range between 12 and 15wk of age, grey symbols). No difference was observed between two different age WT mice groups (*p*= 0.89). All data is shown as mean ± SEM.

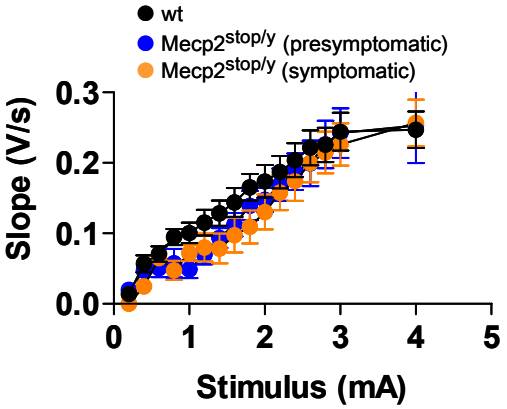

Figure 5.2 Comparison of Input-output curves between *Mecp2-stop* and WT mice.

Stimulus intensity plot showing fEPSP slope (mean±SEM; WT= 16 slices from 13 animals; pre-symptomatic *Mecp2-stop*= 6 slices from 4 animals; symptomatic *Mecp2-stop*= 10 slices from 8 animals) in response to increasing stimulus strength for WT and *Mecp2-stop* samples. *Mecp2-stop* males were used at two developmental time points, pre-symptomatic (severity score <2, blue symbols), and symptomatic (mean severity score 5.3±0.2; generally at between 12 and 15wk of age, orange symbols). No difference was observed in all three mice groups (*p*= 0.42). All data is shown as mean ± SEM.

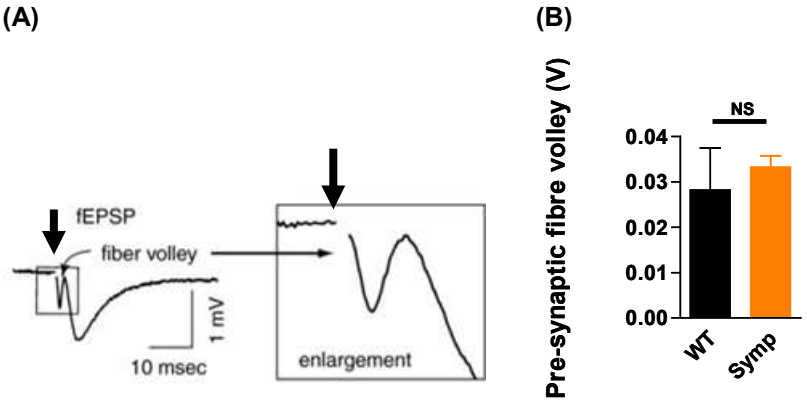

Figure 5.3 Comparison of pre-synaptic fibre volley between *Mecp2-stop* and WT mice groups.

(A) Illustration of measurement of the pre-synaptic fibre volley. In an EPSP trace, immediately after the stimulus (removed and replaced with arrows for clarity), a small field response that precedes the postsynaptic potential and correlates with the number of pre-synaptic afferents activated by the stimulation pulse is the pre-synaptic fibre volley. Adopted and modified from Bortolotto *et al.*, 2011 (Bortolotto *et al.*, 2011). (B) The amplitude of pre-synaptic fibre volley (from baseline) showed no difference between *Mecp2-stop* and WT mice (WT= 0.028 ± 0.009mV, *n*=30 slices from 13 animals; *Mecp2-stop* = 0.033 ± 0.003mV, *n*=30 slices from 12 animals; *p*= 0.61). All data is shown as mean ± SEM.

5.3 LTP in the *Mecp2-stop* hippocampus

5.3.1 HFS-induced LTP was induced in the Mecp2-stop hippocampus

Synaptic plasticity was investigated in acute hippocampal slices from hemizygous male *Mecp2-stop* mice and WT littermates as described in Chapter 2. All brain slices used in one-hour LTP experiments were first recorded for least half hour to assure a stable fEPSP baseline. The stable fEPSP baseline was defined as less than 5% amplitude change for at least 30 minutes recording.

Representative fEPSPs of four different mouse groups are shown in figure 5.4. Field EPSPs recorded for the baseline evaluation were plotted as dotted lines, while the fEPSPs recorded at time 41 to 60 min were plotted as continual lines. Noticeably, all the traces from WT and the pre-symptomatic *Mecp2-stop* groups showed a significant increase before and after HFS; however, the increase in the symptomatic *Mecp2-stop* group was not obvious.

As illustrated in figure 5.5, assessment of LTP revealed that high frequency stimulation (HFS) produced a robust and enduring potentiation of the fEPSP slope in slices from WT mice (WT at 4-5 weeks= 153.1 ± 12.0 % of baseline measured at 41 to 60 min following HFS; n=6 slices from 4 mice; WT at 12-15 weeks= 146.2 ± 3.5 % of baseline measured at 41 to 60 min following HFS; n=10 slices from 9 mice). No difference was observed in the two distinct age WT groups (p= 0.45, repeated-measures ANOVA). Therefore, in the following one-hour LTP experiments, both WT groups' data were pooled.

In figure 5.6, pre-symptomatic *Mecp2-stop* mice showed a robust LTP (155.2 ± 10.4 % of baseline at 41 to 60 min, n= 6 slices from 4 mice) that was similar in magnitude to that evoked in WT controls (p= 0.35, repeated-measures ANOVA). In contrast, brain slices obtained from symptomatic *Mecp2-stop* mice (mean severity score 5.3 ± 0.2) showed a significantly lower LTP (115.7 ± 3.2 % of baseline at 41 to 60 min, n= 10 slices from 8 mice), which represented approximately 40% of the wild-type value, than both the WT and pre-symptomatic groups ($F(2, 28) = 12.14$; $p< 0.001$ for both *post hoc* pairwise comparisons).

(A) Age-matched controls of (B) **(B) Pre-symptomatic group**

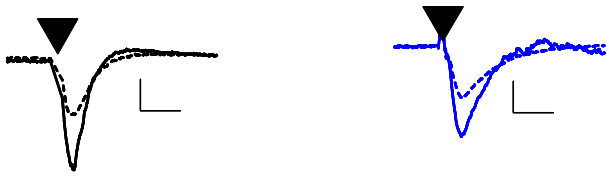

(C) Age-matched controls of (D) **(D) Symptomatic group**

Figure 5.4 Representative fEPSPs for all four groups pre- and post-HFS.

Representative fEPSPs before (dotted lines, obtained from the pre-HFS stage; as indicated as "1" in figure 5.6) and following (continual lines, obtained from the post-HFS stage; as indicated as "2" in figure 5.6) HFS stimulation for each of the four comparison groups. Arrowheads indicate point of stimulus. Scale bars: vertical, 0.2mV; horizontal, 10ms.

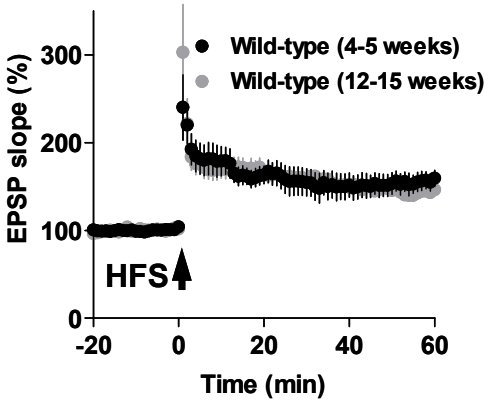

Figure 5.5 HFS-induced LTP experiments in different age WT mice.

EPSP slope was plotted against time after HFS stimulation (large arrow; time 0), as a percentage of the averaged pre-HFS baseline slope for each slice used. The pooled LTP data from 41 to 60 min showed no difference between two different age WT mouse groups (WT at 4-5 weeks= 153.1 ± 12.0 %, *n*= 6 slices from 4 animals; WT at 12-15 weeks= 146.2 ± 3.5 %, *n*= 10 slices from 9 animals; *p*= 0.45, repeated-measures ANOVA). All data is shown as mean ± SEM.

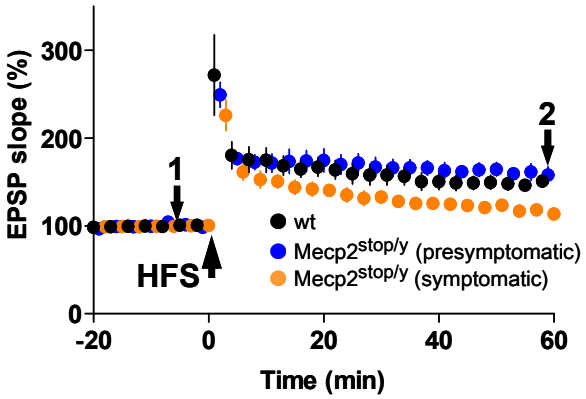

Figure 5.6 HFS-induced LTP experiments in *Mecp2-stop* mice.

EPSP slope was plotted against time after HFS stimulation (large arrow; time 0), as a percentage of the averaged pre-HFS baseline slope for each slice used. The pooled LTP data from 41 to 60 min showed no difference between pre-symptomatic *Mecp2-stop* and WT mice (WT= 152.7 ± 5.3 %, *n*=16 slices from 13 animals; pre-symptomatic *Mecp2-stop* = 155.2 ± 10.4 %, *n*=6 slices from 4 animals; *p*= 0.35), while significant reduction was observed in the symptomatic *Mecp2-stop* mice compared to the WT or pre-symptomatic mice (symptomatic *Mecp2-stop* = 115.7 ± 3.2 %, *n*=10 slices from 8 animals; *p*< 0.001 for *post hoc* pairwise comparisons). All data is shown as mean ± SEM.

5.3.2 Post-tetanic potentiation (PTP) was altered in the symptomatic Mecp2-stop hippocampus

In one-hour LTP experiments of *Mecp2-stop* mice, the post-tetanic potentiation (PTP) could be further analysed. The PTP value in this chapter was averaged from the first three fEPSP slope data following HFS (the fEPSP was measured for every 20 seconds, and the first three fEPSPs were within the first minute after HFS). PTP is regarded to be related to the calcium concentration at the pre-synaptic locus of synapses (Zucker & Regehr, 2002).

As illustrated in figure 5.7, the PTP from two distinct age WT groups were compared and no significant difference was noted (WT at 4-5 weeks= 225.1 ± 41.0 % of baseline measured at 1st min following HFS; *n*=6 slices from 4 mice; WT at 12-15 weeks= 208.6 ± 51.4 % of baseline measured at 1st min following HFS; *n*=10 slices from 9 mice; *p*= 0.62). Since there was no age-dependent difference in the PTP data between both WT groups, the PTP data were pooled for further analyses.

In the same one-hour LTP experiments, PTP were analysed for the pre-symptomatic *Mecp2-stop* group, the symptomatic *Mecp2-stop* group and the WT group. As illustrated in figure 5.8, PTP differed between groups ($F(2, 25) = 3.492$; $p= 0.046$), with symptomatic *Mecp2-stop* mice exhibiting PTP values that were 45 ± 18% of those observed in WT mice (WT= 216 ± 46.2 % of baseline, symptomatic *Mecp2-stop*= 97.8 ± 40.8 %; *post hoc* Tukey test, *p*= 0.036), while pre-symptomatic mice did not differ from wild-type (WT= 216 ± 46.2 % of baseline, pre-symptomatic *Mecp2-stop*= 204.3 ± 18.1 %; *p*= 0.73).

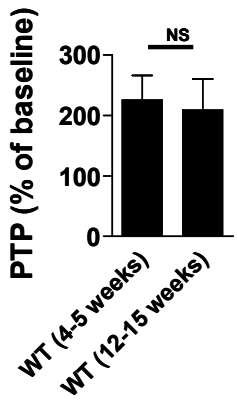

Figure 5.7 PTP comparison between both two different age WT groups.

The amplitude of PTP (compared to baseline) showed no difference between two different aged WT mice groups (WT at 4-5 weeks= 225.1 ± 41.0 %, *n*=6 slices from 4 animals; WT at 12-15 weeks= 208.6 ± 51.4 %, *n*=10 slices from 9 animals; *p*= 0.62). All data is shown as mean ± SEM.

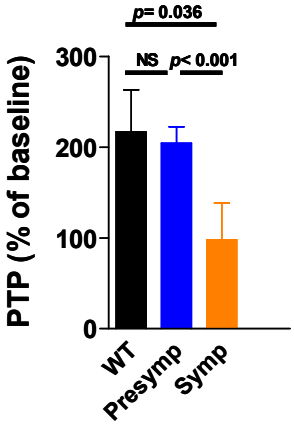

Figure 5.8 PTP analyses of *Mecp2-stop* mice.

The amplitude of PTP (compared to baseline) showed no difference between pre-symptomatic *Mecp2-stop* and WT mice (WT= 216 ± 46.2 %, *n*=13 slices from 16 animals; pre-symptomatic *Mecp2-stop* = 204.3 ± 18.1 %, *n*= 6 slices from 4 animals; *p*= 0.73), while significant reduction was observed in the symptomatic *Mecp2-stop* mice compared to the WT mice (WT= 216 ± 46.2 %, *n*=13 slices from 16 animals; symptomatic *Mecp2-stop* = 97.8 ± 40.8 %, *n*= 10 slices from 8 animals; *post hoc* Tukey test, *p*= 0.036). All data is shown as mean ± SEM.

5.3.3 Paired-pulse facilitation (PPF) ratio analyses from one-hour LTP experiments

Paired-pulse facilitation (PPF) is the increased amplitude of a second synaptic response when triggering stimuli are delivered in pairs. The phenomenon is considered to be mediated by residual calcium accumulation in the axonal terminal and is generally regarded as a pre-synaptic functional assessment (Zucker & Regehr, 2002). Paired pulses with 50ms interval were delivered every 20 seconds. In figure 5.9, two representative traces from pre-symptomatic and symptomatic *Mecp2-stop* mice were demonstrated. As described in Chapter 2, the PPF ratio was calculated as the amplitude of the second fEPSP divided by the amplitude of the first fEPSP. The PPF ratio of the representative trace in the pre-symptomatic *Mecp2-stop* mice was significantly higher than that of the symptomatic *Mecp2-stop* mice.

As illustrated in figure 5.10, PPF ratios were compared in two different age WT groups. No age-dependent difference was observed between these two WT groups (WT at 4-5 weeks= 1.85 ± 0.05; n=6 slices from 4 mice; WT at 12-15 weeks= 1.82 ± 0.08; n=10 slices from 9 mice; p= 0.71). Therefore, data from two WT groups were pooled for further analyses.

Tested by repeated-measures ANOVA, there were significant differences between the symptomatic *Mecp2-stop* group and the other two (WT and pre-symptomatic *Mecp2-stop*) groups ($F(2, 29) = 16.978$; $p< 0.001$). As shown in figure 5.11, the paired-pulse ratio was observed to be of similar magnitude in pre-symptomatic *Mecp2-stop* mice (1.85 ± 0.04) and WT controls (1.84 ± 0.02) (p= 0.89). In contrast, symptomatic *Mecp2-stop* mice showed a significant reduction in baseline paired pulse ratio (ratio=1.43 ± 0.02; *post hoc* Tukey test $p< 0.001$) compared to age-matched WT controls. PPF analysis over the duration of the LTP experiments revealed that the symptomatic mice showed a consistent deficit relative to both other groups (before and after the induction of LTP), with the exception of a brief period immediately following high-frequency stimuli (coinciding with the peak of the PTP) during which all groups showed a similar reduced peak ratio.

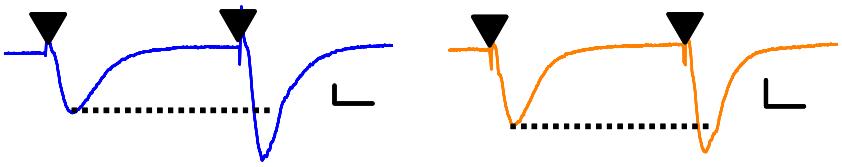

Figure 5.9 Representative fEPSPs in response to paired stimuli of pre-symptomatic and symptomatic *Mecp2-stop* mice.

Representative EPSPs observed in response to paired stimuli (arrowheads) from the pre-symptomatic (blue) and symptomatic *Mecp2-stop* (orange) mice groups. The interval between the paired stimuli was set as 50ms. Scale bars: vertical, 0.2mV; horizontal, 10ms.

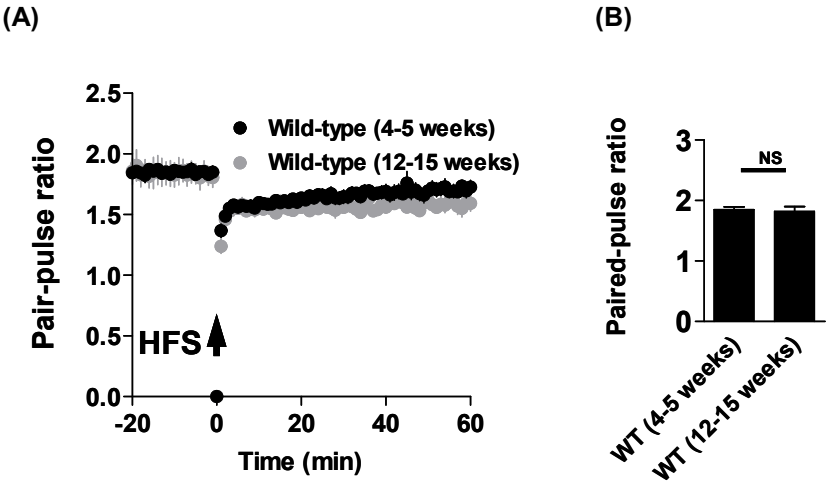

Figure 5.10 Pair-pulse facilitation (PPF) ratio comparison between both two different age WT groups.

(A) Paired-pulse facilitation (PPF) ratios were plotted as mean±SEM (WT at 4-5 wks= 6 slices from 4 animals; WT at 12-15 wks= 9 slices from 10 animals). The slope ratio time course was plotted relative to the delivery of HFS stimulation (time= 0). (B) The mean PPF data at baseline recording showed no age-dependent changes between two different age WT mice groups (WT at 4-5 wks= 1.85 ± 0.05; WT at 12-15 wks= 1.82 ± 0.08; *p*= 0.71). All data is shown as mean ± SEM.

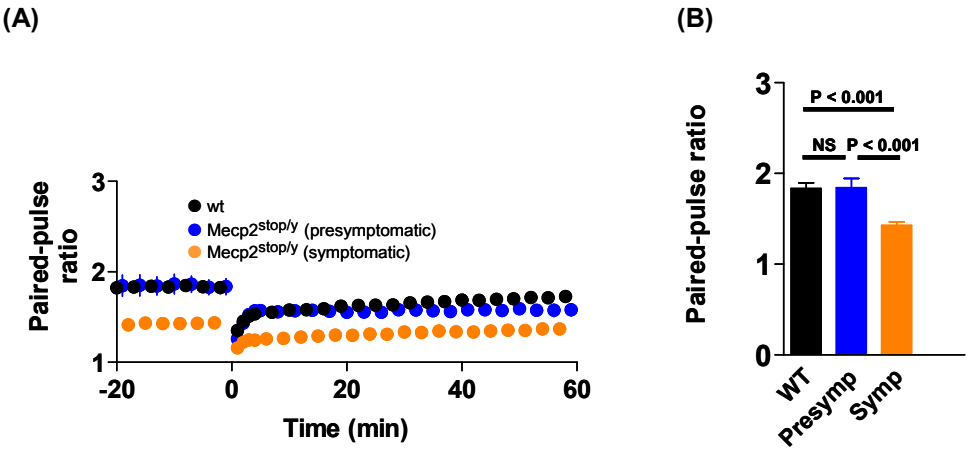

Figure 5.11 Paired-pulse facilitation (PPF) ratios of *Mecp2-stop* mice.

(A) Paired-pulse facilitation (PPF) ratios were plotted as mean±SEM (*n*= 6–10 slices, four to nine mice per group). The slope ratio time course was plotted relative to the delivery of HFS stimulation (time= 0). (B) The mean PPF data at baseline recording showed no difference between pre-symptomatic *Mecp2-stop* and WT mice (WT= 1.84 ± 0.02; pre-symptomatic *Mecp2-stop*= 1.85 ± 0.04; *p*= 0.89), while significant reduction was observed in the symptomatic *Mecp2-stop* mice compared to the WT mice (WT= 1.84 ± 0.02; symptomatic *Mecp2-stop*= 1.43 ± 0.02; *p*< 0.001). All data is shown as mean ± SEM.

5.4 LTP saturation experiments

5.4.1 LTP saturation experiments in Mecp2-stop brain slices

After analysing the LTP, PTP, and PPF results of *Mecp2-stop* mice, we concluded that functional knock-out of MeCP2 is characterised by both the pre-synaptic and the post-synaptic deficits in symptomatic *Mecp2-stop* mice. Here we introduced another experimental design in order to further assess how the LTP is compromised in the *Mecp2-stop* brain. The principle was to deliver repetitive high-frequency stimuli (HFS) at regular intervals (for example 15-20 minutes), and the fEPSP amplitude gradually reached the plateau after repetitive inductions. Multiple HFS induced a cumulated form LTP rather than a single potentiated event following a single HFS. This scheme was adopted in an attempt to detect more subtle deficits in synaptic plasticity. Therefore, not only the symptomatic *Mecp2-stop* and their WT littermates were assessed in the LTP saturation experiments, but also the mild symptomatic *Mecp2-stop* mice (score ranged from 2 to 4). The results were beneficial for further analysing the effect of symptom progression on the alteration of synaptic plasticity in *Mecp2-stop* brains.

In figure 5.12, the representative fEPSP traces from the symptomatic *Mecp2-stop* and WT brain slices were plotted. The letter “b” labels the initial baseline trace before HFS, and the numbers label traces five minutes after each HFS stimulation. In the WT brain slices, the amplitude of LTP increased after each HFS stimulation towards a “saturated” or “plateau” state, while in the symptomatic *Mecp2-stop* brain slices, the amplitude of LTP did not increase but decreased back to the baseline level after multiple HFS inductions.

As illustrated in figure 5.13(A), the assessment of plasticity defects in *Mecp2-stop* mice was conducted by delivering repeated episodes of HFS (see methods detailed in Chapter 2) to investigate possible saturation effects. In WT mice synaptic tone increased over four successive rounds of HFS at fifteen-minute intervals, each successive increase in fEPSP slope being smaller than the previous one such that a plateau was being approached at around the one-hour mark. In contrast, strongly symptomatic *Mecp2-stop* mice showed, in addition to their deficit in the response to the initial HFS, a profound inability to generate

further LTP following subsequent HFS episodes and even a modest depression in the most symptomatic mice. Slices obtained from mildly symptomatic (phenotype score of 2-4) mice, which did not display overt LTP deficits after the first HFS over fifteen minutes, did reveal intermediate but significant additional LTP deficits in response to subsequent episodes of HFS. As the quantification analyses of 15 min LTPs following each consecutive HFS in figure 5.13(B) show, in the WT brain slices, the increase of LTPs after each HFS stimulations was smaller compared to the previous one; however, in the symptomatic *Mecp2-stop* brain slices, a reduced propensity to produce further LTP enhancement was observed.

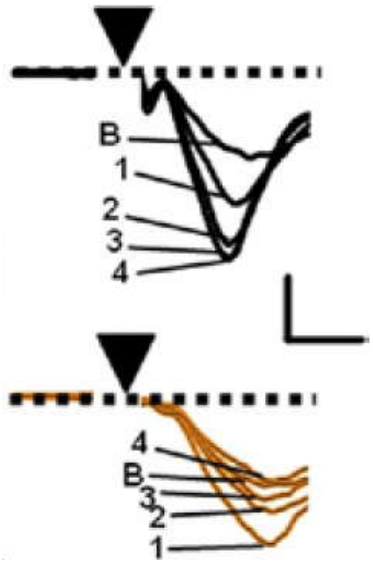

Figure 5.12 Representative EPSP traces after each HFS in the LTP saturation experiments of symptomatic *Mecp2-stop* and WT mice groups.

Representative traces from a WT (top, black) and symptomatic *Mecp2-stop* (bottom, orange) mice. The letter "b" labels the initial baseline trace before HFS, and the numbers label traces five minutes after each HFS stimulation. Scale bar 0.25mV, 5ms. Stimulus (artefact removed for clarity) is indicated by the inverted arrow head.

(A)

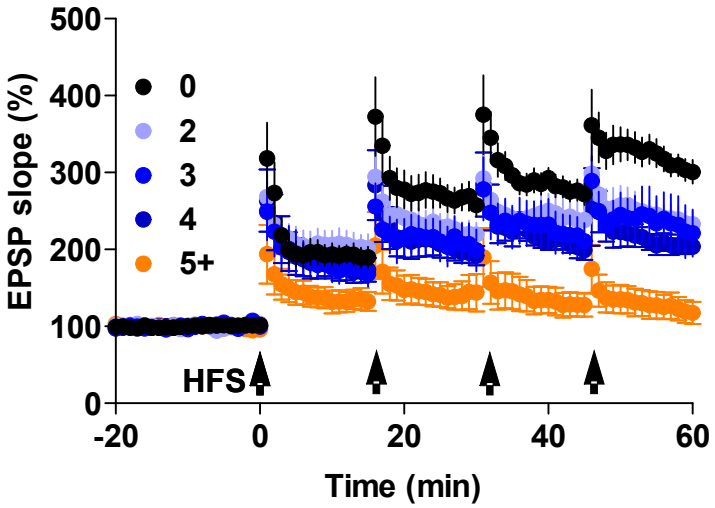

(B)

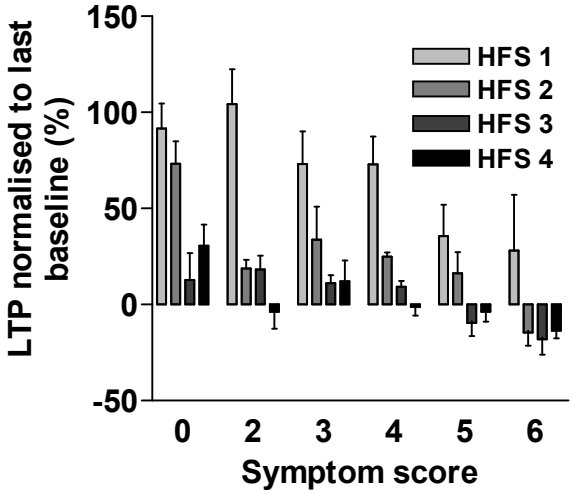

Figure 5.13 LTP showed pronounced saturated phenomenon in symptomatic *Mecp2-stop* mice.

(A) Time plot shows mean fEPSP slope upon repeated high frequency stimulation of afferents in hippocampal slices prepared from WT (score 0) and increasingly symptomatic (symptom score range 2–6) *Mecp2-stop* mice. (B) Bar plot shows 15 min LTPs (mean±SEM, *n*=7–10 slices, four to eight mice from each symptom-scored group) following each consecutive HFS, normalised to the preceding pre-HFS baseline. Note that fEPSP slope shows a robust further LTP enhancement in response to second and subsequent HFS in WT mice but a reduced propensity to produce further LTP enhancement in brain slices from symptomatic *Mecp2-stop* mice. All data is shown as mean ± SEM.

5.4.2 PTP was induced in mild symptomatic and symptomatic *Mecp2-stop* mice

In section 5.3.2, the PTP was analysed and the results indicated potential pre-synaptic deficits in symptomatic *Mecp2-stop* mice brains. In order to further characterise short-term plasticity, brain slices from a range of mildly to severely symptomatic *Mecp2-stop* mice were assessed for post-tetanic potentiation.

Analysis of PTPs in LTP saturation experiments (figure 5.14) revealed a similar impairment in symptomatic *Mecp2-stop* mice that tended to increase with increasing symptom score (R^2= 0.074 in a linear regression of PTP versus aggregate symptom score, *n*= 29; WT mice were treated as having a symptom score of 1 for this test to mimic linearity, pre-symptomatic *Mecp2-stop* mice were with scores of 2 to 4, and symptomatic *Mecp2-stop* mice were with scores of 5 to 6).

The PTP amplitude had a negative correlation with the symptom progress. As illustrated in figure 5.14, when plotting PTP levels versus symptoms scoring, the PTP decreased as the scoring increased. This was an essential finding as previous reports described the pre-synaptic deficit only in symptomatic RTT mice brains; however, it appeared to be that the PTP deficit was accumulated throughout the developing process and eventually became significant at the severe symptomatic stage. The result was in line with previous sections that the pre-synaptic and post-synaptic deficits co-existed in RTT mouse brains.

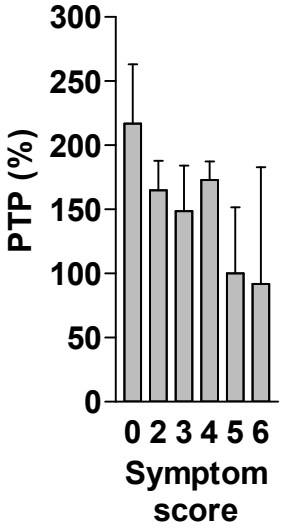

Figure 5.14 Quantification analyses of initial PTP in the LTP saturation experiments of *Mecp2-stop* mice.

Bar plot shows level of post-tetanic potentiation (PTP; mean±SEM, *n*=7–10 slices, four to eight mice from each symptom-scored group) following HFS in WT littermate controls (score 0) and progressively more symptomatic *Mecp2-stop* mice (score range 5-6). The PTP is presented as the percentage of baseline level (100%). All data is shown as mean ± SEM.

5.5 Effects of memantine on synaptic plasticity deficits in symptomatic *Mecp2-stop* mice

5.5.1 In vitro memantine treatment on Mecp2-stop brain slices

In previous sections, LTP deficits were observed in the *Mecp2-stop* hippocampus and these deficits were shown to be associated with an aspect of LTP-saturation-like effect. Interestingly, identical LTP saturation has been reported in Alzheimer disease models and models of NMDA receptor hyper-stimulation (Frankiewicz & Parsons, 1999). Furthermore, these reports indicated that such abnormalities can be reversed by the Alzheimer disease drug memantine (Frankiewicz & Parsons, 1999). Memantine, a weak NMDA receptor antagonist, is thought to bind the NMDA receptor on the post-synaptic terminus to prevent excessive basal stimulation whilst at the same time allowing NMDA receptor activation upon appropriate plasticity-producing stimulus. Clinically memantine was reported to slow down the progression of memory dysfunction in Alzheimer disease. Since the synaptic plasticity defects were similar in nature to those reported due to NMDA over-stimulation, memantine was applied to symptomatic *Mecp2-stop* brain slices to further assess the potential for reversing the LTP saturation deficits in the *Mecp2-stop* brain.

LTP saturation experiments were repeated (as in previous sections) in brain slices pre-incubated for one hour and bathed for the recording duration in 1μM memantine (dissolved in 1x ACSF). As shown in figure 5.15, memantine was assessed on control brain slices from WT mice and showed no significant alterations in LTP, PTP or LTP saturation. In contrast, as illustrated in figure 5.16, in brain slices from symptomatic (mean score =5.3 ± 0.2, *n*=7) *Mecp2-stop* mice, memantine produced a significant enhancement of both PTP and the first 15-minute LTP, restoring these parameters to WT levels (+memantine: 100% of WT first 15-minute LTP, 104% of WT PTP; untreated: 69% of WT first 15-minute LTP and 61% of WT PTP). In response to subsequent episodes of HFS, memantine-treated brain slices from symptomatic *Mecp2-stop* mice showed enhanced PTP and short-term plasticity, but the potentiation rapidly decayed to the preceding baseline level within the 15-minute inter-HFS period.

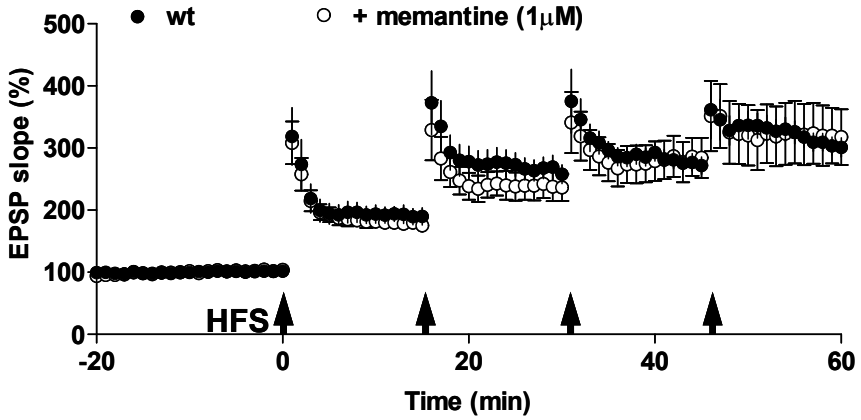

Figure 5.15 Partial reversal of plasticity deficits in symptomatic *Mecp2-stop* mice by memantine.

Time plot shows that memantine did not affect LTP, PTP or LTP saturation in brain slices obtained from WT memantine-treated mice (black empty dots, eight slices from five mice) to WT age-matched controls (black dots, 10 slices from eight mice). Arrows indicate points of afferent HFS every 15 minutes for four instances. All data is shown as mean ± SEM.

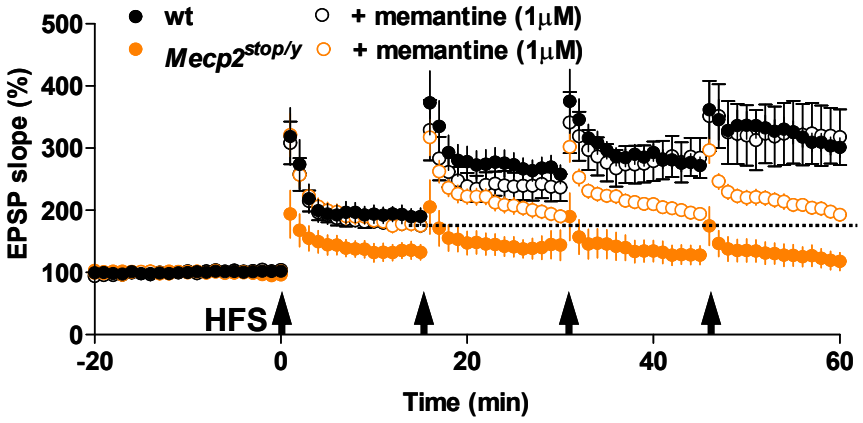

Figure 5.16 Partial reversal of plasticity deficits in symptomatic *Mecp2-stop* mice by memantine.

Time plot shows reduced hippocampal LTP and PTP and elevated synaptic saturation in brain slices from symptomatic *Mecp2-stop* mice (orange dots, seven slices from four mice) compared to WT littermate controls (black dots, 10 slices from eight mice). LTP/PTP reduction and LTP saturation were partially reversed in *Mecp2-stop* slices incubated in 1 μM memantine (orange empty dots, 10 slices from five mice). In contrast, memantine did not affect LTP, PTP or LTP saturation in slices obtained from wild-type mice (black empty dots, eight slices from five mice). Arrows indicate points of afferent HFS every 15 minutes for four instances. The dotted line indicates the mean LTP level 15 min after the first HFS in memantine-treated *Mecp2-stop* mice for easier comparison with subsequent 15min post-HFS time points. All data is shown as mean ± SEM.

5.5.2 In vivo memantine treatment on Mecp2-stop mice

In section 5.5.1, memantine restored the first 15-minute LTP and PTP in the symptomatic *Mecps2-stop* hippocampus. In order to further evaluate the *in vivo* effects of memantine, *Mecp2-stop* mice and their WT littermates were dosed daily from five to eight weeks old with a dose (30mg/Kg) shown previously to achieve the therapeutic serum level of memantine in mice (Minkeviciene *et al.*, 2004). Control groups consisted of age-matched *Mecp2-stop* and WT mice and were also administrated with vehicles (normal saline) daily for four weeks (5 to 8 weeks old). The symptom progress and the life span of all four groups were recorded for further analyses and comparisons.

As shown in figure 5.17, memantine administered daily from five weeks old in *Mecp2-stop* mice (*n*= 7) for a four-week period revealed no significant difference in severity or progression of RTT-like signs from vehicle-treated *Mecp2-stop* mice (*n*= 8). As expected, WT mice scored 0 throughout the study and memantine administration did not affect this score. With regard to the survival plot in figure 5.18, *Mecp2-stop* mice had a reduced survival, but again this was not altered by the memantine treatment.

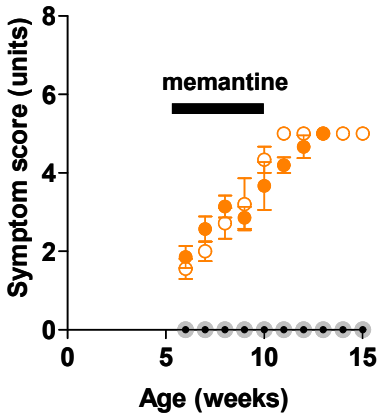

Figure 5.17 Memantine did not affect progression of *Mecp2-stop* mice phenotypes.

Plot shows phenotypic severity progression in WT (mice treated with memantine, grey symbols, *n*=7 animals; mice treated with vehicle, black symbols, *n*=8 animals) and *Mecp2-stop* (orange symbols) mice treated with memantine (oral dosing 30 mg/kg, open symbols, *n*=7 animals) or vehicle (closed symbols, *n*=8 animals). The treatment was administered between 5 and 8 weeks of age, continually for 28 days with a daily dose (shown as black bar). All data is shown as mean ± SEM.

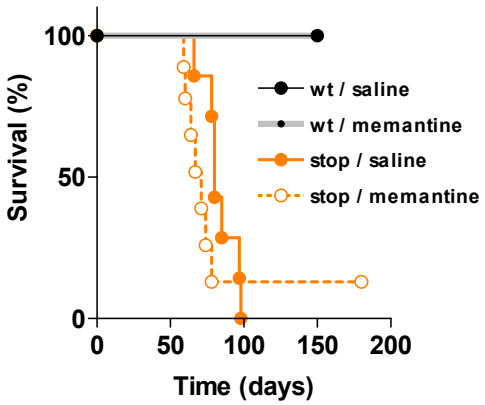

Figure 5.18 Memantine did not affect survival of *Mecp2-stop* mice.

Survival curves plotted for the same four groups of mice as indicated in figure 5.18 (WT mice treated with memantine, grey symbols, *n*=7 animals; WT mice treated with vehicle, black symbols, *n*=8 animals; *Mecp2-stop* mice treated with memantine, orange open symbols, *n*=7 animals; mice treated with vehicle, orange closed symbols, *n*=8 animals). Note that vertical steps indicate deaths due to culling under the humane culling policy (see Chapter 2, determined by symptom scores) rather than natural lifespan of *Mecp2-stop* mice.

5.6 Discussion

The major finding in this chapter is that both short-term and long-term plasticity deficits were detected in symptomatic *Mecp2-stop* brains. In addition, in the LTP saturation experiment, both short-term and long-term plasticity were observed to be connected to the progression of RTT-like symptoms. Furthermore, the effectiveness of memantine on the symptomatic *Mecp2-stop* brain was assessed and it was concluded that memantine can partially restore synaptic plasticity deficits, particularly the short-term plasticity deficit.

An important observation is that classic LTP was not impaired in *Mecp2-stop* mice during the first postnatal weeks, but rather the deficits appeared with the onset of overt RTT-like symptoms. These data mirrored earlier studies conducted in male *Mecp2*-null mice (Asaka *et al.*, 2006) as well as with studies in symptomatic female *Mecp2-stop* mice which developed symptoms later (the symptom onset was around 6 to 9 months) (Guy *et al.*, 2007). In contrast, those studies reporting the absence of deficits have mainly been limited to experiments conducted using relatively immature brain tissues from presumably asymptomatic mice (Dani & Nelson, 2009).

In addition to long-term potentiation, the PTP and PPF analyses showed that short-term forms of plasticity were impaired in symptomatic *Mecp2-stop* mice. Whilst this was the first report addressing short-term plasticity in the *Mecp2-stop* mouse, similar observations have been made in *Mecp2*-null mice (Asaka *et al.*, 2006) and the *Mecp2*^{308} line (Moretti *et al.*, 2006). Both PTP and PPF are believed to represent plasticity processes with largely pre-synaptic loci of expression (Zucker & Regehr, 2002). In contrast, sustained LTP at 41 to 60 minutes following HFS has been shown to be mainly of post-synaptic origin at the Schaffer collateral-to-CA1 pyramidal cell synapse (Nicoll, 2003). It is obvious that the deficits in the two forms of plasticity (LTP and PTP) showed strong parallelism. However, it was unclear from the extracellular recording data whether this relationship could be explained by some overlap in the underlying mechanisms or whether the reduction in LTP is a direct consequence of reduced PTP mediated via a predominantly pre-synaptic dysfunction. In summary, it appeared that both pre-synaptic and post-synaptic elements contributed to the deficits in hippocampal synaptic plasticity in symptomatic *Mecp2-stop* mice.

In the LTP saturation experiments, the inability to produce cumulative LTP in response to repeated HFS in hippocampal slices from symptomatic *Mecp2-stop* mice was observed. Another important finding of the LTP saturation experiment was that deficits in synaptic plasticity could be revealed in very mildly symptomatic male mice (from around five weeks old) by adopting appropriate plasticity induction paradigms which assess cumulative synaptic potentiation (see section 5.4). With symptom progression, these subtle abnormalities in synaptic plasticity became more overt and could be detected by a single HFS protocol for LTP induction. These findings indicated synaptic plasticity deficits as an early indicator of the disease process, although the precise cellular and synaptic dysfunctions and their mechanistic link with MeCP2 deficiency remain obscure.

The PTP analyses suggested pre-synaptic deficits in symptomatic *Mecp2-stop* hippocampal slices, and the PTP analyses from the LTP saturation experiments showed similar results. As with LTP analyses in the LTP saturation experiments, the PTP deficits became more pronounced with symptom progression. From the extracellular recording data, it was difficult to determine the exact mechanism underlying the synaptopathy occurring in RTT mice brains; however, both pre-synaptic and post-synaptic deficits in the *Mecp2-stop* hippocampus seemed to be consistent with the symptom progression and severity. Our result was the first to report this conclusion in an experimental animal model of RTT.

One possibility for the LTP deficits detected in the *Mecp2-stop* mice was that an overall reduction in plasticity existed, or that the apparent reduced LTP was due to synapses operating close to a maximal “ceiling”. The latter hypothesis was supported by the fact that repeated HFS stimuli in hippocampal slices from symptomatic *Mecp2-stop* mice could not induce cumulative LTPs. This phenomenon further supported the hypothesis that neurotransmission at the Schaffer collateral-to-CA1 pyramidal cell synapses in symptomatic *Mecp2-stop* mice operated in a state that was closer to saturation than in pre-symptomatic or WT mice.

A previous study showed that LTP saturation effects could be overcome by memantine, a drug prescribed to Alzheimer’s disease patients (Frankiewicz & Parsons, 1999); therefore memantine was applied in both *in vitro* and *in vivo*

experiments to assess the therapeutic potential for amending synaptic plasticity deficits in symptomatic *Mecp2-stop* mice. The results of this chapter showed that memantine applied to the symptomatic *Mecp2-stop* hippocampal slices at clinically-relevant concentrations (Frankiewicz & Parsons, 1999; Minkeviciene *et al.*, 2004) induced a heightened synaptic potentiation following HFS. In particular, memantine had a marked effect on the response to the first HFS (elevated LTP). However, the effect of memantine on the subsequent episodes of HFS was limited to a transient boost of short-term plasticity which typically decayed to baseline within a 15 minute period. This was a specific action targeting the MeCP2-related pathophysiology, as memantine had no effect on basal evoked synaptic transmission or control hippocampal slices from WT littermates subjected to the LTP saturation paradigm.

In contrast to the clear actions of memantine on hippocampal synaptic transmission *in vitro* under the disease state, the long-term daily dosing of *Mecp2-stop* mice with memantine did not change either the progression of symptoms or affect the survival profile. Memantine has been used successfully to amend aspects of hippocampus-dependent dysfunction in a transgenic model of Alzheimer disease (Minkeviciene *et al.*, 2004) and has been shown recently to normalise cognitive functions and synaptic marker levels in a mouse model of Down syndrome (Rueda *et al.*, 2010). The absence of any detectable improvement in RTT-like phenotypes suggested that this drug may not hold promise in treating the full range of symptoms of RTT. However, *Mecp2-stop* males were very severely affected by loss of MeCP2, and it remains to be tested whether memantine could be beneficial in heterozygous *Mecp2-stop* females, which display a milder and more stable phenotype. In addition, the plasticity impairments demonstrated here *ex vivo* may manifest in a range of subtle cognitive and behavioural aspects of the Rett-like phenotype rather than affecting the observable signs and lethality. Thus, assessing the potential for memantine to improve the phenotype *in vivo* may require appropriate behavioural assays to evaluate the outcome after memantine treatment. However, male *Mecp2-stop* mice have severe motor deficits and were difficult to screen in most cognitive assays. The phenotypic assessment adopted in this thesis did not involve a specific measure of hippocampal dysfunction and it was

therefore difficult to draw comparisons between the data obtained here *in vitro* and *in vivo*.

6 General discussion

6.1 Major findings

The major findings of this study are as follows:

Firstly, from the electrophysiology experiments, I report for the first time, pronounced hippocampal synaptic plasticity in the hemizygous *Mecp2-stop* brain. Moreover, I show a strong relationship between the degree of synaptic plasticity impairment and the overt neurological phenotype as assessed by observational signs at the whole animal level. Further analysis revealed significant deficits in both long-term (LTP) and short-term (PTP, PPF) forms of synaptic plasticity. In addition, the Alzheimer drug, Memantine, partially ameliorated synaptic plasticity deficits in symptomatic hemizygous *Mecp2-stop* hippocampi, particularly the short-term plasticity deficits.

Clinically, reports suggested RTT to be associated with a reduced head size and an increase in neuronal density. In the current study, I showed several findings in the immunohistochemistry experiments; firstly, cell density alteration in the somatosensory cortex was associated with volume change in symptomatic hemizygous *Mecp2-stop* mice. Besides this, a decrease in density of calretinin- (CR) and somatostatin- (SOM) positive inhibitory neurons was observed in the somatosensory cortex of symptomatic hemizygous *Mecp2-stop* mice. Furthermore, the gross distribution patterns of inhibitory neuron subtypes in the hippocampus of symptomatic *Mecp2-stop* mice were not significantly altered.

6.1.1 Synaptic plasticity deficits in Mecp2-stop mice

In Chapter five, synaptic plasticity deficits were reported in the *Mecp2-stop* mouse brain. In the HFS-induced LTP experiments, LTP deficit was observed in symptomatic *Mecp2-stop* hippocampi. LTP deficits shown here were in line with previous reports in various *Mecp2-mutant* models (Asaka *et al.*, 2006; Moretti *et al.*, 2006; Guy *et al.*, 2007). In a different *Mecp2* knock-out model, LTP deficits were detected under either HFS or theta burst LTP induction schemes in symptomatic mice (Asaka *et al.*, 2006). In the $Mecp2^{308/y}$ animal model, in which a truncated MeCP2 protein is expressed, LTP deficits were observed in hippocampal and cortical regions (Moretti *et al.*, 2006). Previously, Guy *et al.* demonstrated LTP deficits in HFS-induced LTP experiments in "symptomatic" (the same symptom scoring system was adopted; score=5 or more) heterozygous $Mecp2^{stop/+}$ mice brains (Guy *et al.*, 2007). In summary, MeCP2 obviously plays an important role in the mechanism of long-term plasticity.

In the HFS-induced LTP experiments of this thesis, not only the long-term plasticity but also the short-term plasticity was observed when MeCP2 was functionally knocked-out. The PTP analyses showed a reduced PTP in symptomatic *Mecp2-stop* mouse brains. Furthermore, the PPF analyses in the same experiments also revealed a decreased ratio in symptomatic *Mecp2-stop* mice brains. PTP and PPF are the representative assessment for short-term plasticity (Zucker & Regehr, 2002), and both results were consistent with the conclusion that short-term plasticity deficits exist in symptomatic *Mecp2-stop* mice brains. However, Asaka *et al.* reported that no significant reduced potentiation in the PTP assessment at Schaffer collateral but only a reduced PPF ratio was detected in symptomatic *Mecp2* knock-out mice (Asaka *et al.*, 2006). One difference between Asaka *et al.* and my studies was the age; most "symptomatic" mice used in Asaka's study were over 6wks of age, while in this thesis "symptomatic" (score=5 or more) *Mecp2-stop* mice referred to 12-15wk old mice. The discrepancy between Asaka and my studies may be due to the fact that PTP deficits developed later, or due to the basic differences between these two model designs.

The LTP saturation experiment, whereby repeated HFS stimuli led to a "plateau" or "saturation" state, proved a valuable means of further investigating plasticity

deficits in the *Mecp2-stop* mice. Specifically, it revealed that synaptic plasticity deficits occurred very early in the disease phenotype (mice scoring only 2 or more on the phenotype severity scale). Under this experimental scheme, more subtle alterations in the LTP could be revealed. In chapter 5, not only symptomatic but also very mildly symptomatic (score 2-4) *Mecp2-stop* mice were used in LTP saturation experiments. My data showed that mild symptomatic *Mecp2-stop* mice demonstrated a significant reduction of LTP after the second or third repetitive stimulus. Most synaptic plasticity studies of the *Mecp2*-mutant mice reported that LTP deficits only existed in "symptomatic" mutant mice (Asaka *et al.*, 2006; Moretti *et al.*, 2006; Guy *et al.*, 2007). However, in this thesis, LTP deficits were shown in mildly symptomatic (score=2-4) *Mecp2-stop* mice under the LTP saturation experimental paradigm. This is an important and novel finding since it indicated LTP alterations may accumulate through neurodevelopmental stages.

PTP was also analysed in the LTP saturation experiments. My data showed that symptomatic *Mecp2-stop* mice had a significant reduction in the initial PTP amplitude. Generally, the age of "symptomatic" (score=5 or more) mice in this thesis ranged from 12-15wks old. In the synaptic plasticity study of Asaka *et al.*, "symptomatic" mice referred to those with ages ranged above 6wks old (Asaka *et al.*, 2006), and there was no difference in the PTP amplitude between symptomatic and WT groups in their study. Once again, PTP deficits in *Mecp2*-null mouse models might occur rather late after symptoms develop and this is proved by the finding of no significant alteration to PTP at earlier stages in both Asaka's and my studies.

To conclude, the synaptic plasticity results observed in both classical HFS-induced LTP and LTP saturation experiments verified that RTT animal models display deficits in both short-term and long-term synaptic plasticity. This adds to the prevalent finding of plasticity deficits in various neurodevelopmental disorder models, such as Down's syndrome, Fragile-X syndrome, etc (Yun & Trommer, ; Rueda *et al.*, 2010). The exact mechanism underlying the synaptopathy of RTT needs to be further addressed to clarify the role MeCP2 plays in hippocampal neuronal circuits.

6.1.2 Memantine partially improved synaptic plasticity deficits in symptomatic Mecp2-stop mice

Memantine is classified as a weak NMDA receptor antagonist and has been widely used for treating Alzheimer's disease clinically (Rammes *et al.*, 2008). In an Alzheimer's animal model, a previous study reported that Memantine has been used successfully to amend aspects of hippocampus-dependent dysfunction (Minkeviciene *et al.*, 2004).

In the results shown in Chapter 5, memantine was applied in the LTP saturation experiments at the therapeutic level. The LTP of the WT hippocampus was not significantly altered after memantine treatment. In contrast, the LTP of the hemizygous symptomatic *Mecp2-stop* hippocampus was partially restored in the LTP saturation experiments. The improvement was significant, particularly after the first HFS stimulus and the LTP of symptomatic *Mecp2-stop* mice showed no difference compared to the initial LTP of WT littermates. However, repeated HFS stimuli on memantine-treated symptomatic *Mecp2-stop* brain slices showed that only the short-term plasticity was restored. It was difficult to determine the mechanism by which memantine ameliorates short-term synaptic plasticity deficits by analysis of extracellular recordings; however, this mechanism was associated with the pathophysiology of RTT, since the LTP of WT brain slices was not altered but only effective on *Mecp2-stop* brain slices. It will be worth assessing whether memantine is beneficial in the heterozygous *Mecp2-stop* brain, since both WT and mutant cells co-exist in the heterozygous brain and the genotype is identical to that of human RTT patients.

6.1.3 Alterations of cell densities in the somatosensory cortex but preserved distribution patterns in the hippocampus in symptomatic Mecp2-stop mice

Previous reports have shown a reduced brain volume in RTT patients (Reiss *et al.*, 1993). In *Mecp2*-mutant models, anatomical studies also revealed that brain cells had a higher packing rate (Chen *et al.*, 2001; Taneja *et al.*, 2009). Since autopsy analyses showed there was no significant apoptosis or necrosis in RTT brains (Armstrong, 2005), the higher cell packing rate may originate solely from the volume change in RTT brains. In order to confirm this hypothesis, both DAPI- and NeuN- positive cell densities were quantified in the somatosensory cortex of symptomatic *Mecp2-stop* and WT mice. The DAPI- and NeuN- positive cell densities were elevated in the symptomatic *Mecp2-stop* brain, and the chi-square analysis showed no significant difference in the ratios of both DAPI- and NeuN- positive cells. This conclusion is in line with previous observations that no significant cell death had occurred in a rather smaller RTT brain (Armstrong, 2005).

One of the characteristic features of RTT is the development of seizure disorders. Previous report showed that an excitatory/inhibitory (E/I) imbalance existed in the *Mecp2*-mutant brains and served as the pathology of seizure disorders in RTT (Dani *et al.*, 2005; Zhang *et al.*, 2008; Wood & Shepherd, 2010). The E/I imbalance may be due to the dysfunctions of excitatory, inhibitory, or both neuronal cell types. Recently, the functional knock-out of MeCP2 selectively in inhibitory neurons has been shown to recapitulate most RTT-like symptoms in mice, including seizure disorders (Chao *et al.*, 2010). Therefore, the dysfunction of inhibitory neurons may directly contribute to the mechanism underling seizure disorders in RTT. In mammalian brains, inhibitory cortical neurons can be further classified into distinct populations by protein markers, and it was of interest to investigate the alteration of different inhibitory neuron subtypes in *Mecp2-stop* brains. In Chapter 4, cell densities of four different inhibitory neuron populations (PV, SOM, CR, and CR) were quantified. Since the NeuN-positive (neuronal) density was elevated in the *Mecp2-stop* brain, the raw cell density data of each inhibitory neuron subtype was further standardised by the *Mecp2*/WT NeuN correcting factor. The results showed that CR- and SOM-positive neuronal densities in symptomatic *Mecp2-stop* mice were decreased compared

to those of WT mice. However, both PV- and CB-positive cell densities remained unchanged in the symptomatic *Mecp2-stop* brain. This is the first report showing the decrease in cell density of specific inhibitory neurons in *Mecp2*-null animals. This decrease may be associated with deficits in the neurogenesis stage or, it may be that specific neuronal subtypes were more vulnerable in the symptomatic *Mecp2-stop* brain. This finding indicated that the dysfunction of inhibitory neurons in RTT brains may originate directly or indirectly from the alteration of specific inhibitory neuron populations.

Regarding the distribution patterns of distinct neuronal subtypes, I assessed four neuronal subtypes (PV, SOM, CR and CB) in the hippocampus in the symptomatic *Mecp2-stop* mice under microscopic examinations, and the results showed a grossly similar distribution pattern to that of WT mice. To conclude, the distribution patterns of these four neuronal subtypes in the hippocampus of symptomatic *Mecp2-stop* mice were not altered; however, since this work was only performed in the hippocampal region, it is not possible to draw any conclusion about whether the lack of MeCP2 influences the distribution patterns of cortical neuronal subtypes or not.

6.2 Significance of this study

The importance of this investigation is outlined in the following key points.

1. In my thesis, both short-term and long-term synaptic plasticity were shown in "symptomatic" *Mecp2-stop* mouse brain. The long-term synaptic plasticity deficit of "symptomatic" *Mecp2-stop* mice was in line with previous reports demonstrating LTP deficits in *Mecp2*-mutant mice (Asaka *et al.*, 2006; Moretti *et al.*, 2006; Guy *et al.*, 2007). Regarding the short-term plasticity deficit, my thesis was the first to report a reduction of both PTP and PPF in "symptomatic" *Mecp2*-mutant mice.

2. In my thesis, the PTP and LTP deficits were examined both in "symptomatic" (age range 12-15wks) and "mild symptomatic" (age range 6-10wks) *Mecp2-stop* mice hippocampi. The LTP deficit was observed in "mild symptomatic" under the LTP saturation experimental scheme. The PTP deficit was only shown in "symptomatic" group, however, PTP analyses from "mild symptomatic" groups showed no significant difference to that of WT littermates, but a decreasing trend of PTP amplitude as symptoms progressed. The studies reported here are the first to link the symptom score progression to both short-term and long-term plasticity deficits in *Mecp2*-mutant mice. Moreover, it may suggest that subtle deficits in synaptic signalling may occur very early in disease pathogenesis but may be undetected by classical assays (for example, the one-hour HFS-induced LTP assessment).

3. The Alzheimer's drug memantine was applied in the current study and my thesis was the first to assess the therapeutic potential of memantine on *Mecp2*-mutant animal models. The results in Chapter 5 showed that memantine partially amended synaptic plasticity deficits, particularly regarding short-term plasticity, while the WT littermates were not altered by memantine administration. My data also demonstrated that memantine was not beneficial to symptom progression or survival in hemizygous *Mecp2-stop* mice. All the three significant findings above have already been published in my recent paper (Weng *et al.*, 2011).

4. In the immunohistochemistry experiments on symptomatic *Mecp2-stop* brains, my thesis was the first to identify specific inhibitory neuronal loss in the *Mecp2*-mutant brain. Both CR- and SOM-positive cells in the somatosensory cortex had a reduced cellular density compared to those of WT littermates. However, this was carried out only in a single region of the brain and it may or may not be representative.

5. In my thesis, I examined the distribution patterns of four neuronal populations (PV, SOM, CB and CR) in symptomatic *Mecp2-stop* mice brains, and there was no significant difference from that of WT mice. The preserved targeting pattern may be directly or indirectly linked to the pathophysiology of RTT.

6.3 Technical considerations

In the immunohistochemistry experiments, the cell density quantification inside image stacks was carried out by manual counting. The disector principle (see Chapter 2 for details) was applied to avoid overlapped counting. Several types of software, such as Image J or Image Pro Plus, have been used in the past for automated counting in this study; however, my experience was that manual counting was more reliable. The first reason for this is that any one cell can exist in adjacent image planes of the image stack. It was difficult to avoid repeated counting solely by the parameter adjustment of the software settings. The second reason is that manual counting was beneficial in differentiating real cells from artefacts by recognising the characteristics of cells. Cells containing identical markers may have varying shapes or sizes. It was difficult to set the parameters in automated cell counting for discriminating cells and artefacts in commercialised software. Therefore, the most reliable method was still manual counting, although it was a time-consuming experimental design. The cell density results in this thesis were further verified by comparing with previous studies quantifying the neuronal cell density in rodent neocortex layer five (Bass *et al.*, 1971), and with reports of the percentage of distinct cortical inhibitory neuronal subtypes (Wonders & Anderson, 2006). To conclude, manual counting was regarded as the most reliable and accurate method in a cell density quantification experiment from 3D image stacks.

6.4 Future studies

The results in this thesis have initiated the prelude for a full investigation of MeCP2 involvement in modulating synaptic plasticity and regulating inhibitory neuron subtype development. These pioneering experiments have laid the groundwork for more detailed future studies. Several further experiments emerging from this thesis have been highlighted in previous discussion. There are many unresolved questions that are worthy of further investigation:

1. How are the pre-synaptic and post-synaptic deficits related in *Mecp2-stop* models? In Chapter 5, both the short-term and long-term plasticity deficits were observed in symptomatic *Mecp2-stop* mice. Since short-term plasticity is generally linked to the pre-synaptic mechanism while the long-term plasticity is principally mediated by the post-synaptic mechanism, the conclusion in this thesis supported the hypothesis that both short- and long-term plasticity deficits co-existed in symptomatic *Mecp2-stop* brains. The two forms of synaptic plasticity deficits showed strong parallelism (Zucker & Regehr, 2002), and it was difficult to determine how they are related solely from the extracellular recording data. Single-cell recording could be applied to assess the relationship between the two forms of synaptic plasticity in the lack of MeCP2.

2. The memantine treatment in symptomatic *Mecp2-stop* hippocampi seemed to partially restore the synaptic plasticity deficit, particularly in the short-term plasticity. When it applied to the WT groups, no obvious alteration was observed. The improvement of memantine on short-term plasticity deficits in symptomatic *Mecp2-stop* brain slices may be directly connected to the RTT pathophysiology, and this will be worthy for further investigation. Whole cell recording could be applied to assess how memantine improves the synaptic plasticity of MeCP2-null cells. The answer will provide further information for treating human RTT in which both the mutant and WT cells co-exist as a mosaic pattern in the brain, and this information will be beneficial for exploring more suitable drugs for future treatment of RTT.

3. In Chapter 4, a decrease in density of calretinin- (CR) and somatostatin- (SOM) positive inhibitory neurons was observed in the somatosensory cortex of symptomatic hemizygous *Mecp2-stop* mice. However, further investigation

addressing the underlying mechanism of the decrease of specific neuronal subtype in the symptomatic *Mecp2-stop* brain needs to be assessed to clarify the MeCP2 role in the whole neurodevelopment from embryonic to adult stages. In addition, it will be essential to investigate the cell density alteration in the heterozygous *Mecp2-stop* mice, in which the genotype is identical to human RTT patients, since the answer will provide further understanding of the development of inhibitory neurons in RTT patients (this project has already been initiated in Dr Stuart Cobb's lab at the University of Glasgow).

4. Since the hippocampus laminar structure is well-investigated, it provides an excellent platform for assessing the distribution pattern of specific neuronal subtypes. However, the distribution pattern could be normal in the hippocampus but abnormal in other regions of the symptomatic *Mecp2-stop* brain. It is worth further characterising the distribution patterns of specific neuronal subtypes in distinct regions of the symptomatic *Mecp2-stop* brain.

5. The phenotype score system of *Mecp2-stop* mice served as an excellent indicator for selecting animals for different experimental use. However, the phenotype score system could be further expanded from the original one adopted from Guy *et al.* (Guy *et al.*, 2007), and might provide more subtle behavioural information for the interpretation of the role that MeCP2 plays in the RTT-like phenotype progression.

To conclude, it is clear that the current study has commenced a new area of research that MeCP2 has an overt action on synaptic plasticity and specific neuronal subtype development. Clearly, this research has laid a strong foundation for a number of other important questions which are necessary to solve in the future for further understanding the role which MeCP2 plays in both normal and diseased brains.

7 References

Al-Humadi H, Zarros A, Al-Saigh R & Liapi C (2010) Genetic basis and gene therapy trials for thyroid cancer. *Cancer Genomics Proteomics* **7**, 31-49.

Amir RE, Van den Veyver IB, Wan M, Tran CQ, Francke U & Zoghbi HY (1999) Rett syndrome is caused by mutations in X-linked MECP2, encoding methyl-CpG-binding protein 2. *Nat Genet* **23**, 185-188.

Archer H, Evans J, Leonard H, Colvin L, Ravine D, Christodoulou J, Williamson S, Charman T, Bailey ME, Sampson J, de Klerk N & Clarke A (2007) Correlation between clinical severity in patients with Rett syndrome with a p.R168X or p.T158M MECP2 mutation, and the direction and degree of skewing of X-chromosome inactivation. *J Med Genet* **44**, 148-152.

Armstrong D, Dunn JK, Antalffy B & Trivedi R (1995) Selective dendritic alterations in the cortex of Rett syndrome. *J Neuropathol Exp Neurol* **54**, 195-201.

Armstrong DD (2005) Neuropathology of Rett syndrome. *J Child Neurol* **20**, 747-753.

Armstrong DD, Dunn K & Antalffy B (1998) Decreased dendritic branching in frontal, motor and limbic cortex in Rett syndrome compared with trisomy 21. *J Neuropathol Exp Neurol* **57**, 1013-1017.

Asaka Y, Jugloff DG, Zhang L, Eubanks JH & Fitzsimonds RM (2006) Hippocampal synaptic plasticity is impaired in the Mecp2-null mouse model of Rett syndrome. *Neurobiol Dis* **21**, 217-227.

Ascoli GA, Alonso-Nanclares L, Anderson SA, Barrionuevo G, Benavides-Piccione R, Burkhalter A, Buzsaki G, Cauli B, Defelipe J, Fairen A, Feldmeyer D, Fishell G, Fregnac Y, Freund TF, Gardner D, Gardner EP, Goldberg JH, Helmstaedter M, Hestrin S, Karube F, Kisvarday ZF, Lambolez B, Lewis DA, Marin O, Markram H, Munoz A, Packer A, Petersen CC, Rockland KS, Rossier J, Rudy B, Somogyi P, Staiger JF, Tamas G, Thomson AM, Toledo-Rodriguez M, Wang Y, West DC &

Yuste R (2008) Petilla terminology: nomenclature of features of GABAergic interneurons of the cerebral cortex. *Nat Rev Neurosci* **9**, 557-568.

Ballas N, Lioy DT, Grunseich C & Mandel G (2009) Non-cell autonomous influence of MeCP2-deficient glia on neuronal dendritic morphology. *Nat Neurosci* **12**, 311-317.

Barrionuevo G, Schottler F & Lynch G (1980) The effects of repetitive low frequency stimulation on control and "potentiated" synaptic responses in the hippocampus. *Life Sci* **27**, 2385-2391.

Bartos M, Vida I & Jonas P (2007) Synaptic mechanisms of synchronized gamma oscillations in inhibitory interneuron networks. *Nat Rev Neurosci* **8**, 45-56.

Bashir ZI & Collingridge GL (1994) An investigation of depotentiation of long-term potentiation in the CA1 region of the hippocampus. *Exp Brain Res* **100**, 437-443.

Bashir ZI, Jane DE, Sunter DC, Watkins JC & Collingridge GL (1993) Metabotropic glutamate receptors contribute to the induction of long-term depression in the CA1 region of the hippocampus. *Eur J Pharmacol* **239**, 265-266.

Bass NH, Hess HH, Pope A & Thalheimer C (1971) Quantitative cytoarchitectonic distribution of neurons, glia, and DNa in rat cerebral cortex. *J Comp Neurol* **143**, 481-490.

Belichenko PV, Hagberg B & Dahlstrom A (1997) Morphological study of neocortical areas in Rett syndrome. *Acta Neuropathol* **93**, 50-61.

Belichenko PV, Wright EE, Belichenko NP, Masliah E, Li HH, Mobley WC & Francke U (2009) Widespread changes in dendritic and axonal morphology in Mecp2-mutant mouse models of Rett syndrome: evidence for disruption of neuronal networks. *J Comp Neurol* **514**, 240-258.

Bennett MV (1997) Gap junctions as electrical synapses. *J Neurocytol* **26**, 349-366.

Bennett MV & Zukin RS (2004) Electrical coupling and neuronal synchronization in the Mammalian brain. *Neuron* **41**, 495-511.

Bentivoglio M, Tassi L, Pech E, Costa C, Fabene PF & Spreafico R (2003) Cortical development and focal cortical dysplasia. *Epileptic Disord* **5 Suppl 2**, S27-34.

Best PJ & White AM (1999) Placing hippocampal single-unit studies in a historical context. *Hippocampus* **9**, 346-351.

Bliss TV & Collingridge GL (1993) A synaptic model of memory: long-term potentiation in the hippocampus. *Nature* **361**, 31-39.

Bliss TV, Errington ML & Lynch MA (1990a) Long-term potentiation in the dentate gyrus in vivo is associated with a sustained increase in extracellular glutamate. *Adv Exp Med Biol* **268**, 269-278.

Bliss TV, Errington ML, Lynch MA & Williams JH (1990b) Presynaptic mechanisms in hippocampal long-term potentiation. *Cold Spring Harb Symp Quant Biol* **55**, 119-129.

Bliss TV & Gardner-Medwin AR (1973) Long-lasting potentiation of synaptic transmission in the dentate area of the unanaestetized rabbit following stimulation of the perforant path. *J Physiol* **232**, 357-374.

Bliss TV & Lomo T (1973) Long-lasting potentiation of synaptic transmission in the dentate area of the anaesthetized rabbit following stimulation of the perforant path. *J Physiol* **232**, 331-356.

Bortolotto ZA, Amici M, Anderson WW, Isaac JT & Collingridge GL (2011) Synaptic plasticity in the hippocampal slice preparation. *Curr Protoc Neurosci* **Chapter 6**, Unit 6 13.

Bortolotto ZA, Fitzjohn SM & Collingridge GL (1999) Roles of metabotropic glutamate receptors in LTP and LTD in the hippocampus. *Curr Opin Neurobiol* **9**, 299-304.

Boss BD, Peterson GM & Cowan WM (1985) On the number of neurons in the dentate gyrus of the rat. *Brain Res* **338**, 144-150.

Boss BD, Turlejski K, Stanfield BB & Cowan WM (1987) On the numbers of neurons in fields CA1 and CA3 of the hippocampus of Sprague-Dawley and Wistar rats. *Brain Res* **406**, 280-287.

Boyer P, Phillips JL, Rousseau FL & Ilivitsky S (2007) Hippocampal abnormalities and memory deficits: new evidence of a strong pathophysiological link in schizophrenia. *Brain Res Rev* **54**, 92-112.

Brendel C, Klahold E, Gartner J & Huppke P (2009) Suppression of nonsense mutations in Rett syndrome by aminoglycoside antibiotics. *Pediatr Res* **65**, 520-523.

Brucke T, Sofic E, Killian W, Rett A & Riederer P (1987) Reduced concentrations and increased metabolism of biogenic amines in a single case of Rett-syndrome: a postmortem brain study. *J Neural Transm* **68**, 315-324.

Burke SN & Barnes CA (2006) Neural plasticity in the ageing brain. *Nat Rev Neurosci* **7**, 30-40.

Calabresi P, Pisani A, Mercuri NB & Bernardi G (1992) Long-term Potentiation in the Striatum is Unmasked by Removing the Voltage-dependent Magnesium Block of NMDA Receptor Channels. *Eur J Neurosci* **4**, 929-935.

Calfa G, Percy AK & Pozzo-Miller L (2011) Experimental models of Rett syndrome based on Mecp2 dysfunction. *Exp Biol Med (Maywood)* **236**, 3-19.

Celio MR & Heizmann CW (1981) Calcium-binding protein parvalbumin as a neuronal marker. *Nature* **293**, 300-302.

Chahrour M, Jung SY, Shaw C, Zhou X, Wong ST, Qin J & Zoghbi HY (2008) MeCP2, a key contributor to neurological disease, activates and represses transcription. *Science* **320**, 1224-1229.

Chahrour M & Zoghbi HY (2007) The story of Rett syndrome: from clinic to neurobiology. *Neuron* **56**, 422-437.

Chang YS, Wang L, Suh YA, Mao L, Karpen SJ, Khuri FR, Hong WK & Lee HY (2004) Mechanisms underlying lack of insulin-like growth factor-binding protein-3 expression in non-small-cell lung cancer. *Oncogene* **23**, 6569-6580.

Chao HT, Chen H, Samaco RC, Xue M, Chahrour M, Yoo J, Neul JL, Gong S, Lu HC, Heintz N, Ekker M, Rubenstein JL, Noebels JL, Rosenmund C & Zoghbi HY (2010) Dysfunction in GABA signalling mediates autism-like stereotypies and Rett syndrome phenotypes. *Nature* **468**, 263-269.

Chao HT, Zoghbi HY & Rosenmund C (2007) MeCP2 controls excitatory synaptic strength by regulating glutamatergic synapse number. *Neuron* **56**, 58-65.

Chen RZ, Akbarian S, Tudor M & Jaenisch R (2001) Deficiency of methyl-CpG binding protein-2 in CNS neurons results in a Rett-like phenotype in mice. *Nat Genet* **27**, 327-331.

Chen WG, Chang Q, Lin Y, Meissner A, West AE, Griffith EC, Jaenisch R & Greenberg ME (2003) Derepression of BDNF transcription involves calcium-dependent phosphorylation of MeCP2. *Science* **302**, 885-889.

Colledge M, Snyder EM, Crozier RA, Soderling JA, Jin Y, Langeberg LK, Lu H, Bear MF & Scott JD (2003) Ubiquitination regulates PSD-95 degradation and AMPA receptor surface expression. *Neuron* **40**, 595-607.

Collingridge GL, Herron CE & Lester RA (1988) Synaptic activation of N-methyl-D-aspartate receptors in the Schaffer collateral-commissural pathway of rat hippocampus. *J Physiol* **399**, 283-300.

Collins AL, Levenson JM, Vilaythong AP, Richman R, Armstrong DL, Noebels JL, David Sweatt J & Zoghbi HY (2004) Mild overexpression of MeCP2 causes a progressive neurological disorder in mice. *Hum Mol Genet* **13**, 2679-2689.

Connors BW & Gutnick MJ (1990) Intrinsic firing patterns of diverse neocortical neurons. *Trends Neurosci* **13**, 99-104.

D'Cruz JA, Wu C, Zahid T, El-Hayek Y, Zhang L & Eubanks JH (2010) Alterations of cortical and hippocampal EEG activity in MeCP2-deficient mice. *Neurobiol Dis* **38**, 8-16.

Dani VS, Chang Q, Maffei A, Turrigiano GG, Jaenisch R & Nelson SB (2005) Reduced cortical activity due to a shift in the balance between excitation and inhibition in a mouse model of Rett syndrome. *Proc Natl Acad Sci U S A* **102**, 12560-12565.

Dani VS & Nelson SB (2009) Intact long-term potentiation but reduced connectivity between neocortical layer 5 pyramidal neurons in a mouse model of Rett syndrome. *J Neurosci* **29**, 11263-11270.

Davies JC & Alton EW (2010) Gene therapy for cystic fibrosis. *Proc Am Thorac Soc* **7**, 408-414.

DeFelipe J (1997) Types of neurons, synaptic connections and chemical characteristics of cells immunoreactive for calbindin-D28K, parvalbumin and calretinin in the neocortex. *J Chem Neuroanat* **14**, 1-19.

DeFelipe J (1999) Chandelier cells and epilepsy. *Brain* **122 (Pt 10)**, 1807-1822.

Deguchi K, Antalffy BA, Twohill LJ, Chakraborty S, Glaze DG & Armstrong DD (2000) Substance P immunoreactivity in Rett syndrome. *Pediatr Neurol* **22**, 259-266.

Diehl KH, Hull R, Morton D, Pfister R, Rabemampianina Y, Smith D, Vidal JM & van de Vorstenbosch C (2001) A good practice guide to the administration of substances and removal of blood, including routes and volumes. *J Appl Toxicol* **21**, 15-23.

Dolphin AC, Errington ML & Bliss TV (1982) Long-term potentiation of the perforant path in vivo is associated with increased glutamate release. *Nature* **297**, 496-498.

Druga R (2009) Neocortical inhibitory system. *Folia Biol (Praha)* **55**, 201-217.

Dudek SM & Bear MF (1992) Homosynaptic long-term depression in area CA1 of hippocampus and effects of N-methyl-D-aspartate receptor blockade. *Proc Natl Acad Sci U S A* **89**, 4363-4367.

Dudek SM & Bear MF (1993) Bidirectional long-term modification of synaptic effectiveness in the adult and immature hippocampus. *J Neurosci* **13**, 2910-2918.

Eccles JC (1982) The synapse: from electrical to chemical transmission. *Annu Rev Neurosci* **5**, 325-339.

Ehlers MD (2000) Reinsertion or degradation of AMPA receptors determined by activity-dependent endocytic sorting. *Neuron* **28**, 511-525.

Elde R, Hokfelt T, Johansson O, Schultzberg M, Efendic S & Luft R (1978) Cellular localization of somatostatin. *Metabolism* **27**, 1151-1159.

Feldman DE, Nicoll RA, Malenka RC & Isaac JT (1998) Long-term depression at thalamocortical synapses in developing rat somatosensory cortex. *Neuron* **21**, 347-357.

Frankiewicz T & Parsons CG (1999) Memantine restores long term potentiation impaired by tonic N-methyl-D-aspartate (NMDA) receptor activation following reduction of Mg2+ in hippocampal slices. *Neuropharmacology* **38**, 1253-1259.

Freund TF & Buzsaki G (1996) Interneurons of the hippocampus. *Hippocampus* **6**, 347-470.

Frey U, Krug M, Reymann KG & Matthies H (1988) Anisomycin, an inhibitor of protein synthesis, blocks late phases of LTP phenomena in the hippocampal CA1 region in vitro. *Brain Res* **452**, 57-65.

Fukuda T, Itoh M, Ichikawa T, Washiyama K & Goto Y (2005) Delayed maturation of neuronal architecture and synaptogenesis in cerebral cortex of Mecp2-deficient mice. *J Neuropathol Exp Neurol* **64**, 537-544.

Gadalla KK, Bailey ME & Cobb SR (2011) MeCP2 and Rett syndrome: reversibility and potential avenues for therapy. *Biochem J* **439**, 1-14.

Galarreta M & Hestrin S (2001) Electrical synapses between GABA-releasing interneurons. *Nat Rev Neurosci* **2**, 425-433.

Garcia-Segura LM, Baetens D, Roth J, Norman AW & Orci L (1984) Immunohistochemical mapping of calcium-binding protein immunoreactivity in the rat central nervous system. *Brain Res* **296**, 75-86.

Giacometti E, Luikenhuis S, Beard C & Jaenisch R (2007) Partial rescue of MeCP2 deficiency by postnatal activation of MeCP2. *Proc Natl Acad Sci U S A* **104**, 1931-1936.

Guy J, Gan J, Selfridge J, Cobb S & Bird A (2007) Reversal of neurological defects in a mouse model of Rett syndrome. *Science* **315**, 1143-1147.

Guy J, Hendrich B, Holmes M, Martin JE & Bird A (2001) A mouse Mecp2-null mutation causes neurological symptoms that mimic Rett syndrome. *Nat Genet* **27**, 322-326.

Hagberg B (2005) Rett syndrome: long-term clinical follow-up experiences over four decades. *J Child Neurol* **20**, 722-727.

Hagberg B, Aicardi J, Dias K & Ramos O (1983) A progressive syndrome of autism, dementia, ataxia, and loss of purposeful hand use in girls: Rett's syndrome: report of 35 cases. *Ann Neurol* **14**, 471-479.

Hagberg G, Stenbom Y & Witt Engerstrom I (2000) Head growth in Rett syndrome. *Acta Paediatr* **89**, 198-202.

Hamberger A, Gillberg C, Palm A & Hagberg B (1992) Elevated CSF glutamate in Rett syndrome. *Neuropediatrics* **23**, 212-213.

Harris EW & Cotman CW (1986) Long-term potentiation of guinea pig mossy fiber responses is not blocked by N-methyl D-aspartate antagonists. *Neurosci Lett* **70**, 132-137.

Hendrich B & Bird A (1998) Identification and characterization of a family of mammalian methyl-CpG binding proteins. *Mol Cell Biol* **18**, 6538-6547.

Herculano-Houzel S & Lent R (2005) Isotropic fractionator: a simple, rapid method for the quantification of total cell and neuron numbers in the brain. *J Neurosci* **25**, 2518-2521.

Herman ST (2006) Clinical trials for prevention of epileptogenesis. *Epilepsy Res* **68**, 35-38.

Heynen AJ, Quinlan EM, Bae DC & Bear MF (2000) Bidirectional, activity-dependent regulation of glutamate receptors in the adult hippocampus in vivo. *Neuron* **28**, 527-536.

Hof PR & Sherwood CC (2005) Morphomolecular neuronal phenotypes in the neocortex reflect phylogenetic relationships among certain mammalian orders. *Anat Rec A Discov Mol Cell Evol Biol* **287**, 1153-1163.

Hoffbuhr KC, Moses LM, Jerdonek MA, Naidu S & Hoffman EP (2002) Associations between MeCP2 mutations, X-chromosome inactivation, and phenotype. *Ment Retard Dev Disabil Res Rev* **8**, 99-105.

Holtmaat A & Svoboda K (2009) Experience-dependent structural synaptic plasticity in the mammalian brain. *Nat Rev Neurosci* **10**, 647-658.

Horike S, Cai S, Miyano M, Cheng JF & Kohwi-Shigematsu T (2005) Loss of silent-chromatin looping and impaired imprinting of DLX5 in Rett syndrome. *Nat Genet* **37**, 31-40.

Huang YY, Colino A, Selig DK & Malenka RC (1992) The influence of prior synaptic activity on the induction of long-term potentiation. *Science* **255**, 730-733.

Huber KM, Kayser MS & Bear MF (2000) Role for rapid dendritic protein synthesis in hippocampal mGluR-dependent long-term depression. *Science* **288**, 1254-1257.

Ide S, Itoh M & Goto Y (2005) Defect in normal developmental increase of the brain biogenic amine concentrations in the mecp2-null mouse. *Neurosci Lett* **386**, 14-17.

Isoda K, Morimoto M, Matsui F, Hasegawa T, Tozawa T, Morioka S, Chiyonobu T, Nishimura A, Yoshimoto K & Hosoi H (2010) Postnatal changes in serotonergic innervation to the hippocampus of methyl-CpG-binding protein 2-null mice. *Neuroscience* **165**, 1254-1260.

Itoh M, Ide S, Takashima S, Kudo S, Nomura Y, Segawa M, Kubota T, Mori H, Tanaka S, Horie H, Tanabe Y & Goto Y (2007) Methyl CpG-binding protein 2 (a mutation of which causes Rett syndrome) directly regulates insulin-like growth factor binding protein 3 in mouse and human brains. *J Neuropathol Exp Neurol* **66**, 117-123.

Jessell TM & Kandel ER (1993) Synaptic transmission: a bidirectional and self-modifiable form of cell-cell communication. *Cell* **72 Suppl**, 1-30.

Jian L, Nagarajan L, de Klerk N, Ravine D, Bower C, Anderson A, Williamson S, Christodoulou J & Leonard H (2006) Predictors of seizure onset in Rett syndrome. *J Pediatr* **149**, 542-547.

Jinno S & Kosaka T (2006) Cellular architecture of the mouse hippocampus: a quantitative aspect of chemically defined GABAergic neurons with stereology. *Neurosci Res* **56**, 229-245.

Jonas P, Bischofberger J, Fricker D & Miles R (2004) Interneuron Diversity series: Fast in, fast out--temporal and spatial signal processing in hippocampal interneurons. *Trends Neurosci* **27**, 30-40.

Jugloff DG, Vandamme K, Logan R, Visanji NP, Brotchie JM & Eubanks JH (2008) Targeted delivery of an Mecp2 transgene to forebrain neurons improves the behavior of female Mecp2-deficient mice. *Hum Mol Genet* **17**, 1386-1396.

Julu PO, Kerr AM, Apartopoulos F, Al-Rawas S, Engerstrom IW, Engerstrom L, Jamal GA & Hansen S (2001) Characterisation of breathing and associated central autonomic dysfunction in the Rett disorder. *Arch Dis Child* **85**, 29-37.

Kauer JA, Malenka RC & Nicoll RA (1988) NMDA application potentiates synaptic transmission in the hippocampus. *Nature* **334**, 250-252.

Kaufmann WE & Moser HW (2000) Dendritic anomalies in disorders associated with mental retardation. *Cereb Cortex* **10**, 981-991.

Kemp N & Bashir ZI (1999) Induction of LTD in the adult hippocampus by the synaptic activation of AMPA/kainate and metabotropic glutamate receptors. *Neuropharmacology* **38**, 495-504.

Kemp N & Bashir ZI (2001) Long-term depression: a cascade of induction and expression mechanisms. *Prog Neurobiol* **65**, 339-365.

Kirkwood A & Bear MF (1994) Homosynaptic long-term depression in the visual cortex. *J Neurosci* **14**, 3404-3412.

Kishi N & Macklis JD (2004) MECP2 is progressively expressed in post-migratory neurons and is involved in neuronal maturation rather than cell fate decisions. *Mol Cell Neurosci* **27**, 306-321.

Klausberger T & Somogyi P (2008) Neuronal diversity and temporal dynamics: the unity of hippocampal circuit operations. *Science* **321**, 53-57.

Kline DD, Ogier M, Kunze DL & Katz DM (2010) Exogenous brain-derived neurotrophic factor rescues synaptic dysfunction in Mecp2-null mice. *J Neurosci* **30**, 5303-5310.

Klose RJ & Bird AP (2006) Genomic DNA methylation: the mark and its mediators. *Trends Biochem Sci* **31**, 89-97.

Knudsen GP, Neilson TC, Pedersen J, Kerr A, Schwartz M, Hulten M, Bailey ME & Orstavik KH (2006) Increased skewing of X chromosome inactivation in Rett syndrome patients and their mothers. *Eur J Hum Genet* **14**, 1189-1194.

Kubota Y, Hattori R & Yui Y (1994) Three distinct subpopulations of GABAergic neurons in rat frontal agranular cortex. *Brain Res* **649**, 159-173.

Kudo S (1998) Methyl-CpG-binding protein MeCP2 represses Sp1-activated transcription of the human leukosialin gene when the promoter is methylated. *Mol Cell Biol* **18**, 5492-5499.

Kullmann DM & Lamsa KP (2007) Long-term synaptic plasticity in hippocampal interneurons. *Nat Rev Neurosci* **8**, 687-699.

Kutsuwada T, Sakimura K, Manabe T, Takayama C, Katakura N, Kushiya E, Natsume R, Watanabe M, Inoue Y, Yagi T, Aizawa S, Arakawa M, Takahashi T, Nakamura Y, Mori H & Mishina M (1996) Impairment of suckling response, trigeminal neuronal pattern formation, and hippocampal LTD in NMDA receptor epsilon 2 subunit mutant mice. *Neuron* **16**, 333-344.

Lamsa KP, Heeroma JH, Somogyi P, Rusakov DA & Kullmann DM (2007) Anti-Hebbian long-term potentiation in the hippocampal feedback inhibitory circuit. *Science* **315**, 1262-1266.

Lappalainen R, Lindholm D & Riikonen R (1996) Low levels of nerve growth factor in cerebrospinal fluid of children with Rett syndrome. *J Child Neurol* **11**, 296-300.

Lappalainen R & Riikonen RS (1996) High levels of cerebrospinal fluid glutamate in Rett syndrome. *Pediatr Neurol* **15**, 213-216.

LaSalle JM, Goldstine J, Balmer D & Greco CM (2001) Quantitative localization of heterogeneous methyl-CpG-binding protein 2 (MeCP2) expression phenotypes in normal and Rett syndrome brain by laser scanning cytometry. *Hum Mol Genet* **10**, 1729-1740.

Lekman A, Witt-Engerstrom I, Holmberg B, Percy A, Svennerholm L & Hagberg B (1990) CSF and urine biogenic amine metabolites in Rett syndrome. *Clin Genet* **37**, 173-178.

Lewis JD, Meehan RR, Henzel WJ, Maurer-Fogy I, Jeppesen P, Klein F & Bird A (1992) Purification, sequence, and cellular localization of a novel chromosomal protein that binds to methylated DNA. *Cell* **69**, 905-914.

Lisman JE (1985) A mechanism for memory storage insensitive to molecular turnover: a bistable autophosphorylating kinase. *Proc Natl Acad Sci U S A* **82**, 3055-3057.

Lloyd TE & Bellen HJ (2001) pRIMing synaptic vesicles for fusion. *Nat Neurosci* **4**, 965-966.

London M & Hausser M (2005) Dendritic computation. *Annu Rev Neurosci* **28**, 503-532.

Luikenhuis S, Giacometti E, Beard CF & Jaenisch R (2004) Expression of MeCP2 in postmitotic neurons rescues Rett syndrome in mice. *Proc Natl Acad Sci U S A* **101**, 6033-6038.

Lynch G, Larson J, Kelso S, Barrionuevo G & Schottler F (1983) Intracellular injections of EGTA block induction of hippocampal long-term potentiation. *Nature* **305**, 719-721.

Lynch GS, Dunwiddie T & Gribkoff V (1977) Heterosynaptic depression: a postsynaptic correlate of long-term potentiation. *Nature* **266**, 737-739.

Madison DV, Malenka RC & Nicoll RA (1991) Mechanisms underlying long-term potentiation of synaptic transmission. *Annu Rev Neurosci* **14**, 379-397.

Maezawa I, Swanberg S, Harvey D, LaSalle JM & Jin LW (2009) Rett syndrome astrocytes are abnormal and spread MeCP2 deficiency through gap junctions. *J Neurosci* **29**, 5051-5061.

Mahanty NK & Sah P (1998) Calcium-permeable AMPA receptors mediate long-term potentiation in interneurons in the amygdala. *Nature* **394**, 683-687.

Malenka RC & Bear MF (2004) LTP and LTD: an embarrassment of riches. *Neuron* **44**, 5-21.

Malenka RC, Kauer JA, Perkel DJ, Mauk MD, Kelly PT, Nicoll RA & Waxham MN (1989) An essential role for postsynaptic calmodulin and protein kinase activity in long-term potentiation. *Nature* **340**, 554-557.

Malenka RC & Nicoll RA (1999) Long-term potentiation--a decade of progress? *Science* **285**, 1870-1874.

Malinow R, Madison DV & Tsien RW (1988) Persistent protein kinase activity underlying long-term potentiation. *Nature* **335**, 820-824.

Malinow R, Mainen ZF & Hayashi Y (2000) LTP mechanisms: from silence to four-lane traffic. *Curr Opin Neurobiol* **10**, 352-357.

Maliszewska-Cyna E, Bawa D & Eubanks JH (2010) Diminished prevalence but preserved synaptic distribution of N-methyl-D-aspartate receptor subunits in the methyl CpG binding protein 2(MeCP2)-null mouse brain. *Neuroscience* **168**, 624-632.

Martin SJ, Grimwood PD & Morris RG (2000) Synaptic plasticity and memory: an evaluation of the hypothesis. *Annu Rev Neurosci* **23**, 649-711.

Martinowich K, Hattori D, Wu H, Fouse S, He F, Hu Y, Fan G & Sun YE (2003) DNA methylation-related chromatin remodeling in activity-dependent BDNF gene regulation. *Science* **302**, 890-893.

Matarazzo V, Cohen D, Palmer AM, Simpson PJ, Khokhar B, Pan SJ & Ronnett GV (2004) The transcriptional repressor Mecp2 regulates terminal neuronal differentiation. *Mol Cell Neurosci* **27**, 44-58.

Matsuishi T, Nagamitsu S, Yamashita Y, Murakami Y, Kimura A, Sakai T, Shoji H, Kato H & Percy AK (1997) Decreased cerebrospinal fluid levels of substance P in patients with Rett syndrome. *Ann Neurol* **42**, 978-981.

Mayer ML, Westbrook GL & Guthrie PB (1984) Voltage-dependent block by Mg2+ of NMDA responses in spinal cord neurones. *Nature* **309**, 261-263.

McNair K, Davies CH & Cobb SR (2006) Plasticity-related regulation of the hippocampal proteome. *Eur J Neurosci* **23**, 575-580.

McNaughton BL, Battaglia FP, Jensen O, Moser EI & Moser MB (2006) Path integration and the neural basis of the 'cognitive map'. *Nat Rev Neurosci* **7**, 663-678.

Medrihan L, Tantalaki E, Aramuni G, Sargsyan V, Dudanova I, Missler M & Zhang W (2008) Early defects of GABAergic synapses in the brain stem of a MeCP2 mouse model of Rett syndrome. *J Neurophysiol* **99**, 112-121.

Meehan RR, Lewis JD, McKay S, Kleiner EL & Bird AP (1989) Identification of a mammalian protein that binds specifically to DNA containing methylated CpGs. *Cell* **58**, 499-507.

Minkeviciene R, Banerjee P & Tanila H (2004) Memantine improves spatial learning in a transgenic mouse model of Alzheimer's disease. *J Pharmacol Exp Ther* **311**, 677-682.

Mojumder DK, Wensel TG & Frishman LJ (2008) Subcellular compartmentalization of two calcium binding proteins, calretinin and calbindin-28 kDa, in ganglion and amacrine cells of the rat retina. *Mol Vis* **14**, 1600-1613.

Moretti P, Levenson JM, Battaglia F, Atkinson R, Teague R, Antalffy B, Armstrong D, Arancio O, Sweatt JD & Zoghbi HY (2006) Learning and memory and synaptic plasticity are impaired in a mouse model of Rett syndrome. *J Neurosci* **26**, 319-327.

Moretti P & Zoghbi HY (2006) MeCP2 dysfunction in Rett syndrome and related disorders. *Curr Opin Genet Dev* **16**, 276-281.

Mount RH, Hastings RP, Reilly S, Cass H & Charman T (2001) Behavioural and emotional features in Rett syndrome. *Disabil Rehabil* **23**, 129-138.

Mulkey RM, Endo S, Shenolikar S & Malenka RC (1994) Involvement of a calcineurin/inhibitor-1 phosphatase cascade in hippocampal long-term depression. *Nature* **369**, 486-488.

Mulkey RM, Herron CE & Malenka RC (1993) An essential role for protein phosphatases in hippocampal long-term depression. *Science* **261**, 1051-1055.

Mulkey RM & Malenka RC (1992) Mechanisms underlying induction of homosynaptic long-term depression in area CA1 of the hippocampus. *Neuron* **9**, 967-975.

Mullen RJ, Buck CR & Smith AM (1992) NeuN, a neuronal specific nuclear protein in vertebrates. *Development* **116**, 201-211.

Nag N, Moriuchi JM, Peitzman CG, Ward BC, Kolodny NH & Berger-Sweeney JE (2009) Environmental enrichment alters locomotor behaviour and ventricular volume in Mecp2 1lox mice. *Behav Brain Res* **196**, 44-48.

Nan X, Campoy FJ & Bird A (1997) MeCP2 is a transcriptional repressor with abundant binding sites in genomic chromatin. *Cell* **88**, 471-481.

Nan X, Cross S & Bird A (1998) Gene silencing by methyl-CpG-binding proteins. *Novartis Found Symp* **214**, 6-16; discussion 16-21, 46-50.

Nan X, Meehan RR & Bird A (1993) Dissection of the methyl-CpG binding domain from the chromosomal protein MeCP2. *Nucleic Acids Res* **21**, 4886-4892.

Nelson ED, Kavalali ET & Monteggia LM (2006) MeCP2-dependent transcriptional repression regulates excitatory neurotransmission. *Curr Biol* **16**, 710-716.

Nelson ED, Kavalali ET & Monteggia LM (2008) Activity-dependent suppression of miniature neurotransmission through the regulation of DNA methylation. *J Neurosci* **28**, 395-406.

Neul JL, Fang P, Barrish J, Lane J, Caeg EB, Smith EO, Zoghbi H, Percy A & Glaze DG (2008) Specific mutations in methyl-CpG-binding protein 2 confer different severity in Rett syndrome. *Neurology* **70**, 1313-1321.

Neul JL, Kaufmann WE, Glaze DG, Christodoulou J, Clarke AJ, Bahi-Buisson N, Leonard H, Bailey ME, Schanen NC, Zappella M, Renieri A, Huppke P & Percy AK (2010) Rett syndrome: revised diagnostic criteria and nomenclature. *Ann Neurol* **68**, 944-950.

Nicoll RA (2003) Expression mechanisms underlying long-term potentiation: a postsynaptic view. *Philos Trans R Soc Lond B Biol Sci* **358**, 721-726.

Nicoll RA & Schmitz D (2005) Synaptic plasticity at hippocampal mossy fibre synapses. *Nat Rev Neurosci* **6**, 863-876.

Nomura Y (2005) Early behavior characteristics and sleep disturbance in Rett syndrome. *Brain Dev* **27 Suppl 1**, S35-S42.

Nowak L, Bregestovski P, Ascher P, Herbet A & Prochiantz A (1984) Magnesium gates glutamate-activated channels in mouse central neurones. *Nature* **307**, 462-465.

Okabe S, Collin C, Auerbach JM, Meiri N, Bengzon J, Kennedy MB, Segal M & McKay RD (1998) Hippocampal synaptic plasticity in mice overexpressing an embryonic subunit of the NMDA receptor. *J Neurosci* **18**, 4177-4188.

Oliet SH, Malenka RC & Nicoll RA (1997) Two distinct forms of long-term depression coexist in CA1 hippocampal pyramidal cells. *Neuron* **18**, 969-982.

Olowoyeye A & Okwundu CI (2010) Gene therapy for sickle cell disease. *Cochrane Database Syst Rev*, CD007652.

Palmer A, Qayumi J & Ronnett G (2008) MeCP2 mutation causes distinguishable phases of acute and chronic defects in synaptogenesis and maintenance, respectively. *Mol Cell Neurosci* **37**, 794-807.

Pelka GJ, Watson CM, Radziewic T, Hayward M, Lahooti H, Christodoulou J & Tam PP (2006) Mecp2 deficiency is associated with learning and cognitive deficits and altered gene activity in the hippocampal region of mice. *Brain* **129**, 887-898.

Percy AK (1992) Neurochemistry of the Rett syndrome. *Brain Dev* **14 Suppl**, S57-62.

Percy AK (2008) Rett syndrome: recent research progress. *J Child Neurol* **23**, 543-549.

Perez Y, Morin F & Lacaille JC (2001) A hebbian form of long-term potentiation dependent on mGluR1a in hippocampal inhibitory interneurons. *Proc Natl Acad Sci U S A* **98**, 9401-9406.

Perumbeti A & Malik P (2010) Therapy for beta-globinopathies: a brief review and determinants for successful and safe correction. *Ann N Y Acad Sci* **1202**, 36-44.

Quaderi NA, Meehan RR, Tate PH, Cross SH, Bird AP, Chatterjee A, Herman GE & Brown SD (1994) Genetic and physical mapping of a gene encoding a methyl CpG binding protein, Mecp2, to the mouse X chromosome. *Genomics* **22**, 648-651.

Rammes G, Danysz W & Parsons CG (2008) Pharmacodynamics of memantine: an update. *Curr Neuropharmacol* **6**, 55-78.

Rastegar M, Hotta A, Pasceri P, Makarem M, Cheung AY, Elliott S, Park KJ, Adachi M, Jones FS, Clarke ID, Dirks P & Ellis J (2009) MECP2 isoform-specific vectors with regulated expression for Rett syndrome gene therapy. *PLoS ONE* **4**, e6810.

Reiss AL, Faruque F, Naidu S, Abrams M, Beaty T, Bryan RN & Moser H (1993) Neuroanatomy of Rett syndrome: a volumetric imaging study. *Ann Neurol* **34**, 227-234.

Rett A (1966) [On a unusual brain atrophy syndrome in hyperammonemia in childhood]. *Wien Med Wochenschr* **116**, 723-726.

Riikonen R & Vanhala R (1999) Levels of cerebrospinal fluid nerve-growth factor differ in infantile autism and Rett syndrome. *Dev Med Child Neurol* **41**, 148-152.

Rogers JH (1987) Calretinin: a gene for a novel calcium-binding protein expressed principally in neurons. *J Cell Biol* **105**, 1343-1353.

Roux JC, Dura E, Moncla A, Mancini J & Villard L (2007) Treatment with desipramine improves breathing and survival in a mouse model for Rett syndrome. *Eur J Neurosci* **25**, 1915-1922.

Rueda N, Llorens-Martin M, Florez J, Valdizan E, Banerjee P, Trejo JL & Martinez-Cue C (2010) Memantine normalizes several phenotypic features in the Ts65Dn mouse model of Down syndrome. *J Alzheimers Dis* **21**, 277-290.

Samaco RC, Mandel-Brehm C, Chao HT, Ward CS, Fyffe-Maricich SL, Ren J, Hyland K, Thaller C, Maricich SM, Humphreys P, Greer JJ, Percy A, Glaze DG, Zoghbi HY & Neul JL (2009) Loss of MeCP2 in aminergic neurons causes cell-autonomous defects in neurotransmitter synthesis and specific behavioral abnormalities. *Proc Natl Acad Sci U S A* **106**, 21966-21971.

Sangro B & Prieto J (2010) Gene therapy for liver cancer: clinical experience and future prospects. *Curr Opin Mol Ther* **12**, 561-569.

Santos M, Summavielle T, Teixeira-Castro A, Silva-Fernandes A, Duarte-Silva S, Marques F, Martins L, Dierssen M, Oliveira P, Sousa N & Maciel P (2010) Monoamine deficits in the brain of methyl-CpG binding protein 2 null mice suggest the involvement of the cerebral cortex in early stages of Rett syndrome. *Neuroscience* **170**, 453-467.

Schanen NC, Dahle EJ, Capozzoli F, Holm VA, Zoghbi HY & Francke U (1997) A new Rett syndrome family consistent with X-linked inheritance expands the X chromosome exclusion map. *Am J Hum Genet* **61**, 634-641.

Schmidt H, Arendt O, Brown EB, Schwaller B & Eilers J (2007) Parvalbumin is freely mobile in axons, somata and nuclei of cerebellar Purkinje neurones. *J Neurochem* **100**, 727-735.

Schultz RJ, Glaze DG, Motil KJ, Armstrong DD, del Junco DJ, Hubbard CR & Percy AK (1993) The pattern of growth failure in Rett syndrome. *Am J Dis Child* **147**, 633-637.

Schwaller B, Meyer M & Schiffmann S (2002) 'New' functions for 'old' proteins: the role of the calcium-binding proteins calbindin D-28k, calretinin and parvalbumin, in cerebellar physiology. Studies with knockout mice. *Cerebellum* **1**, 241-258.

Segawa M & Nomura Y (1990) The pathophysiology of the Rett syndrome from the standpoint of polysomnography. *Brain Dev* **12**, 55-60.

Segawa M & Nomura Y (1992) Polysomnography in the Rett syndrome. *Brain Dev* **14 Suppl**, S46-54.

Shahbazian M, Young J, Yuva-Paylor L, Spencer C, Antalffy B, Noebels J, Armstrong D, Paylor R & Zoghbi H (2002) Mice with truncated MeCP2 recapitulate many Rett syndrome features and display hyperacetylation of histone H3. *Neuron* **35**, 243-254.

Shahbazian MD, Zhang K & Grunstein M (2005) Histone H2B ubiquitylation controls processive methylation but not monomethylation by Dot1 and Set1. *Mol Cell* **19**, 271-277.

Shapovalov AI (1980) Interneuronal synapses with electrical, dual and chemical mode of transmission in vertebrates. *Neuroscience* **5**, 1113-1124.

Shibuki K & Okada D (1992) Cerebellar long-term potentiation under suppressed postsynaptic Ca2+ activity. *Neuroreport* **3**, 231-234.

Skene PJ, Illingworth RS, Webb S, Kerr AR, James KD, Turner DJ, Andrews R & Bird AP (2010) Neuronal MeCP2 is expressed at near histone-octamer levels and globally alters the chromatin state. *Mol Cell* **37**, 457-468.

Smrt RD, Eaves-Egenes J, Barkho BZ, Santistevan NJ, Zhao C, Aimone JB, Gage FH & Zhao X (2007) Mecp2 deficiency leads to delayed maturation and altered gene expression in hippocampal neurons. *Neurobiol Dis* **27**, 77-89.

Soderling TR & Derkach VA (2000) Postsynaptic protein phosphorylation and LTP. *Trends Neurosci* **23**, 75-80.

Stearns NA, Schaevitz LR, Bowling H, Nag N, Berger UV & Berger-Sweeney J (2007) Behavioral and anatomical abnormalities in Mecp2 mutant mice: a model for Rett syndrome. *Neuroscience* **146**, 907-921.

Sterio DC (1984) The unbiased estimation of number and sizes of arbitrary particles using the disector. *J Microsc* **134**, 127-136.

Subramaniam B, Naidu S & Reiss AL (1997) Neuroanatomy in Rett syndrome: cerebral cortex and posterior fossa. *Neurology* **48**, 399-407.

Taneja P, Ogier M, Brooks-Harris G, Schmid DA, Katz DM & Nelson SB (2009) Pathophysiology of locus ceruleus neurons in a mouse model of Rett syndrome. *J Neurosci* **29**, 12187-12195.

Tropea D, Giacometti E, Wilson NR, Beard C, McCurry C, Fu DD, Flannery R, Jaenisch R & Sur M (2009) Partial reversal of Rett Syndrome-like symptoms in MeCP2 mutant mice. *Proc Natl Acad Sci U S A* **106**, 2029-2034.

Vachani A, Moon E, Wakeam E & Albelda SM (2010) Gene therapy for mesothelioma and lung cancer. *Am J Respir Cell Mol Biol* **42**, 385-393.

Viemari JC, Roux JC, Tryba AK, Saywell V, Burnet H, Pena F, Zanella S, Bevengut M, Barthelemy-Requin M, Herzing LB, Moncla A, Mancini J, Ramirez JM, Villard L & Hilaire G (2005) Mecp2 deficiency disrupts norepinephrine and respiratory systems in mice. *J Neurosci* **25**, 11521-11530.

Villard L, Levy N, Xiang F, Kpebe A, Labelle V, Chevillard C, Zhang Z, Schwartz CE, Tardieu M, Chelly J, Anvret M & Fontes M (2001) Segregation of a totally skewed pattern of X chromosome inactivation in four familial cases of Rett syndrome without MECP2 mutation: implications for the disease. *J Med Genet* **38**, 435-442.

Voutsinas GE & Stravopodis DJ (2009) Molecular targeting and gene delivery in bladder cancer therapy. *J Buon* **14 Suppl 1**, S69-78.

Wang SH & Morris RG (2010) Hippocampal-neocortical interactions in memory formation, consolidation, and reconsolidation. *Annu Rev Psychol* **61**, 49-79, C41-44.

Watanabe M, Maemura K, Kanbara K, Tamayama T & Hayasaki H (2002) GABA and GABA receptors in the central nervous system and other organs. *Int Rev Cytol* **213**, 1-47.

Weng SM, McLeod F, Bailey ME & Cobb SR (2011) Synaptic plasticity deficits in an experimental model of rett syndrome: long-term potentiation saturation and its pharmacological reversal. *Neuroscience* **180**, 314-321.

Wenk GL (1997) Rett syndrome: neurobiological changes underlying specific symptoms. *Prog Neurobiol* **51**, 383-391.

Wenk GL & Hauss-Wegrzyniak B (1999) Altered cholinergic function in the basal forebrain of girls with Rett syndrome. *Neuropediatrics* **30**, 125-129.

Wenk GL & Mobley SL (1996) Choline acetyltransferase activity and vesamicol binding in Rett syndrome and in rats with nucleus basalis lesions. *Neuroscience* **73**, 79-84.

Whitlock JR, Heynen AJ, Shuler MG & Bear MF (2006) Learning induces long-term potentiation in the hippocampus. *Science* **313**, 1093-1097.

Wilson DA & Racine RJ (1983) The postnatal development of post-activation potentiation in the rat neocortex. *Brain Res* **283**, 271-276.

Wilson MA & McNaughton BL (1993) Dynamics of the hippocampal ensemble code for space. *Science* **261**, 1055-1058.

Wonders CP & Anderson SA (2006) The origin and specification of cortical interneurons. *Nat Rev Neurosci* **7**, 687-696.

Wood L & Shepherd GM (2010) Synaptic circuit abnormalities of motor-frontal layer 2/3 pyramidal neurons in a mutant mouse model of Rett syndrome. *Neurobiol Dis* **38**, 281-287.

Wu LG & Saggau P (1994) Presynaptic calcium is increased during normal synaptic transmission and paired-pulse facilitation, but not in long-term potentiation in area CA1 of hippocampus. *J Neurosci* **14**, 645-654.

Yun SH & Trommer BL Fragile X mice: reduced long-term potentiation and N-Methyl-D-Aspartate receptor-mediated neurotransmission in dentate gyrus. *J Neurosci Res* **89**, 176-182.

Yuste R & Bonhoeffer T (2001) Morphological changes in dendritic spines associated with long-term synaptic plasticity. *Annu Rev Neurosci* **24**, 1071-1089.

Zaitsev AV, Gonzalez-Burgos G, Povysheva NV, Kroner S, Lewis DA & Krimer LS (2005) Localization of calcium-binding proteins in physiologically and morphologically characterized interneurons of monkey dorsolateral prefrontal cortex. *Cereb Cortex* **15**, 1178-1186.

Zanella S, Mebarek S, Lajard AM, Picard N, Dutschmann M & Hilaire G (2008) Oral treatment with desipramine improves breathing and life span in Rett syndrome mouse model. *Respir Physiol Neurobiol* **160**, 116-121.

Zhang L, He J, Jugloff DG & Eubanks JH (2008) The MeCP2-null mouse hippocampus displays altered basal inhibitory rhythms and is prone to hyperexcitability. *Hippocampus* **18**, 294-309.

Zhang ZW, Zak JD & Liu H (2010) MeCP2 is required for normal development of GABAergic circuits in the thalamus. *J Neurophysiol* **103**, 2470-2481.

Zhou Z, Hong EJ, Cohen S, Zhao WN, Ho HY, Schmidt L, Chen WG, Lin Y, Savner E, Griffith EC, Hu L, Steen JA, Weitz CJ & Greenberg ME (2006) Brain-specific phosphorylation of MeCP2 regulates activity-dependent Bdnf transcription, dendritic growth, and spine maturation. *Neuron* **52**, 255-269.

Ziakopoulos Z, Tillett CW, Brown MW & Bashir ZI (1999) Input-and layer-dependent synaptic plasticity in the rat perirhinal cortex in vitro. *Neuroscience* **92**, 459-472.

Zlatanova J (2005) MeCP2: the chromatin connection and beyond. *Biochem Cell Biol* **83**, 251-262.

Zoghbi HY, Milstien S, Butler IJ, Smith EO, Kaufman S, Glaze DG & Percy AK (1989) Cerebrospinal fluid biogenic amines and biopterin in Rett syndrome. *Ann Neurol* **25**, 56-60.

Zoghbi HY, Percy AK, Glaze DG, Butler IJ & Riccardi VM (1985) Reduction of biogenic amine levels in the Rett syndrome. *N Engl J Med* **313**, 921-924.

Zucker RS & Regehr WG (2002) Short-term synaptic plasticity. *Annu Rev Physiol* **64**, 355-405.